NMR Studies on the Electronic Properties of Superconducting Fulleride K_3C_{60}

核磁気共鳴法による超伝導性フラレン化合物K_3C_{60}の電子状態の研究

佐々木　進

NMR Studies on the Electronic Properties of Superconducting Fulleride K_3C_{60}

Thesis

Submitted for the degree of Doctor of Science in Physics,

The University of Tokyo

1996

by

Susumu SASAKI

NTT Basic Research Laboratories,

Nippon Telegraph and Telephone Corporation

Acknowledgments

The present study has been accomplished not only by me but also by many people who have supported me with their kind offers, useful advice, and warm encouragements. I wish to express my sincere appreciation to many people who have supported or have been supporting me.

First of all, I would like to acknowledge Prof. C. W. Chu, who has prepared a good quality sample of superconducting fulleride K_3C_{60}. When he visited our laboratory (May 23rd, 1991), I had a chance to discuss with him and to show him my NMR spectrometer which had attained the desired specifications. Great and famous scientist as he is, he kindly and gently proposed to give us a K_3C_{60} sample for our NMR measurements. Without his kind offer or the well-prepared sample, the present study would not have existed.

I wish to thank Dr. John Michael Albert, secretary to Prof. C. W. Chu, and all the scientists, in the Texas Center for Superconductivity at University of Houston, that were involved in the synthesis and characterization of the sample.

I would like to express my grateful thanks to Prof. Hiroshi Yasuoka. He was my advisor for two years (1987 ~ 1989) when I was a graduate course student at Yasuoka Lab., Institute for Solid State Physics, The University of Tokyo. Owing to his guidance, I could join this fascinating field: the NMR study on solid state materials. I think I have learned from him what experimental researchers in solid state physics should keep in mind. First, physical picture based on precise data using a well-characterized sample. Second, curiosity motivated by a naive question. Third, can-do spirit and positive attitude, never jumping to pessimistic criticism. (The third does not contradict the first, since the optimistic stance lies on the reliable data.) It was very lucky that I could learn these from him in the beginning of my carrier as a researcher.

Although I had to leave Yasuoka Lab. and to go into industry without a doctoral degree from a financial problem due to my father's death, I luckily had a chance to stay in the study of this field.

Dr. Azusa Matsuda, my boss and the Leader of our group, gave me the opportunity to build up an NMR spectrometer at NTT Basic Research Labs., Nippon Telegraph and Telephone Corporation, aiming at investigating the electronic states of superconductors from a microscopic viewpoint. Although it was for only two years that I was trained in Yasuoka Lab., he was generous enough to hire me as a researcher in the NMR field, believing in my potential. In addition, I was greatly indebted from him, particularly in the course of building up the spectrometer. He made me some prototypes of computer programs for controlling the devices and for data acquisition and analyses. He inspired me with his modernized knowledge on electronics. Without his advice, the spectrometer had not attained the present specifications.

Even after leaving Yasuoka Lab., I have been benefited by Prof. Yasuoka mainly from his mental support. He strongly encouraged me to submit a thesis on the present study, after having kept observing the progress of my study. Without his warm observation and frequent encouragement after I left his Lab., I would have missed the opportunity to obtain a doctoral degree.

Prof. Hironori Nishihara, Dr. Masashi Takigawa, Dr. Tadashi Shimizu, Prof. Takashi Imai, who belonged to Yasuoka Lab. while I was a graduate course student, instructed me in the ABC of NMR measurements and the related physics. From fruitful discussions with Dr. Tetsuo Ohama, Dr. Yutaka Itoh, and Kenji Ikushima, the present members at Yasuoka Lab., I have learned a great deal on both physics and techniques. Prof. Toshinobu Tsuda and Prof. Masayuki Itoh, who would often visit Yasuoka Lab. and supported me by their blissful atmospheres in my graduate course, have been stimulating me by useful information and discussion. Dr. Yohsuke Yoshinari, Dr. Jun Kikuchi and Dr. Atsushi Goto, the former students of Prof. Yasuoka, gave me their theses. I would like to express my sincere thanks to these former and present members at Yasuoka Lab.

Dr. Tatsuo Izawa, the Senior Executive Manager of NTT Basic Research Labs., supported me financially a great deal when I joined Materials Science Research Lab. On demand of Dr. Matsuda and me, he made an effort to prepare substantial amount of the initial cost and the space for the spectrometer. Dr. Tomoaki Yamada, the Research Fellow of Yamada Research Lab. at NTT, has been giving me metal support and valuable instructions as a researcher on natural science in a corporation. Dr. Nobuo Matsumoto, the Executive Manager of Materials Science Research Lab., has encouraged me to prepare the present thesis in addition to his constant financial and mental support on my studies. I enjoyed discussion with Prof. Susumu Kurihara. When he was a Group Leader at NTT Basic Research Labs., he gave me instructive advice from theoretical viewpoint. Dr. Michiya Fujiki, a skilled chemist in our Lab., kindly helped me to install the sample from Prof. Chu into our spectrometer.

Dr. Michio Naito and Dr. Hisashi Tara-chan Sato are the present members of Matsuda Research Group in Materials Science Research Lab. at NTT. Since they used to be visitors at Yasuoka Lab., their practical and useful comments on my studies from experimental point of view have been doing me a great deal. I have been enjoying free-style but fruitful discussion with Kouichi Semba, a member of Matsuda Group. Believing in my potential, he was on my side by encouraging me strongly, particularly when the time was against me. He helped me a great deal to survive the hard time.

Prof. Yoshiji Horikoshi is the former Executive Manager of Physical Science Research Lab. at NTT. Although he majors in semi-conductor physics, he was interested in the present study and encouraged me, particularly in the hard time.

I have been enjoying free discussion frequently on physics and the related topics with Dr. Kenji Gee-san Shiraishi, Dr. Tsuneo Fukuda, Dr. Makoto Yamatta-tang Yamashita, Hiroyuki Shibatta-tang Shibata. I really wish to thank these former and present coworkers at NTT Basic Research Labs.

Stimulating private communications with Prof. Kazushi Kanoda inspired me in a number of ideas which are indispensable to the analyses in the present

thesis. The present study would not have produced a consistent physical picture without the studies by him and his coworkers, to whom I wish to express my sincere thanks.

I am grateful to Vincent A. Stenger, Dr. Yohsuke Yoshinari, Dr. Takahito Saito, Dr. Yutaka Maniwa and Prof. Kiyoshi Kume for discussing in details on the NMR studies of fullerides.

I would like to express my appreciation to Prof. Charles P. Slichter. He kindly sent me, on my request, the unpublished theses by Dr. Po-Kang Wang and by Dr. Jean-Philippe Ansermet. I enjoyed and learned a great deal from private communications with Dr. Joseph A. Martindale, the former student of Prof. Slichter. He had the further kindness to send me the theses by him and by Prof. Charles H. Pennington. I wish to express my thanks to these former students of Prof. Slichter. Although I myself have never met them directly, I am benefited from them, particularly on the improvement of the NMR spectrometer.

Finally, I want to thank my father who passed away in 1988. My curiosity in natural science stems from the conversations with him in my childhood. To my many "why's" as a young boy, he tried to answer by discussing with me from a naive viewpoint of a child, never giving a definite answer.

Table of Contents

Chapter 1. Introduction

§1-1. Discovery of Superconducting Fullerides A_3C_{60} (A = alkali metal)

In 1985, Kroto *et al.* succeeded in synthesizing the soccer-ball shaped carbon allotrope C_{60} for the first time [Kroto *et al.*, 1985]. The allotrope was named "Buckminsterfullerene" after the scientist Buckminster Fuller, since it was he that theoretically predicted its existence [Marks *et al.*, 1960]. In the beginning, the main aim of experimental studies was to understand the mechanisms how the long-chain carbon molecules in interstellar space are formed. However, the discovery by Kratschmer *et al.* in 1990 [Kratschmer *et al.*, 1990], the methods of producing and purifying substantial amount of fullerenes, attracted many chemists. In fact, soon after this discovery, Hebard *et al.* have succeeded in synthesizing a potassium doped fulleride K_xC_{60} and found an ambiguous evidence of superconductivity with transition temperature T_C of 18 K [Hebard *et al.*, 1991]. This evoked extensive studies by not only chemists but also physicists from a view point of solid state science. It was not long before Holczer *et al.* demonstrated that, among A_xC_{60} fullerides, only A_3C_{60} compounds show superconductivity [Holczer *et al.*, 1991].

Shown in Fig. 1-1 is the crystal structure of superconducting A_3C_{60} at low temperatures. It is known that the C_{60} molecules start to rotate with increasing temperatures.

§1-2. Physical Properties of A_3C_{60} ---theories and experiments

In the early stage of the studies on the mechanisms of superconductivity in A_3C_{60}, there were some "radical" theories: the pairing mechanisms are due to electronic origin [Chakravarty *et al.*, 1991] or the so-called "negative U"

Fig. 1-1
Crystal structure of superconducting fulleride K_3C_{60}.
Soccer-ball shaped C_{60} molecules form face-centered cubic. Two sites exist for potassiums located between the molecules; T-site (O-site) potassium, which is shown by dark blue (by green), is located at the center of gravity of a tetrahedron (an octahedron) formed by the molecules.

origin [Zhang *et al.*, 1991], mainly because the T_C's of A_3C_{60} are the highest but only those of the cuprate oxides. As shown in Fig. 1-2, band calculations indicate that the highest occupied molecular orbital (HOMO) of both K_3C_{60} and pristine C_{60} is five-fold degenerated and the lowest unoccupied molecular orbital (LUMO), the energy level of which is about 1 eV higher than that of HOMO, is three-fold degenerated [Erwin and Pickett, 1991]. In K_3C_{60}, the electrons, given on the C_{60} molecule by the doped potassium, go into the three-fold degenerated t_{1u} orbitals, resulting in the so-called half-filled metals.

Some experiments in the early stage reported anomalous results: "zero-dimensional" conductivity for thin films [Palstra *et al.*, 1992] and rather small α as the strength of electron-phonon coupling from the measurement of isotope effect [Ramirez *et al.*, 1992]. However, these are found to be experimental artifacts mainly due to the poor quality of the samples: Xiang *et al.* have succeeded in synthesizing high quality single crystals of K_3C_{60} and Rb_3C_{60} instead of thin films [Xiang *et al.*, 1992] and, as shown in Fig. 1-3, they observed not only usual metallic temperature (T) dependence of the conductivity but also three dimensional superconducting fluctuations (which they called "paraconductivity") for the first time [Xiang *et al.*, 1993]. In addition, as shown in Fig. 1-4, using a sample which contains ^{13}C isotope homogeneously, Ebbesen *et al.* made it clear that the superconducting mechanisms strongly suggest the Bardeen -Cooper -Schrieffer (BCS) -type phonon-mediated one instead of extraordinary ones [Ebbesen *et al.*, 1992].

As samples are improved, experiments have led toward the consensus that the normal state of the A_3C_{60} is a Fermi liquid and that a conventional *s*-wave pairing (probably phonon-mediated) is formed in their superconducting state. Most spectroscopic results such as Raman scattering [Mitch *et al.*, 1992], optical reflectivity [Degiorgi *et al.*, 1992], and muon spin rotation (μSR) [Kiefl *et al.*, 1993], suggest that the coupling is weak, whereas the low-temperature scanning tunneling microscopy (STM) indicates that it is strong [Zhang *et al.*,

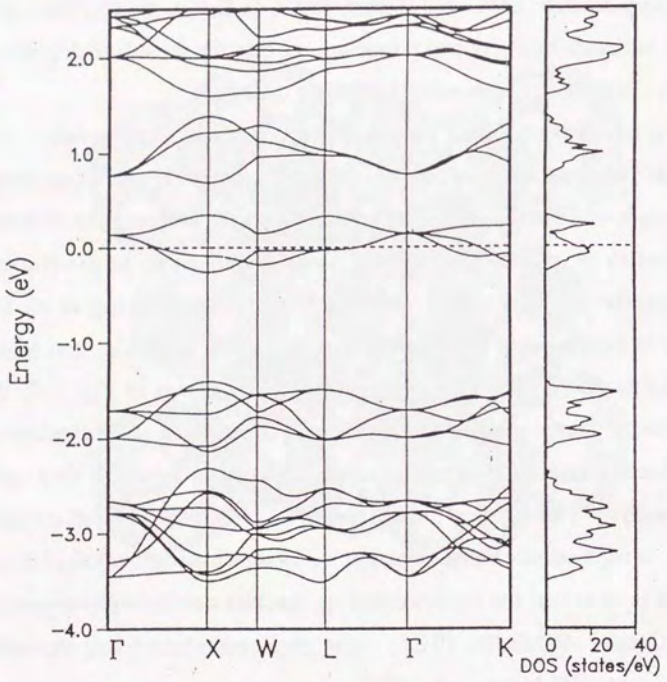

Fig. 1-2

Self-consistent electronic band structure of K_3C_{60} [Erwin and Pickett, 1991]. The zero of energy is defined by the Fermi level. The density of states is for both spins.

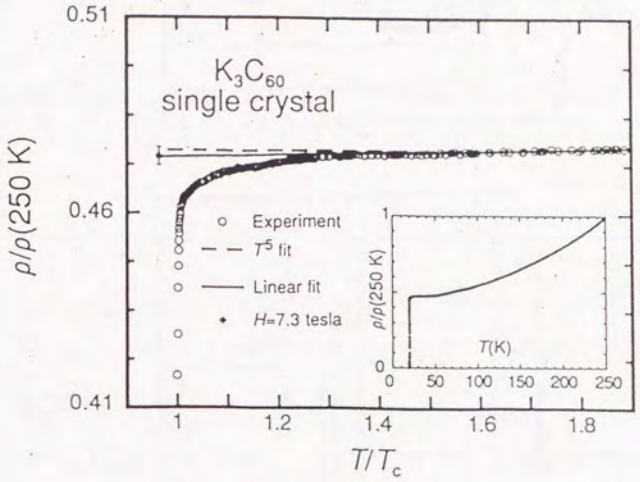

Fig. 1-3

Normalized resistivity as a function of T/T_C for K_3C_{60}. Xiang *et al.* observed three-dimensional fluctuation conductivity for the first time using the well-characterized single crystal [Xiang *et al.*, 1993].

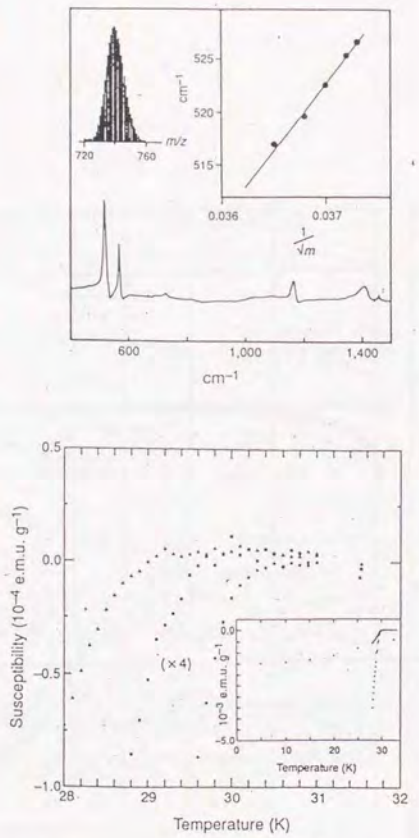

Fig. 1-4

Isotope effect on superconductivity in Rb_3C_{60} [Ebbesen *et al.*, 1992].

Upper: Infrared spectrum of C_{60} containing 33 % ^{13}C and its mass distribution. Inset: dependence of the infrared peak position on the average mass of C_{60}. The isotope is homogeneously doped.

Lower: Meissner (field-cooling) curves as a function of T showing in detail the T_C onset for three different ^{13}C content, (circles: 1.1 %; squares: 31 %; triangles: 33 %). The curve for 31 % has been multiplied by 4 to separate it more clearly from the 33 % curve. Inset: zero-field-cooled and field-cooled curves for C_{60} with 1.1 % ^{13}C content.

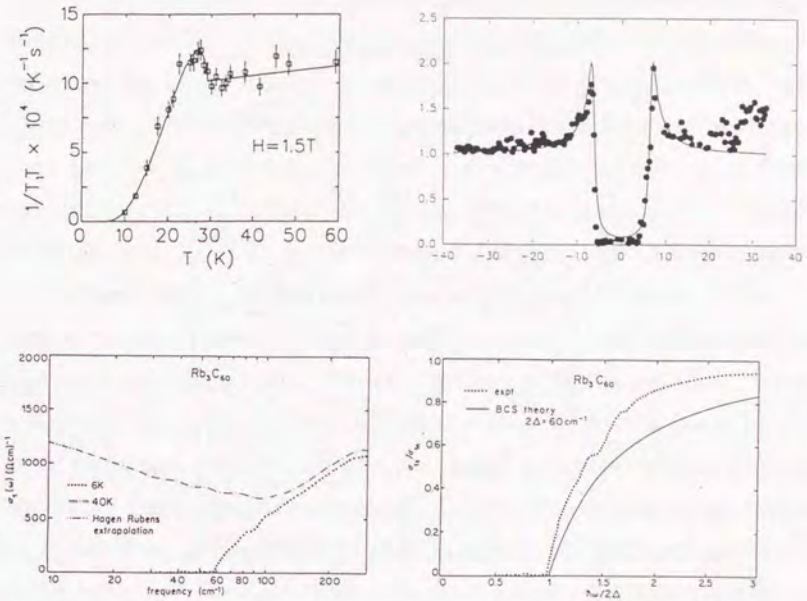

Fig. 1-5

Spectroscopic results indicating the Bardeen -Cooper -Schriefer (BCS) -type superconductivity in Rb_3C_{60}.

Upper-Left: T dependence of muon spin-lattice relaxation rate $1/(T_1T)$ for Rb_3C_{60} [Kiefl *et al.*, 1993]. A clear-cut coherence peak is observed just below T_C. The data is well reproduced by the so-called Dynes' density of states (shown by the solid curve) and the reduced gap $2\Delta/k_BT_C$ is found to be 3.63.

Upper-Right: dI/dV is plotted as a function of V in the low T scanning tunneling microscopy (STM) for Rb_3C_{60} [Zhang *et al.*, 1991]. Divergent behavior in the density of states (proportional to dI/dV) is observed. The data is fitted by the Dynes' density of states with $2\Delta/k_BT_C = 5.3$.

Lower: Optical conductivity for Rb_3C_{60} [Degiorgi *et al.*, 1992]. The conductivity well below T_C (shown by dotted curve in the left) clearly has a gap at frequency of ~60 cm^{-1} whereas that above T_C (broken curve in the left) does not. As illustrated in the right figure, the data well below T_C (dotted curve) is well reproduced by the so-called Mattis-Bardeen (i.e., BCS) theory with $2\Delta/k_BT_C = 3.52$.

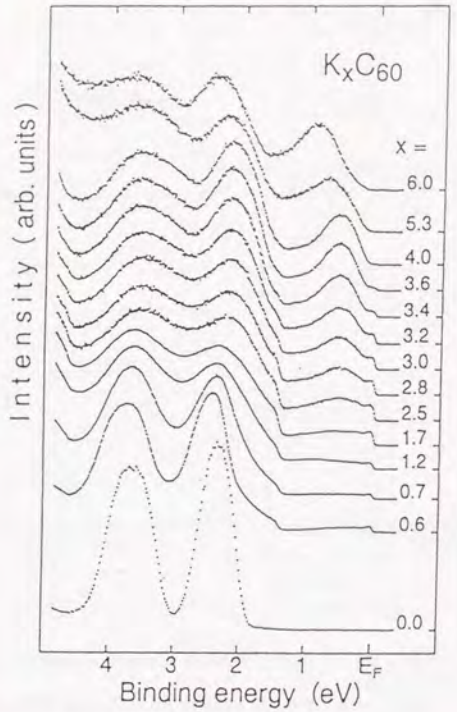

Fig. 1-6
Photoemmision spectra of K_xC_{60} measured with energy resolution of 35 meV at 40 K [Morikawa and Takahashi, 1993]. Around x = 3.0 (superconducting phase), a clear-cut Fermi edge is observed, which is a direct proof of a Fermi liquid.

1991]. As shown in Fig. 1-5, these results clearly indicate that A_3C_{60} behaves as a conventional superconductor although the obtained coupling strengths are different.

Within the conventional framework of the A_3C_{60} superconductivity, however, some anomalous electronic properties are observed by other experiments which are now widely accepted. Firstly, A_3C_{60} is a type II superconductor with a large value of λ/ξ: the superconducting coherence length ξ is found to be very small (25 ~35 Å; note that the diameter of C_{60} molecule is 7.1 Å) from magnetization measurements [Holczer *et al.*, 1991; Johnson *et al.*, 1992; Boebinger *et al.*, 1992]. The penetration depth λ obtained by μSR measurements is very large (4800 Å for K_3C_{60}) [Uemura *et al.*, 1991]. Secondly, A_3C_{60} is a dirty metal: the resistivity at room T is extremely large (5 mΩ-cm) even in the high quality single crystal whose resistivity shows the metallic T-linear dependence [Xiang *et al.*, 1992]. Thirdly, the effect of electron interaction is likely not to be negligible: basically, the electronic state of A_3C_{60} is a Fermi liquid since Fermi edges (direct proof of a Fermi liquid) are clearly observed in highly resoluted photoemission spectra [Morikawa and Takahashi, 1993], as shown in Fig. 1-6. However, Coulomb interaction on the C_{60} molecule is found to be 1.6 eV from Auger spectra by Lof *et al.* [Lof *et al.*, 1992], whereas the band width is obtained to be 0.4 ~ 0.6 eV from band calculations (Fig. 1-2) [Erwin and Pickett, 1991].

§1-3. Organization of This Thesis

The organization of the present thesis is as follows.

In Chapter 2, we briefly describe basic concepts for ^{13}C and ^{39}K NMR which are inevitable for the following discussion. In Chapter 3, after surveying the findings and the problems in the precedent NMR studies on the electronic states of A_3C_{60}, which were published in 1992 ~ 1994 by other groups, we present the motivation of this study. In Chapter 4, we describe the experimental procedures

for this study: sample preparation, our spectrometer, and measurement conditions. Chapters 5 and 6 are the bodies of the thesis. In Chapter 5, after showing the results of ^{13}C NMR spectra, we present the results of ^{13}C NMR spin-lattice relaxation time measurements, focusing on not the C_{60} molecular motion but the electronic states. Based on consistent analyses of these static and dynamical information on the carbon sites, we discuss the electronic states of K_3C_{60} from the viewpoint of anisotropy in hyperfine coupling of conduction electrons, validity of the Korringa relation, superconducting mechanisms, and electron interaction. In Chapter 6, we first present the results of ^{39}K NMR spectra. Together with the results of ^{13}C NMR, the analyses of the potassium sites give us the information on the C_{60} molecules as well as on the potassium sites. In this chapter, we discuss some properties of the low-T phase of K_3C_{60} where the C_{60} molecular motion is frozen: orientational disorder of the molecules and the absence of local density of states on the molecules. Finally, in Chapter 7, by summing up the experimental results and giving answers to the questions presented in Chapter 3, we conclude a consistent physical picture on the electronic properties of K_3C_{60} superconductor, which has been made clear by this study.

Chapter 2.

Basic Concepts for ^{13}C and ^{39}K NMR

§2-1. Hyperfine Interaction

The NMR-related area is so wide that it would be impossible to describe all the concepts including the first steps of measurements and the related physics. In this chapter, therefore, we only briefly introduce some basic concepts of ^{13}C and ^{39}K NMR that the author considers to be the musts for the present study.

The advantage of NMR measurements lies on the fact that they can detect the microscopic electronic states since the "probe" is the microscopic nucleus. This is possible because, in addition to the applied static magnetic field ($\boldsymbol{H}^{ext}$), the nucleus is coupled to the environment via magnetic and/or electric interaction. The total Hamiltonian for a nucleus consists of three terms as

$$\mathcal{H} = \mathcal{H}^{Zeeman} + \mathcal{H}^{mag} + \mathcal{H}^{el}. \tag{2-1}$$

The first is the nuclear Zeeman term expressed as

$$\mathcal{H}^{Zeeman} = -\gamma_n \hbar \boldsymbol{I} \cdot \boldsymbol{H}^{ext}, \tag{2-2}$$

where $\boldsymbol{H}^{ext}$ represents the applied magnetic field, $\boldsymbol{I}$ is the nuclear spin operator divided by $\hbar$. γ_n is the gyromagnetic ratio of the nucleus, and $\hbar$ is the Planck's constant divided by 2π. The second (the third) term in Eq. (2-1) represents the magnetic (the electric) interaction between the nuclear spin $\boldsymbol{I}$ (the nuclear quadrupole moment Q) and the local magnetic field (the local electric field gradient) acted on the nucleus by the environment. The interaction is called magnetic (electric) *hyperfine interaction* [Jaccarino, 1967].

The magnetic hyperfine interaction consists of three parts as

$$\mathcal{H}^{mag} = \boldsymbol{I} \cdot \boldsymbol{A}^{spin} \cdot \boldsymbol{S} + \boldsymbol{I} \cdot \boldsymbol{A}^{VV} \cdot \boldsymbol{L} + \boldsymbol{I} \cdot \boldsymbol{A}^{core} \cdot \boldsymbol{l}, \tag{2-3}$$

where $\boldsymbol{S}$ is the electron spin.

The presence of $\boldsymbol{H}^{ext}$ makes the electron orbital, which is ordinarily quenched in a crystal by the presence of the crystal field, "revive" to some extent as a result of the effect of the second-order perturbation. The second term in Eq. (2-3) represents the interaction between the nuclear spin $\boldsymbol{I}$ and the electron orbital $\boldsymbol{L}$ induced by this effect, via the hyperfine coupling A^{VV}. This term is called *Van-Vleck term* because it represents the "microscopic version" of the Van-Vleck susceptibility. Alternatively, it is called *paramagnetic term*, after the name of the electric current (*paramagnetic current*) which corresponds to the induced orbital $\boldsymbol{L}$. It is to be noted that, from the viewpoint of quantum mechanics, the paramagnetic current is described as $(e/2mi)[\Psi^*\nabla\Psi - \Psi\nabla\Psi^*]$, where e (m) is the charge (mass) of electron and the change in the wave function Ψ results from applying $\boldsymbol{H}^{ext}$ [Slichter, 1989].

In addition to the paramagnetic current, the presence of $\boldsymbol{H}^{ext}$ induces *diamagnetic* electric current (with orbital moment $\boldsymbol{l}$) on the electron core. As a result, the external field $\boldsymbol{H}^{ext}$ is shielded by the electron core. In other words, the electron core acts as a superconductor to the nucleus. Specifically, to apply the external field (hence the presence of the corresponding vector potential $\mathcal{A}$) results in diamagnetic current density which is expressed as $(e^2/m)[\mathcal{A}\Psi^*\Psi]$ [Slichter, 1989]. For this reason, the diamagnetic effect due to the third term is referred to as *chemical shielding* [Bovey, 1988].

The first term in Eq. (2-3) represents the interaction between the nuclear spin and the electron spin. For metals and magnetic materials, this term plays an important role because this is usually larger by the order of 2 ~ 3 than the other two terms. On the other hand, for nonmagnetic insulators (usually organic materials) which are studied by chemists, it is the latter two terms that count since the first term is zero due to the quenching of the total electron spin (S = 0), and the latter terms reflect the states of chemical bondings.

The magnetic hyperfine coupling A^{spin} consists of such two terms as the *Fermi contact* term (which is isotropic) and *electron dipolar* one (which is anisotropic),

which is denoted as A_{iso}^{spin} and A^{dipole}, respectively. The isotropic Fermi contact A_{iso}^{spin} is expressed as

$$A_{iso}^{spin} = \mu_B(8\pi/3)\langle u(0)\rangle^2, \tag{2-4}$$

where μ_B is Bohr magneton. For conventional metals where the band picture holds (including K_3C_{60}), $u(0)$ represents the amplitude at the nucleus of the *Bloch* wave function, and the average $\langle ...\rangle$ is taken for all the *conduction electrons* near the *Fermi surface*. The sign of the resultant A_{iso}^{spin} is *positive*. In the case of ^{13}C- (^{39}K-) NMR on K_3C_{60}, the average is taken for all those conduction electrons near the Fermi surface which reside on the carbon (the potassium) *s*-orbitals. (In the cases of transition metals, magnetic materials, or cuprate oxides, the finite amplitude at the nucleus is also due to the *core polarization* of closed inner *s*-shells which is caused by an unpaired electron spin at outer 3*d*-orbital. The exchange interaction between the electron spin in the closed *s*-shells and the unpaired spin at the 3*d*-orbital causes the difference between the up and down spin of the inner *s*-shells by way of virtual mixing with higher *s*-orbitals. This results in the *imbalance* of the up and down spins of the *s*-shells, hence the finite spin amplitude at the nucleus. The sign of the resultant A_{iso}^{spin} in the presence of core polarization is ordinarily *negative*.)

The anisotropic magnetic dipolar hyperfine coupling A^{dipole} is expressed as

$$A^{dipole} = \mu_B\langle\textstyle\sum_k(1/r_k^3)[S_k - \{3(S_k\cdot r_k)r_k\}/r_k^2]\rangle, \tag{2-5}$$

where S_k is the k-th electron spin, r_k (r_k) is the vector (the distance) from the nucleus to the k-th electron, and the average $\langle ...\rangle$ is taken for the electrons on the wave function in concern. In the case of ^{13}C NMR on the carbon-based conductors (including K_3C_{60}), the average is taken for all the *conduction* electrons near the *Fermi surface* residing on the carbon 2*p*-orbitals. On the other hand, in the case of the ^{39}K NMR on K_3C_{60}, the absence of *p*-orbitals on the potassium ions causes no magnetic dipolar hyperfine coupling.

The electric hyperfine interaction $\mathcal{H}^{el}$ in Eq. (2-3) is expressed as

$$\mathcal{H}^{el} = e^2qQ\,(3I_z^2 - I^2) / 4I(2I - 1). \tag{2-6a}$$

In the coordinates where the electric potential V is diagonalized, the electric field gradient (EFG, denoted as eq) is defined as

$$eq = \partial^2 V / \partial z^2. \tag{2-6b}$$

In Eq. (2-6a), Q is the nuclear quadrupole moment and $\boldsymbol{I}$ is the nuclear spin operator divided by $\hbar$. It is to be noted that the electric term appears *only when* the nucleus has finite value of Q, or equivalently, in the case of $I \geq 3/2$. Since the nuclear spin of ^{13}C (^{39}K) is $^{13}I = 1/2$ ($^{39}I = 3/2$), the electric hyperfine interaction should be taken into account only for the ^{39}K NMR but not for the ^{13}C NMR.

§2-2. NMR Frequency Shift

In the present ^{39}K NMR study, the electric hyperfine term $\mathcal{H}^{el}$ in the total Hamiltonian expressed by Eq. (2-1) is taken to be a perturbation effect to the other Zeeman and magnetic hyperfine terms. This is because the value of eq is considered to be close to zero due to the fact that the potassiums in K_3C_{60} are located at the center of gravity of the tetrahedron or of the octahedron formed by the C_{60} molecules. Indeed, as is described in Chapter 6, this will be experimentally confirmed. In the case of ^{13}C NMR, as already mentioned, the electric hyperfine term $\mathcal{H}^{el}$ is zero in principle. Thus, we neglect the $\mathcal{H}^{el}$ term in the total Hamiltonian of Eq. (2-1) for the moment in what follows. In this case, the unperturbed Hamiltonian $\mathcal{H}_0$ is expressed as

$$\mathcal{H}_0 \equiv \mathcal{H}^{Zeeman} + \mathcal{H}^{mag} = -\gamma_n \hbar \boldsymbol{I} \cdot \langle \boldsymbol{H}^{loc} \rangle. \tag{2-7}$$

Using the coordinates which diagonalize the magnetic hyperfine couplings, the local magnetic field in Eq. (2-7) is expressed as

$$H_i^{loc} = H_i^{ext} - (gA_i^{spin} S_i + gA_i^{VV} L_i + gA_i^{core} l_i), \tag{2-8}$$

where i stands for x-, y-, and z- component, and the diagonalized magnetic hyperfine coupling A_{ii}^{k} is abbreviated as A_i^{k} (k = spin, VV, core). Generally, the following relation holds for the respective susceptibility as

$$\chi^{spin} = - (g\mu_B S_i) / H_i^{ext}, \tag{2-9a}$$

$$\chi^{VV} = - (g\mu_B L_i) / H_i^{ext}, \tag{2-9b}$$

$$\chi^{core} = - (g\mu_B l_i) / H_i^{ext}. \tag{2-9c}$$

By dividing the both sides of Eq. (2-8) by H_i^{ext} and using Eq. (2-9), we obtain

$$(1/\mu_B) [A_i^{spin}\chi^{spin} + A_i^{VV}\chi^{VV} + A_i^{core}\chi^{core}] = [H_i^{loc} - H_i^{ext}]/ H_i^{ext}. \tag{2-10}$$

As seen from Eqs. (2-1) and (2-2), the value of $\gamma_n H_i^{ext}$ ($\equiv (\omega^{ext})_i$) represents the resonance frequency if the nucleus were to couple only to H_i^{ext}. In reality, however, the resonance occurs at the frequency $\gamma_n H_i^{loc}$ ($\equiv (\omega^{res})_i$) instead of $\gamma_n H_i^{ext}$, because the nuclear spin $\boldsymbol{I}$ interacts with the local magnetic field $\boldsymbol{H}^{loc}$ not with the external field $\boldsymbol{H}^{ext}$. Specifically, this is expressed as,

$$[H_i^{loc} - H_i^{ext}]/ H_i^{ext} = [(\omega^{res})_i - (\omega^{ext})_i]/ (\omega^{ext})_i. \tag{2-11}$$

In other words, the effect of the environment which originates from the magnetic hyperfine term $\mathcal{H}^{mag}$ in Eq. (2-7) or, equivalently, the local magnetic field at the nucleus *other than* $\boldsymbol{H}^{ext}$, is observed as the *difference* in the resonance frequency of $[(\omega^{res})_i - (\omega^{ext})_i]$. The value defined by the right-side of Eq. (2-11), which does not depend on H_i^{ext} (or equivalently, $(\omega^{ext})_i$), is called *NMR frequency shift* and is expressed by K_i throughout this thesis. As seen from Eqs. (2-10) and (2-11), K_i consists of three terms as

$$K_i = K_i^{spin} + K_i^{VV} + K_i^{core}, \tag{2-12a}$$

$$K_i^{spin} = (1/\mu_B) [A_i^{spin}\chi^{spin}], \tag{2-12b}$$

$$K_i^{VV} = (1/\mu_B) [A_i^{VV}\chi^{VV}], \tag{2-12c}$$

$$K_i^{core} = (1/\mu_B) [A_i^{core}\chi^{core}]. \tag{2-12d}$$

As is defined in Eq. (2-9), the corresponding susceptibility χ^k (k = spin, VV, core) is in the units of c.g.s. per atom.

The first term in Eq. (2-12a), K_i^{spin}, is called *Knight shift*. The other term of $K_i^{VV} + K_i^{core}$, which is expressed by K_i^{orb}, is named as *chemical shift*. For nonmagnetic insulators, since the Knight shift is equal to zero ($K_i^{spin} = 0$) due to $S = 0$, the resultant NMR shift is equal to the chemical shift ($K_i = K_i^{orb}$). In this case, the "absolute value" of K_i^{orb} could be obtained in principle if the value of γ_n were to be measured precisely within the error of 10^{-8} from the

resonance frequency of the "bare" nucleus, as is seen from Eqs. (2-10) and (2-11). In practice, however, the value of K_i^{orb} of a certain nucleus in a certain material is defined as the *difference* from the resonance frequency of the same nucleus in a *standard material* (which is, needless to say, nonmagnetic insulator), instead of going so far as to obtain the precise gyromagnetic ratio on the "bare" nucleus. For instance, tetramethylsilane (TMS) is used as the standard material for ^{13}C NMR. Owing to this *relative* definition, precise value of K_i^{orb} has become available, in addition to the improvement in the homogeneity of superconducting magnet and in the resolution and stability of frequency oscillator. For conventional metals, not only K_i^{orb} but also K_i^{spin} is observed due to the finite value of S_i, as seen from Eqs. (2-9a) and (2-12b). In many cases, since the Knight shift is larger than the chemical shift by the order of $2 \sim 3$ ($K_i^{spin} \gg K_i^{orb}$), the resultant NMR shift is equal to the Knight shift to a good approximation ($K_i \approx K_i^{spin}$). (For this reason, physicists prefer to call K_i as *Knight shift* instead of NMR frequency shift, and K_i^{spin} (K_i^{orb}) as *spin part* (*orbital part*) *of the Knight shift* instead of Knight shift (chemical shift).) Under this approximation, the "absolute" value of the Knight shift can be defined by using the gyromagnetic ratio in a table (whose error is within $\sim 10^{-5}$).

In the case of, for instance, the ^{89}Y NMR in a cuprate oxide superconductor $YBa_2Cu_3O_{6+x}$ or the ^{13}C- and ^{39}K-NMR in K_3C_{60}, the chemical shift is comparable to the Knight shift ($K_i^{orb} \sim K_i^{spin}$) mainly because the values of K_i^{core} are not negligible. Thus, in this thesis, we use the exact expression for the NMR shift defined by Eq. (2-12).

For conventional metals where the value of χ^{spin} remains finite, the magnetic hyperfine term $\mathcal{H}^{mag}$ in Eq. (2-7) (due to the additional local magnetic field other than $\boldsymbol{H}^{ext}$), which can be treated as a perturbation to the Zeeman term $\mathcal{H}^{Zeeman}$ (due to the applied field), is observed as a frequency *shift*. On the contrary, for *magnetic materials* where the time average of $\boldsymbol{S}$ is finite ($\langle \boldsymbol{S} \rangle_{time} \neq 0$), the $\mathcal{H}^{mag}$ term is dominant or comparable to the Zeeman term $\mathcal{H}^{Zeeman}$. In

this case, the magnetic resonance can be observed, and is usually done, under *zero magnetic field* ($\boldsymbol{H}^{ext} = 0$) because the internal magnetic field due to the ordered magnetic moment substitutes for the applied magnetic field. This is called *zero field resonance* [Gossard and Portis, 1959].

In general, as Eq. (2-12) indicates, both K_i^{spin} and K_i^{orb} are anisotropic due to the anisotropy in the corresponding magnetic hyperfine couplings. The anisotropy in A_i^{spin} (A_i^{orb}) stems from the presence of asymmetric p- or d-electron orbitals where the conduction (the valence) electrons reside. As a result, the observed NMR shift K_i (or, resonance frequency $(\omega^{res})_i$) is also anisotropic. If a single crystal is employed as a sample, a single NMR line is observed at the resonance frequency of $(\omega^{res})_x$, $(\omega^{res})_y$, and $(\omega^{res})_z$ by applying the external magnetic field in the x-, y-, and z- direction, respectively. On the other hand, in the case of a powder sample, instead of a single line, the spectrum has a finite width of $(\omega^{res})_x$ - $(\omega^{res})_z$ (here we assume $(\omega^{res})_x > (\omega^{res})_y > (\omega^{res})_z$), with two edges at $(\omega^{res})_x$ and $(\omega^{res})_z$, and a divergent intensity at $(\omega^{res})_y$. Between $(\omega^{res})_x$ and $(\omega^{res})_z$, the intensity is described as an elliptic function of ω [Slichter, 1989]. This line shape is called a *powder pattern* [Bloembergen and Rowland, 1953].

For the ^{13}C nuclei in K_3C_{60}, the local structure of a C_{60} molecule is, as seen from the nucleus length scale, regarded as an almost "planar segment" formed by two C-C bonds and one C=C bond, and the planar segments are randomly oriented with respect to the applied magnetic field. Thus, it is expected that the ^{13}C NMR spectra show powder patterns. Indeed, as will be shown in Chapter 5, the ^{13}C NMR spectra are well reproduced by powder patterns. For the ^{39}K nuclei in K_3C_{60}, on the other hand, the magnetic hyperfine couplings are considered to be isotropic, since the potassiums are located in the form of spherical ions between the C_{60} molecules. Thus, it is not the anisotropy in the magnetic hyperfine interaction $\mathcal{H}^{mag}$ but the electric interaction $\mathcal{H}^{el}$ that should be taken into account for the ^{39}K NMR in K_3C_{60}, because of the finite value of ^{39}Q.

Under the first order perturbation of the electric hyperfine interaction to both Zeeman and magnetic hyperfine interaction, i.e.,

$$\mathcal{H}^{el} \ll \mathcal{H}_0 \equiv \mathcal{H}^{Zeeman} + \mathcal{H}^{mag}, \tag{2-13}$$

Equation (2-6) gives us the eigenvalues of the total Hamiltonian which are expressed as

$$E_m = -\gamma_n \hbar H_i^{loc} m + [e^2qQ / 4I(2I-1)][(3\cos^2\theta - 1)/2][3m^2 - I(I+1)] \tag{2-14}$$

where m is the magnetic quantization number of the nucleus ($-I \le m \le I$), $\gamma_n H_i^{loc}$ (= $(\omega^{res})_i$) is the resonance frequency in the absence of the electric hyperfine interaction, and θ stands for the angle between the $\boldsymbol{H}_i^{loc}$ and the principal axis of the EFG. For the ^{39}K nuclei in K_3C_{60}, the condition of (2-13) holds due to the small amount of eq. The ^{39}K nulear energy diagram is shown in Fig. 2-1(a). In the case of $\theta = 0$ for simplicity, the presence of $\mathcal{H}^{el}$ raises the $m = \pm 3/2$ levels and lowers the $m = \pm 1/2$ levels by the same energy $\Delta^{el}(\theta = 0) = +e^2qQ/4$. The spectral absorption is illustrated in Fig. 2-1(b). Under the first order perturbation, it should be noted that the central $m = -1/2 \leftrightarrow +1/2$ transition is unaffected. The absorption line corresponding to the $m = -3/2 \leftrightarrow -1/2$ (to the $m = +3/2 \leftrightarrow +1/2$) transition appears at higher (lower) resonance frequency than the central absorption line. The change in the absorption spectrum caused by the electric hyperfine interaction is called *quadrupole splitting* or *eqQ splitting.* (The additional lines are named *eqQ satellite lines*, the number of which is $2I - 1$.) The difference in the resonance frequencies of the two satellite lines is $4\Delta^{el}(\theta = 0)/\hbar = +e^2qQ/\hbar$. For a powder sample, since the value of θ distributes randomly, the overall spectrum shows a powder pattern with divergences in the intensity at ω^{res} (the central line), $\omega^{res} \pm e^2qQ/4\hbar$ (the satellite lines for $\theta = \pi/2$), and edges at $\omega^{res} \pm e^2qQ/2\hbar$ (the satellite lines for $\theta = 0$). The effect of the random distribution of θ is referred to as *quadrupole broadening*.

Since the values of eq for the ^{39}K nuclei in K_3C_{60} are close to zero due to their high symmetry locations, it is expected that the electric interaction, if any, results in the quadrupole *broadening* without splitting clearly the central line. This is discussed in Chapter 6.

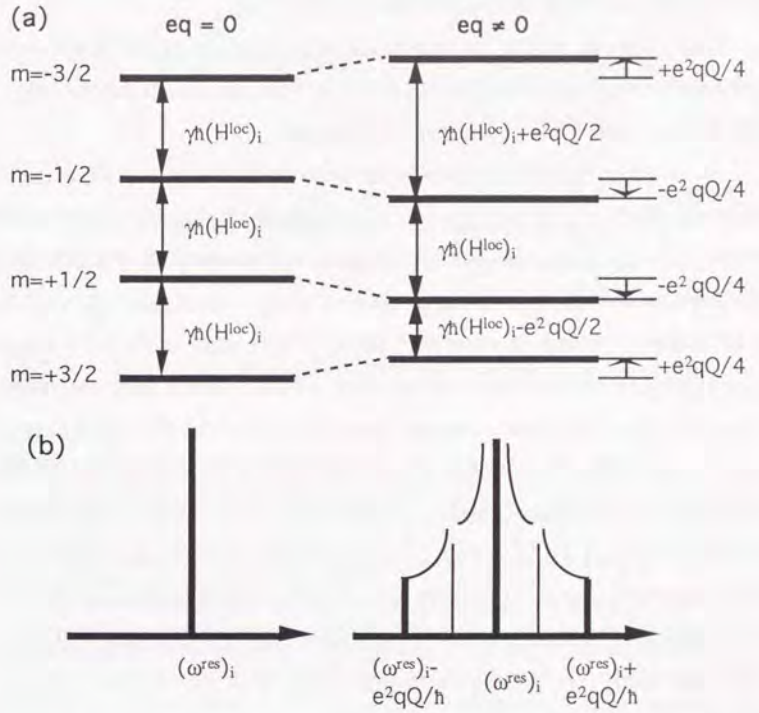

Fig. 2-1

(a) Energy diagram of a nucleus of spin $I = 3/2$ under a static magnetic field $(H_{loc})_i$. In the absence of electric interaction, the four levels are equally spaced, as shown in the left.
Under the first-order perturbation of the electric term to the Zeeman and magnetic terms, the $m = \pm 1/2$ (the $\pm 3/2$) levels are decreased (increased) by $e^2qQ/4$ for the $\theta = 0$ direction, as illustrated in the right.

(b) Energy spectrum in the absence of electric interaction (corresponding to the diagram of the left in (a)) shows a single resonance line at $(\omega^{res})_i$ ($\equiv \gamma(H_{loc})_i$).
In the presence of the electric term, three resonance lines (shown by bold lines) appear, as seen from the diagram of the right in (a). The resonance frequency of the center line is unchanged by the first-order perturbation. Two satellite lines appear above and below the center line. It should be noted that for a powder sample, since the electric term depends on θ, the resonance frequency of the $m = -3/2 \leftrightarrow -1/2$ (the $m = +1/2 \leftrightarrow +3/2$) transition ranges between $(\omega^{res})_i - e^2qQ/2\hbar$ and $(\omega^{res})_i + e^2qQ/\hbar$ ($(\omega^{res})_i - e^2qQ/\hbar$ and $(\omega^{res})_i + e^2qQ/2\hbar$), even in the absence of the distribution in the value of eq. The resultant powder pattern is illustrated by the thin curve. Two thin lines between the bold lines represent the resonances for the $\theta = \pi/2$ direction.

§2-3. Spin-Lattice Relaxation Time (T_1)

In this section, we discuss spin-lattice relaxation time (T_1) on those nuclei which possess spin one-half ($I = 1/2$), since the T_1 measurement is done only for the ^{13}C nucleus ($^{13}I = 1/2$) of the K_3C_{60} sample.

As shown in Fig. 2-2, the population of nuclear spins, which are at the thermal equilibrium of temperature T, is proportional to the Boltzmann factor $\exp(-\Delta_N/k_BT)$, where Δ_N is the energy difference in the two levels. The difference in the population at the two levels produces the net nuclear magnetic moment M_0. Irradiating a radio frequency (RF) pulse of the energy of Δ_N for a certain duration (typically of the order of μsec) results in raising the spin temperature to $T_{spin} = \infty$. The RF pulse is named *saturation pulse* and the spin system is called *saturated*. Since the nuclear spins are coupled to their environment other than themselves (the environment is called *lattice* in the NMR field) via the hyperfine couplings A_i^k (k = spin, VV, core) as mentioned in the previous section, the nuclear spin system will recover to the initial thermal equilibrium state by dissipating its energy. Since the net magnetization at time t after saturation (denoted as $M(t)$) for nuclei with spin one-half ($I = 1/2$) follows a single-exponential time evolution, there exists only one time constant in the recovery process. The time constant is called *spin-lattice relaxation time* T_1, namely,

$$M(t) = M_0 [1 - \exp(-t/T_1)]. \qquad (2\text{-}15)$$

In general, spin-lattice relaxation rate $1/T_1$ is described as [Moriya, 1963]

$$(1/T_1)_c^k = (\gamma_n^2 k_B T/\mu_B^2)[(A_a^k)^2 + (A_b^k)^2]\sum_q[\chi''(q, \omega_0)/\omega_0], \qquad (2\text{-}16)$$

where ω_0 is the resonance frequency, a, b, and c stand for the x-, y-, and z-axis. k represents "spin", "orb" or "core", and $\chi''(q, \omega_0)$ stands for the imaginary part of the generalized susceptibility expressed as

$$\chi''(q, \omega) = (\mu_B^2 \omega / k_B T) \int \langle\{S_q(t)S_{-q}(0)\}\rangle \cos(\omega t)\, dt. \qquad (2\text{-}17)$$

Equation (2-16) tells us that $1/T_1$ probes the low-frequency component ($\omega_0 \ll \omega$) of the wave-vector (q) summation of $\chi''(q, \omega_0)$. Equation (2-17) means that $\chi''(q, \omega)$ represents the auto-correlation function of time on the local magnetic

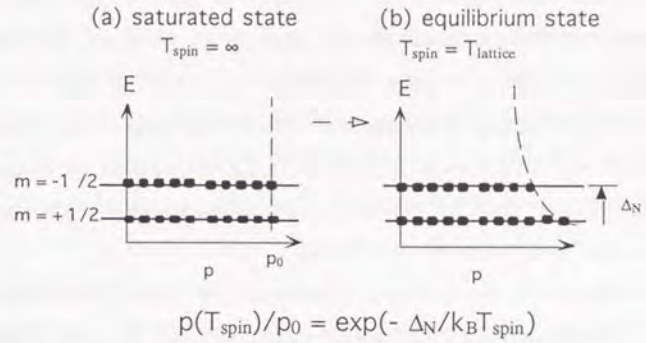

Fig. 2-2

Spin-lattice relaxation process in the case of two-energy levels ($I = 1/2$).

(a) Irradiating a saturation RF pulse of the energy of Δ_N makes the system saturated state ($T_{spin} = \infty$). On the Cartesian coordinates whose xy-plane is rotating around the z-axis (the external magnetic field H_0 is applied in the z-axis) at the resonance frequency, the z-component of the total nuclear magnetization M_z is zero in the case of $T_{spin} = \infty$, as illustrated in the left below.

(b) With a time constant (= spin-lattice relaxation time, T_1), the system will recover to the thermal equilibrium state ($T_{spin} = T_{lattice}$). In the equilibrium state, the value of M_z is maximum. However, it is to be noted that even in this state, close to half of the spins are *anti-parallel* to H_0, as seen from the population diagram. In other words, "high temperature approximation" is generally valid for nuclear spin systems ($\Delta_N \sim$ mK and $k_BT >$ ~K). During this process ($T_{lattice} < T_{spin} < \infty$), the value of M_z increases (i.e., the energy of the spin system decreases) via the fluctuation of the local magnetic field.

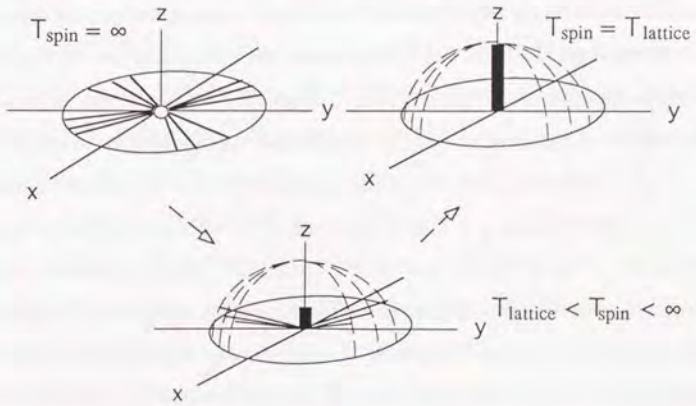

field. Thus, the energy of the nuclear spins is *dissipated* into the surrounding "lattice" by the *fluctuation* of the local magnetic field *perpendicular* to the quantization axis. Here it should be noted that Eqs. (2-16) and (2-17) hold quite generally *irrespective of the materials*, that is, for metals, superconductors, magnetic or nonmagnetic materials, and so forth. However, since the relations of $(1/T_1)_i^{spin} \gg (1/T_1)_i^{orb}$ and $(1/T_1)_i^{spin} \gg (1/T_1)_i^{core}$ hold in most cases, we neglect the $(1/T_1)_i^{orb}$ and $(1/T_1)_i^{core}$ terms in the presence of $(1/T_1)_i^{spin}$, and omit the superscript "spin" of the term hereafter.

By taking into account the electron - electron interaction under the random phase approximation (RPA), the relaxation rate in a Fermi liquid is expressed as [Moriya, 1963]

$$T_1T(K^{spin})^2 = (\hbar/4\pi k_B)(\gamma_e/\gamma_n)/K(\alpha), \tag{2-18a}$$

$$K(\alpha) = (1-\alpha)^2/\langle\{1 - \alpha[\chi_0(q,0)/\chi_0(0,0)]\}^2\rangle_{Fermi} \tag{2-18b}$$

$$\alpha = JN_0 \tag{2-18c}$$

where γ_e is the electron gyromagnetic ratio, J stands for exchange energy between the conduction electrons which is assumed to be *independent* of the wave-vector (q), and N_0 is the density of states. In Eq. (2-18b), $\chi_0(q,0)$ represents the q-dependent and static ($\omega = 0$) susceptibility in the absence of electron interaction, and the average $\langle ... \rangle_{Fermi}$ is taken over the q vectors connecting two points on the Fermi surface. In the case of $J = 0$, i.e., non-interacting Fermi *gas*, the value of $K(\alpha)$ is unity and Eq. (2-18a) is reduced to the so-called *Korringa relation*. In other words, the Korringa relation is corrected by the $K(\alpha)$ term which specifies the electron interaction. If the electron interaction is *ferromagnetic* (i.e., $\chi_0(q,0)$ is enhanced at $q \approx 0$), $K(\alpha)$ is *smaller* than unity. On the contrary, if $\chi_0(q,0)$ is enhanced at $q \approx Q$ (for instance, at around an *antiferromagnetic* wave vector), $K(\alpha)$ is *larger* than unity. Thus, $K(\alpha)$ is an important quantity which describes the electron interaction within the RPA treatment. In this thesis, we refer to Eq. (2-18) as the *modified* Korringa relation. It is to be noted that the relaxation rate is, as is seen from Eq. (2-18b), corrected by $\chi_0(q,0)$ at *finite*

value of q, whereas the Knight shift is enhanced by the factor of $(1 - \alpha)^{-1}$, the usual Stoner enhancement.

In using Eq. (2-18), we cannot be too careful on the following two points. First, the relation is applicable *only to* the case where the coupling between the nucleus and conduction electrons is *isotropic* ; $K^{spin} \equiv K_x^{spin} = K_y^{spin} = K_z^{spin}$, $(1/T_1) \equiv (1/T_1)_x = (1/T_1)_y = (1/T_1)_z$. To be more specific, it describes the relaxation process via *only* the Fermi contact hyperfine coupling A_{iso}^{spin}. In other words, it is *incorrect* to use the Korringa relation to those nuclei (such as ^{13}C, ^{17}O, $^{63/65}Cu$ *etc.*) which can possess conduction electrons on their p- or d-orbitals, since the relation does not take into account the relaxation process via anisotropic electron dipolar hyperfine couplings.

Second, it is also *incorrect* to regard "constancy of T_1T" directly as "Korringa relation", or as "an NMR evidence of a Fermi liquid". This argument is correct *if and only if* the isotropic Knight shift K^{spin} is T independent. Within the framework of a Fermi liquid, a T dependence of K^{spin}, if any, originates from a T-dependent density of states $N_0(T)$, as is seen from the relations of $K^{spin} \propto \chi^{spin}$ (Eq. (2-12b)) and $\chi^{spin} \propto N_0$. In this case, since the T_1T *does depend* on T, *the validity of a Korringa relation should be proved by the constancy of* $T_1T(K^{spin})^2$ *instead of* T_1T.

Quite generally, regardless of the relaxation mechanisms, the presence of anisotropy in the hyperfine couplings (AHC) causes the anisotropy in the relaxation rate, as is seen from Eq. (2-16). If the hyperfine couplings (where k = spin) are axially symmetric, i.e., $A_x^{spin} = A_y^{spin} \equiv A_{x/y}^{spin} \neq A_z^{spin}$, the anisotropic $(1/T_1)_i$ is, from Eq. (2-16), expressed as

$$(1/T_1)_z \propto 2\,(A_{x/y}^{spin})^2, \tag{2-19a}$$

$$(1/T_1)_{x/y} \propto [(A_z^{spin})^2 + (A_{x/y}^{spin})^2]. \tag{2-19b}$$

If the sample is a single crystal, one can separately obtain the value of $(1/T_1)_z$ ($(1/T_1)_{x/y}$) by applying the external field perpendicular to the xy-plane, i.e., H^{ext} // z-axis (parallel to the xy-plane, i.e., $H^{ext} \perp z$-axis), and, for $I = 1/2$, the nuclear

magnetization shows a single-exponential time evolution, Eq. (2-15). On the contrary, this is not the case for a powder sample, since the z-axis of each crystalline in the powder has random direction to H^{ext}. As the result, the magnetization does not satisfy Eq. (2-15) but instead shows a *non-single* exponential recovery (NSER). In this case, it should be noted that the NSER is observed even for the nuclei of *magnetically single sites*, since the difference between $(1/T_1)_z$ and $(1/T_1)_{x/y}$ comes from *only* the AHC for the *same* dynamical susceptibility $\chi''(q, \omega)$, as seen from Eq. (2-16). In other words, in a powder sample, the AHC causes an NSER as well as an asymmetric line shape (i.e., a powder pattern), *even in the absence of inequivalent sites*. Recently, Kawamoto *et al.* have succeeded in extending the modified Korringa relation to this case [Kawamoto *et al.*, 1995a]. It is expressed as

$$T_1{}^S T(K_{iso}{}^{spin})^2 = S / [K(\alpha)\{1 + 2(A_{ax}{}^{spin}/A_{iso}{}^{spin})^2\}], \quad (2\text{-}20a)$$

where $T_1{}^S$ is given by the initial slope of the magnetization recovery, S is the Korringa constant ($= (\hbar/4\pi k_B)(\gamma_e/\gamma_n)$). The hyperfine couplings are defined as

$$A_{iso}{}^{spin} = [\ 2(A_{x/y}{}^{spin}) + (A_z{}^{spin})\ ]/3,$$
$$A_{ax}{}^{spin} = [\ (A_z{}^{spin}) - (A_{x/y}{}^{spin})\ ]/3. \quad (2\text{-}20b)$$

As discussed in the previous section, a C_{60} molecule in K_3C_{60} is *effectively* regarded as a *powder sample* under an external magnetic field, if the molecular motion is frozen and there exists the AHC at the ^{13}C nucleus. Thus, if the ^{13}C NMR spectrum in K_3C_{60} shows an asymmetric powder pattern at low T, it is expected that the ^{13}C nuclear magnetization shows an NSER and that the validity of the Fermi-liquid picture (where the electron interaction is treated within the RPA) should be tested whether the *extended* Korringa relation Eq. (2-20) holds or not. This will be discussed in Chapter 5.

From a physical viewpoint, Eq. (2-20a) means that the experimentally observed $1/T_1{}^S$ is *increased* by the factor of $[1 + 2(A_{ax}{}^{spin}/A_{iso}{}^{spin})^2]$ which comes from the AHC, compared to the "*isotropic* $1/T_1$" which could result from the "fictitious" situation where *only* $A_{ax}{}^{spin}$ is 0 *without* changing the value of the dynamical

susceptibility $\chi''(q, \omega)$ *nor* $A_{iso}{}^{spin}$ at the same T. It is interesting to note that, as will be discussed in Chapter 5, this situation is actually realized in the C_{60} molecule at high T where the correlation rate $1/\tau_M$ of the molecular motion is sufficiently fast.

Spin-lattice relaxation which obeys the Korringa relation in the normal state behaves quite differently in the superconducting state. The relaxation rate shows two characteristic T dependences.

First, the so-called *coherence peak* is observed. Specifically, the values of $1/T_1T$ just below T_C are enhanced to those just above T_C. The coherence peak comes from *both* the piling up of the density of states which results from the formation of a superconducting gap Δ , *and* from a "coherence factor" which describes the development of paring. The coherence factor in the case of NMR *enhances* the relaxation rate, whereas that in the case of ultrasonic attenuation *reduces* the relaxation rate [Tinkham, 1975].

Well below T_C, the nuclear spin-lattice relaxation is not caused by the direct excitation of the quasi particles from the Fermi sea across the gap Δ, since the energy which the nuclear spins dissipate is much smaller than the energy gap. Instead, it is the *thermally* excited quasi particles that scatter the nuclei. This process contributes to the relaxation. As a result, the relaxation rate is proportional to $\exp(-\Delta/k_BT)$ because the population of the excited quasi particles depend on T as $\exp(-\Delta/k_BT)$.

The suppression of the coherence peak, which has been actually observed, is ascribed to the *finite lifetime* of the quasi particles (such as electron- phonon strong coupling or short mean- free path) or to the anisotropy in the superconducting gap [MacLaughlin, 1976].

For cuprate oxides or heavy fermion superconductors, a quite different T dependence from that mentioned above is observed below T_C, i.e., $1/T_1 \propto T^n$ ($n = 3 \sim 5$) *without* a coherence peak. This behavior is considered to come from pairing states other than the BCS s-wave singlet.

Chapter 3. Motivation of This Study

§3-1. NMR Reports by Other Groups (~ 1994) --- findings and problems

Prior to this study, other groups reported on NMR studies of A_3C_{60}. In this section, we briefly summarize the findings and the problems of those reports which focused on the *electronic* properties of A_3C_{60}.

[1] ^{13}C NMR ----- spectra

(a) above T_C

In the precedent reports on the ^{13}C NMR spectra of K_3C_{60}, both the Bell and the Orsay group published almost symmetrical line shapes, as shown in Fig. 3-1(a) [Tycko *et al.*, 1992; Holczer *et al.*, 1993]. However, *no physical information* on the electronic states were derived from their spectra, let alone the Knight shifts. It is presumed that this is partly because the ^{13}C NMR signal of substantial amount of unreacted pristine C_{60} is superimposed on the signal of K_3C_{60} , as shown in Fig. 3-1(b) [Yoshinari *et al*, 1993], and partly because they expected the contribution of plural factors to the line shapes. To be specific on the latter, it was proposed that there existed the local density of states (LDOS) at the carbon sites on a C_{60} molecule, corresponding to the crystallographically inequivalent sites at low T where the molecular motion was frozen [Holczer *et al.*, 1993; Antropov *et al.*, 1993]. The LDOS, in addition to the anisotropy in the ^{13}C NMR frequency shifts, was expected to contribute to the line shapes. The author suspects that they attributed the integration of these factors to the apparent almost symmetrical line shapes.

(b) below T_C

Since A_3C_{60} is a type II superconductor, the NMR measurements are done in a vortex state. In this case, observed NMR frequency shift K is contributed *not*

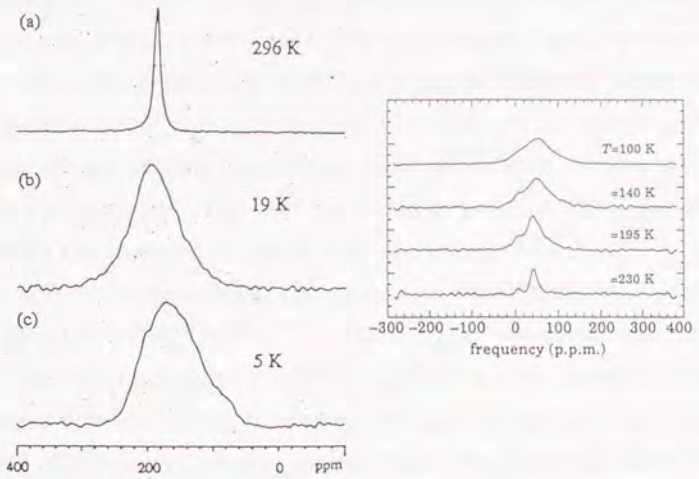

Fig. 3-1(a)

^{13}C NMR spectra of K_3C_{60} published by the Bell group (left) [Tycko *et al.*, 1992] and those by the Orsay group (right) [Holczer *et al.*, 1993].
No physical information on the electronic states of K_3C_{60} was derived from the line shapes, since no quantitative analyses, including the Knight shifts, were obtained in their report.

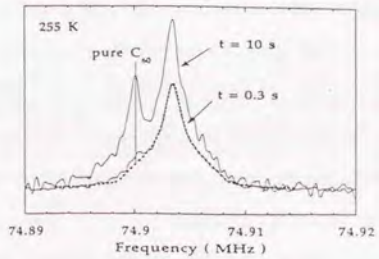

Fig. 3-1(b)

^{13}C NMR spectra of K_3C_{60} at 255 K, reported by the Orsay group [Yoshinari *et al.*, 1993]. The signal at ~74.9 MHz (= ~140 ppm, in reference to the standard material of TMS) which grows at longer pulse repetition time (10 sec) is assigned to the signal of unreacted pristine C_{60}.

only by the Knight shift K^{spin} and the chemical shift K^{orb}, *but also* by the diamagnetism due to superconductivity $\Delta H/H$. This is one of the reasons why the T dependences of the Knight shift K^{spin} had not been reported. However, as shown in Fig. 3-2, the Ohio State University group succeeded in obtaining the T dependence of the spin susceptibility χ^{spin} in the superconducting state by their "multi-nucleus" method [Stenger *et al.*, 1993]: they first observed the NMR frequency shift at the Rb-, Cs-, and C-sites on Rb_2CsC_{60}, which is denoted as ^{87}K, ^{133}K, and ^{13}K, respectively. Then, they used the fact that the diamagnetic contribution $\Delta H/H$ is *cancelled out* in the "subtracted" NMR shifts such as $^{87}K(T) - {}^{133}K(T)$. It is to be noted that, even though the corresponding hyperfine couplings $^{87}A^{spin}$ and $^{133}A^{spin}$ are unknown, the T-dependent $\chi^{spin}(T)$ can be obtained from the relation $^{87}K(T) - {}^{133}K(T) = (^{87}A^{spin} - {}^{133}A^{spin})\chi^{spin}(T) + (^{87}K^{orb} - {}^{133}K^{orb})$, where the value of $(^{87}K^{orb} - {}^{133}K^{orb})$ is T independent. The Ohio State University group argued that the T dependence of $\chi^{spin}(T)$ was well explained by the Yosida function, i.e., the BCS weak-coupling prediction [Yosida, 1958].

[2] ^{13}C NMR ----- T_1

(a) recovery data

As already mentioned in Section 2-3, the T_1-recovery process for ^{13}C nucleus shows a single-exponential time evolution *in principle*. However, the Bell group reported that the recovery data at the ^{13}C sites of both K_3C_{60} and Rb_3C_{60} showed non-single exponential recoveries (NSER), and that *at all T* [Tycko *et al.*, 1992]. Later, the Orsay group extensively studied the recovery shape of K_3C_{60} [Holczer *et al.*, 1993]. In their study, as shown in Fig. 3-3, they argued that the ^{13}C recovery showed a single-exponential function at $T > 250$ K, and the NSER at $T < 250$ K. In addition, they reported the recovery shape at low T (< 100 K) were successfully reproduced by a three-exponential function corresponding to the proposed LDOS. In the fitting, they assumed that the T_1-relaxation was solely caused by the electron dipolar field, using the theoretical calculation by the Max-Planck group which was based on the local density

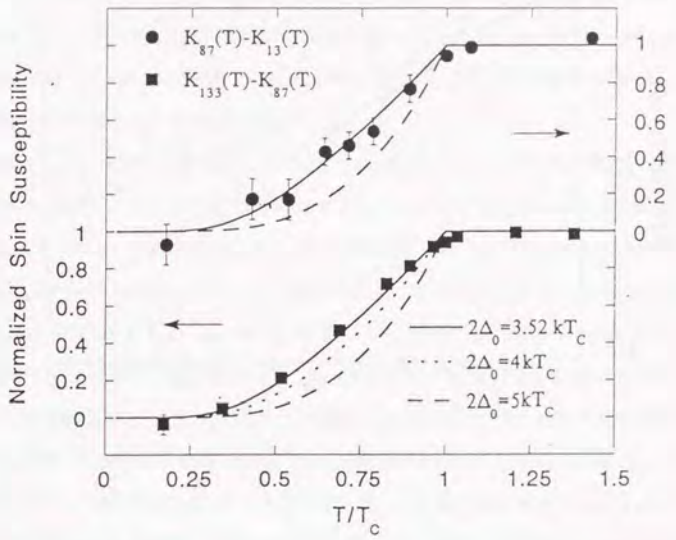

Fig. 3-2

NMR shift differences $(^{87}K - {}^{13}K)$ for Rb_3C_{60} (filled circles) and $(^{133}K - {}^{87}K)$ for Rb_2CsC_{60} (filled squares) versus T/T_C, published by the Ohio State University group [Stenger et al., 1993]. Since these "subtracted" NMR shifts, where the diamagnetic contributions are cancelled out, are proportional to the static spin susceptibility χ^{spin}, the figure shows that their superconductivity is well reproduced by the BCS weak coupling.

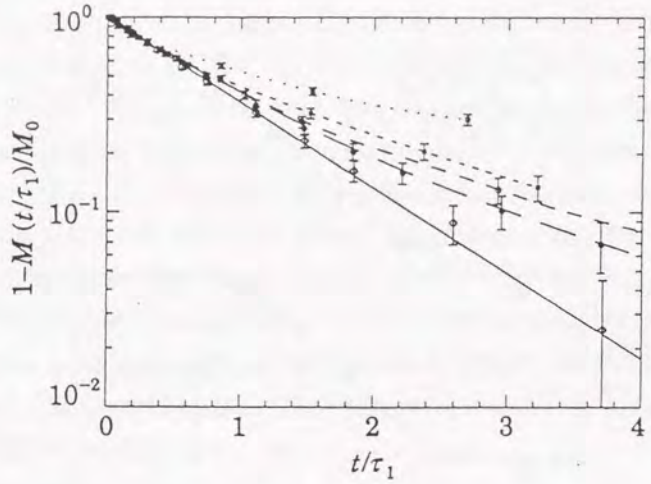

Fig. 3-3
^{13}C NMR spin-lattice relaxation processes of K_3C_{60}, published by the Orsay group [Holczer *et al.*, 1993]. They found that the recovery shapes at $T > 250$ K show single-exponentials and that those at 100 K $< T <$ 250 K deviate from single-exponentials and depend on T. Below $T < 100$ K, they found that the non-single exponential recoveries do not depend on T. In the figure, the open squares represent the data at 335 K, closed circles at 96 K, open circles at 22.4 K, and closed squares at 7.75 K.

approximation [Antropov *et al.*, 1993]. Here it should be noted that the reports are different between the Bell group and the Orsay group in the following two points. First, the Orsay group argued that the recovery shape at high T (> 250 K) showed a single-exponential time evolution, but the Bell group insisted on the NSER. Second, the Bell group reported that the origin of the NSER is not clear, whereas the Orsay group attributed it to the LDOS. The Tokyo Metropolitan University group reported later the same results and the analyses as those of the Orsay group on the recovery data for only $T_C < T <$ 77 K [Maniwa *et al.*, 1994].

(b) Hebel-Slichter coherence peak

Regarding the mechanisms of superconductivity, it does count whether a coherence peak exists or not, because the presence of a coherence peak evidences the *s*-wave Cooper pairing, as mentioned in Section 2-3. However, the precedent NMR reports were controversial: the Bell group was the first that published the T dependence of $1/T_1T$ below T_C at the ^{13}C sites for their K_3C_{60} and Rb_3C_{60} [Tycko *et al.*, 1992]. In their study, as shown in Fig. 3-4(a), they argued that the coherence peak was *clearly absent* without specifying the origin of the absence. It should be noted that this result is totally different from the μSR report where a clear-cut coherence peak is observed and the T dependence is well reproduced by the BCS weak-coupling theory [Kiefl *et al.*, 1993]. On the contrary, in the published data by the Orsay group (Fig. 3-4(b)), one can see a T dependence of $1/T_1T$ which is regarded as a coherence peak [Holczer *et al.*, 1993]. However, to date, they have published no comments on the "apparent" coherence peak.

Regarding the superconducting energy gap, the Bell group reported that the reduced gap $2\Delta/k_BT_C$ is 3.0 (4.1) for their K_3C_{60} (Rb_3C_{60}), based on the confirmation of the activation type T dependences of $1/T_1T$ at low T (< 10 K) [Tycko *et al.*, 1992].

[3] ^{13}C hyperfine coupling

There were no reports on the ^{13}C NMR Knight shifts from the analyses on the line shapes in the normal state, as mentioned above. In addition, it is difficult to

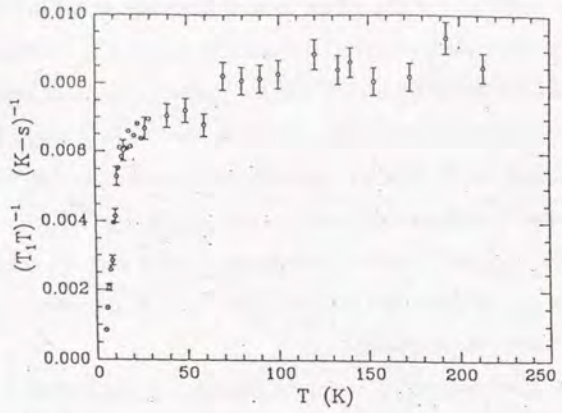

Fig. 3-4(a)

T dependence of $1/T_1T$ of the ^{13}C NMR in K_3C_{60}, published by the Bell group [Tycko *et al.*, 1992]. Below T_C, a Hebel-Slichter coherence peak, which is expected for a BCS *s*-wave superconductor, is *clearly absent*. They did not specify the origin of the absence nor analyzed the T dependence of $1/T_1T$.

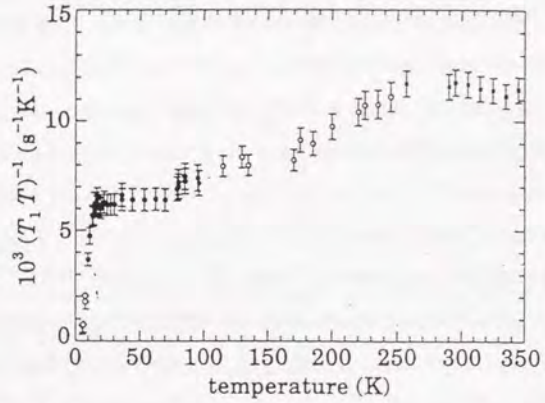

Fig. 3-4(b)

T dependence of $1/T_1T$ of the ^{13}C NMR in K_3C_{60}, published by the Orsay group [Holczer *et al.*, 1993]. Below 250 K where the recovery shapes deviate from a single-exponential function, the "T_1" values are represented by the average values. In the normal state, the values of $1/T_1T$ decrease with decreasing T. Below T_C, one can see a T dependence which is regarded as a Hebel-Slichter coherence peak, but they have not commented on the "apparent" coherence peak to date.

obtain reliable values of bulk susceptibility χ, partly because the observed magnetization is dominated by the T-dependent magnetization of the Pyrex glass (which seals the sample), and partly because the reported spin susceptibility showed upturns toward T_C, probably due to the existence of paramagnetic impurity phases [Wong *et al.*, 1992; Ramirez *et al.*, 1992b]. In general, hyperfine couplings are obtained experimentally by the so-called "K-χ plot" [Clogston *et al.*, 1964]. However, this is impossible since neither the Knight shifts nor the susceptibility was reliable. Therefore, the Bell group was the first to calculated the ^{13}C hyperfine coupling [Tycko *et al.*, 1991b]. This calculation was performed in order to obtain the density of states from the T_1 measurements alone, motivated by their observation of constant-T_1T at high T (140 K < T < 360 K). In their study, they used unrestricted Hartree-Fock approximation and concluded that the ^{13}C hyperfine coupling was dominated by the *isotropic* Fermi contact terms, including the core-polarized ones.

Contrary to the result by the Bell group, the Max-Planck group later reported that the electron dipolar field dominated the ^{13}C hyperfine coupling, based on the local density approximation (LDA) [Antropov *et al.*, 1993]. However, this controversial on theoretical calculation should be solved experimentally, because it so happens that the accuracy of the approximation changes *qualitatively* the contribution of the Fermi contact (i.e., on the nucleus) hyperfine coupling.

§3-2. Motivation of This Study

As mentioned above, the precedent NMR reports had been controversial, and contradicted other spectroscopic results such as scanning tunneling microscope [Zhang *et al.*, 1991], optical conductivity [Degiorgi *et al.*, 1992], and μSR [Kiefl *et al.*, 1993]. Although the molecular *motion* had been studied extensively [Yoshinari *et al.*, 1993], the precedent NMR reports had derived little information on the *electronic* properties of A_3C_{60}. In the opinion of the author, the only exception is the finding that $\chi^{spin}(T)$ below T_C is well explained

by the BCS weak-coupling prediction [Stenger *et al.*, 1993]. This situation is rather surprising, since it is well known that NMR has been applied to clarify the electronic states of the heavy fermions and the cuprate oxides [Pennington and Slichter, 1990] as well as to confirm the BCS theory [MacLaughlin, 1976]. The controversial NMR reports by 1994 can possibly be caused by the following three factors.

First, the sample quality: the advantages of NMR measurements stem from the fact they can give both static and dynamical information on the electronic states from a *microscopic* point of view (namely, the information is site-specific, as in the case for the studies of cuprate oxides). At the same time, however, this means that the NMR results can be misleading, especially when the sample contains *extrinsic* phases exactly because the obtained information is site-specific. Second, the accuracy of the measurements: in general, the NMR signal is weak due to the small value of a nuclear magnetization, which forces us to average the weak signals substantially. This means that insufficient averaging and/or the drift of the spectrometer during the averaging can cause misled experimental results. Third, the way of analyzing the obtained data: the analyses should be performed on a *consistent* physical picture. For example, a picture that explains the NSER in the T_1-process of the ^{13}C NMR should reproduce the line shapes at the same *T as well.*

In the present study, we have done the prescriptions to the above mentioned problems: first, we have used a good quality sample. One of the reason we have chosen K_3C_{60} despite its lowest T_C among A_3C_{60} is that K_3C_{60} is considered to be of the best quality, as typically shown by the sharpest superconducting transition and the largest volume fraction of superconductivity shielding. Indeed, we have confirmed from the ^{13}C NMR spectra that our sample does not contain the unreacted pristine C_{60}. In addition, it is confirmed qualitatively that the bulk susceptibility above T_C does not show the upturn toward T_C. Second, we have tried to obtain precise data by making the use of our knowledge on NMR

measurements as well as improving the spectrometer, although this forced us to spend much time. Third, we analyzed the obtained data systematically: for example, we have successfully proved that *both* the T_1-recovery shape of the ^{13}C NMR at high T (at low T) *and* the symmetrical (asymmetric) line shapes are *qualitatively* reproduced by the anisotropy in the ^{13}C hyperfine coupling.

"Based on these prescriptions, we give an answer to the controversial situation, thereby we deduce a consistent physical picture on the electronic states of K_3C_{60}."

This is the purpose of the present study.

The names of the game of the present thesis are as follows:

[1] Is the K_3C_{60} superconductivity explained by the framework of the BCS theory? : Is the electronic states in the normal state a Fermi liquid? Does the superconducting energy gap show an *s*-wave symmetry? How large is the superconducting gap? Are the Cooper pairs phonon-mediated?

[2] What are the electronic states on the C_{60} molecule like? : Is the value of $1/T_1$ enhanced by electron interaction as in the case of the cuprate oxides? Which is dominant to the carbon hyperfine coupling, isotropic Fermi contact one or anisotropic dipolar one?

[3] Is there any difference in the electronic states between the carbon sites and the potassium sites?

[4] Why is the T_C of K_3C_{60} so high?

In an attempt to give answers to these questions, we obtained precise ^{13}C spin-lattice relaxation time at low temperatures where the C_{60} motion is frozen, as well as highly resoluted ^{13}C- and ^{39}K-NMR spectra below room temperature. In this thesis, by analyzing them systematically, a consistent physical picture to the electronic properties of K_3C_{60} superconductor will be given.

Chapter 4. Experimental Procedures

§4-1. Sample Preparation

The K_3C_{60} sample used in this study was synthesized at Department of Physics & Texas Center for Superconductivity, the University of Houston in the United States of America. The sample was prepared as follows: commercially obtained C_{60} was purified by the standard chromatographic method and by filtration in order to remove undissolved graphite, C_{70}, and other higher fullerenes. The superconducting K_3C_{60} sample was synthesized by reacting the purified C_{60} with potassium (99.95 %, Alfa Aesar) in the stoichiometric composition of $K:C_{60} = 3:1$ in a quartz tube sealed in vacuum at 200 °C for 12 hours until all the potassium was absorbed by the purified C_{60}. The material was then annealed at 250 °C for another 24 hours. The amount of the obtained sample is about 50 mg. Since C_{60} was commercially obtained, ^{13}C in our sample is naturally abundant. The T_C onset, determined by susceptibility measurement under 2 Oe after zero-field cooled, is 19.4 K. The superconducting shielding fraction is 50 % in comparison to that of standard niobium metal. Reliable value of bulk spin susceptibility χ^{spin} is not available above T_C, due to the larger magnetization of the Pyrex glass that seals the sample. Nevertheless, we observed the qualitative behavior that χ^{spin} decreases with decreasing T by subtracting the Pyrex magnetization. In other words, no upturn in χ^{spin} is observed toward T_C with lowering T, unlike the $\chi^{spin}(T)$ behavior in the normal state of A_3C_{60} samples reported previously [Wong *et al.*, 1992; Ramirez *et al.*, 1992b]. In addition, as is discussed in Chapter 5, the ^{13}C NMR study revealed that our sample does not contain the unreacted pristine C_{60} unlike the samples of other groups [Yoshinari *et al.*, 1993]. Thus, our sample is of better quality in the absence of upturn in χ^{spin} and of the unreacted pristine C_{60}.

§4-2. Spectrometer

The pulsed-NMR spectrometer used for the present study is based on that of Prof. Yasuoka's laboratory at ISSP, the University of Tokyo (Tokyo, Japan), and has been built and modified at NTT Basic Research Laboratories by the author since 1990 with the help of Dr. A. Matsuda. As seen from the typical block diagram of Fig. 4-1(a), we employed phase sensitive detection (PSD). This enables one to obtain precise data by averaging very weak signals substantially (In most cases of the present study, the ^{13}C- and ^{39}K-signal-to-noise ratio (S/N) was less than unity). The spectrometer is controlled by the personal computer (HP382) through GPIB cables using programs originally written by Dr. A. Matsuda and modified by the author. These programs help one to run the spectrometer easily with parameters on time, frequency and so forth. In addition to controlling the devices, the personal computer receives the averaged signals from signal storages (IWATSU DM2350 and SM2100C) and processes the data by fast Fourier transformation or by obtaining spin-lattice relaxation recovery data.

The PSD requires two radio frequency (RF) channels and the detection is optimized by changing the difference in their phases. In usual cases, the RF delay lines are used for controlling the phase difference in the two channels as a *phase shifter*. In our case, we employed a two-channel RF synthesizer (HP3326A) instead. This enabled us not only to obtain a highly stable phase difference for long time measurements but also to control and reproduce it digitally by the computer. However, the maximum frequency which HP3326A generates is 13 MHz. Therefore, as shown in Fig. 4-1(b), a desired frequency more than 13 MHz is obtained by combining the frequency generated by HP3326A (13 MHz) and that by HP8657B (HP8656B) for the "main channel" (for the "reference channel"). The frequencies are combined by double balanced mixers and the resultant side-band frequencies are cut-off by band-pass filters (Tamagawa-Denshi Tunable Filter VVF-134) which are made to our order.

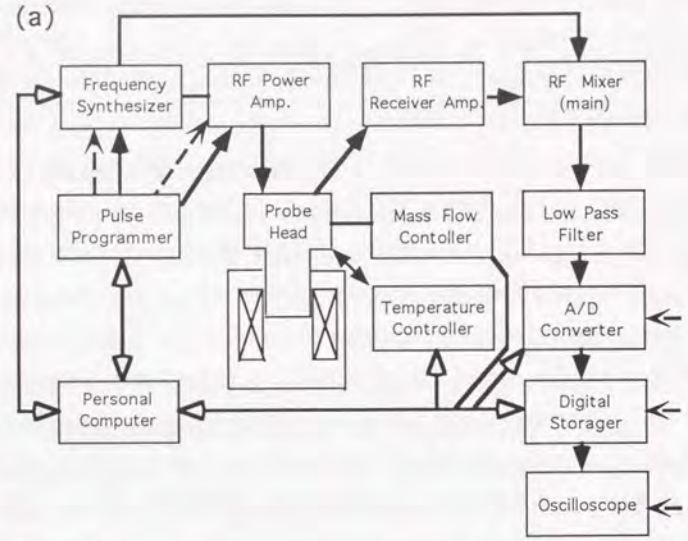

Fig. 4-1

(a) Typical block diagram of the spectrometer. Solid line with solid head indicates the signal input / output. Most components are controlled by a personal computer. The GPIB command input / outputs are represented by a solid line with an open head at both ends. Since the NMR measurements are done by pulsed method, the trigger pulses are needed. The trigger, produced by the pulse programmer, is put in to the RF synthesizer, the RF power amplifier, the A/D converter, the digital storage, and the oscilloscope. The trigger pulses are shown by a broken line with a solid arrow.

(b) For the stability and accuracy in the phase difference between the "main channel" and the "reference channel", the phase is controlled by a two channel RF synthesizer (HP3326A). A desired RF is generated by double balanced mixers and band pass filters, as shown below. The RF's are given by three synthesizers (HP8657B, 8656B, and 3326A) whose time base are governed by a highly-resoluted and highly-stable oscillator (HP option001).

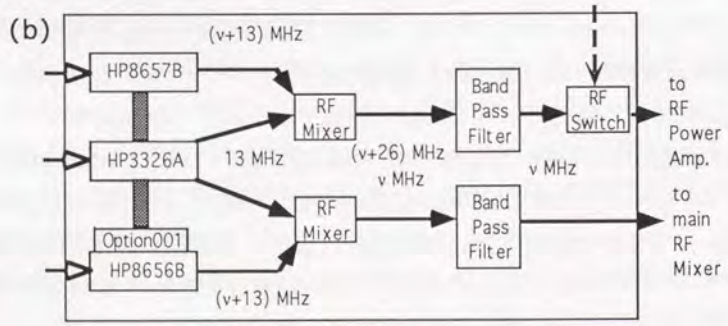

A desired T is obtained by cooling the sample with the helium gas flow in a cryostat and, at the same time, by heating the sample through a wire wound on a surface of a copper can which shields the resonance circuit electromagnetically. The sample T is monitored by a AuFe Chromel thermocouple sensor which is calibrated at both 77 K and 4.2 K after it is equipped to the probe. The sensor, which is thermally anchored to the ground of the resonance circuit, is touched on the sample coil in order to avoid the T gradient between the sample and the sensor. However, this results in picking up the electromagnetic noise from outside the can though the sensor to the NMR pick-up coil. Thus, we attached a home-made passive noise filter at the top of the probe to eliminate the noise. The flow of helium gas for the cooling is obtained by a mass-flow controller (Ohkura Electronic MF5041A). Based on the monitored T, the desired T, and the parameters input from the personal computer, the T controller (Lake Shore DRC-91C) produces the suitable electric current for the heater (the wire on the can). As a result, the desired T is controlled within the error of $\pm$ 0.1 K.

In order to obtain better S/N, we tried to match the impedance of the resonance circuit by making the use of a network analyzer (HP8752A). Although our resonance circuit, as shown in Fig. 4-2, is not equipped with two variable capacitors for perfect matching, we have confirmed that the impedance is matched satisfactory: specifically, its imaginary part is zero and its real part is 40~60 Ω in many cases (The spectrometer is 50 Ω-impedance type). The typical sensitivity of our spectrometer is 0.1 μV.

In addition to the above mentioned modifications by the author to the NMR spectrometer for the studies of solid state physics (denoted as *broadband use* hereafter), we have done extra upgrades for the study of the K_3C_{60} fulleride. First, the resolution of the spectrometer is improved, since the widths of the ^{13}C- and ^{39}K-NMR spectra of fullerides are by the orders of 1~3 smaller than those of usual metals. By employing a highly homogeneous superconducting magnet (Oxford 300/89), we achieved a resolution of 0.2 ppm. This is ~50

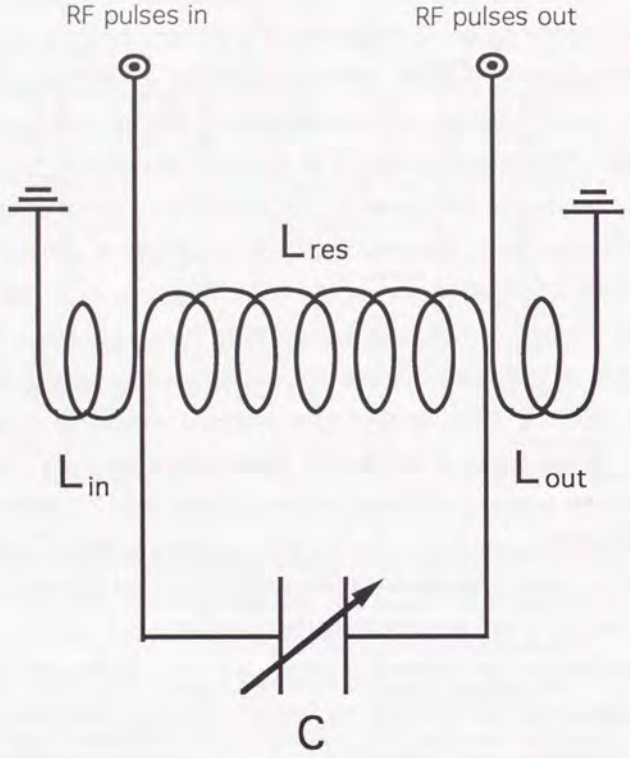

Fig. 4-2

Resonance circuit used in the present NMR study. Although it is impossible to match the impedance of the circuit at an arbitrary frequency in principle, it was confirmed by using a network analyzer that the impedance is matched satisfactorily in practice; its imaginary part is 0 Ω and the real part is 40 ~60 Ω, at both frequencies of ~70 MHz (for the ^{13}C NMR) and ~14 MHz (for the ^{39}K NMR).
RF pulses are put in from the inductor L_{in}, which is coupled to the resonance coil L_{res}. Output signal from the nuclei in concern is picked up by the inductor L_{out}. The three inductors are wound on a cylinder and electrically insulated from each other in order to avoid arching between L_{in} and L_{res}, and between L_{res} and L_{out}. The material for the insulation is glass-paste (epoxy) for the ^{13}C NMR (for the ^{39}K NMR) which does not contain carbon (potassium) nuclei. The better the impedance is matched, the more likely the aching happens at the variable capacitor. Thus, a method, which was invented by the author and is in appliance for a patent, is prescribed for the insulation.

times better than that for the broadband use (~10 ppm). Second, in addition to the homogeneity, it is indispensable to improve the stability since the measurement at a fixed T takes very long time for precise data (one hour at shortest and a few weeks at longest). The required stability is, however, not achieved by employing the Oxford 300/89 magnet alone, although its magnetic field is more stable than 0.1 ppm/day. This is because the frequency of the oscillator (HP 8656B/8657B) depends on the room temperature substantially (2 ppm/5 °C), which is a problem for the present study. One solution is to control the room temperature within ±1 °C. However, this is found to be insufficient, particularly for the measurements of the ^{13}C-NMR T_1 at higher T or the ^{39}K-NMR spectra because of the sharpness of the line shapes. Thus, we employed a highly stable and T compensated oscillator (HP8656B with Option 001). As a result, the spectrometer achieved a stability (better than 0.1 ppm/day) and a homogeneity (better than 0.2 ppm) which were found to be sufficient for the present study.

§4-3. ^{13}C and ^{39}K NMR Measurements

The K_3C_{60} sample synthesized at Texas was carried to us in an ampule made of Pyrex glass (about 10 cm) with inert helium gas. Since the static magnetic field is applied vertically in the case of our spectrometer, the sample coil should be placed horizontally in principle. However, the accessible diameter of our NMR probe is 35 mm. Therefore, we had to transfer the sample into another tube which could be placed in our NMR probe. The procedures for the transfer were done very carefully by a skilled chemist Dr. M. Fujiki in our laboratory, using a grove box when the sample was out of the tube. This is because exposing the sample to air or moisture immediately changes the properties of the sample in addition to destroying its superconductivity. The procedures are as follows: one of the edges of a newly cut Pyrex tube was sealed and then bent into an L-shape. The prepared tube was dried in a grove box for 24 hours at 200 °C in order to purge moisture, oxygen, and other gases adsorbed on the

surface of the tube. The K_3C_{60} powder was extracted by cutting the ampule from Texas and then put into the prepared L-shaped tube. Then, the sample was sealed completely in a vacuum by closing the other edge of the tube. Hereafter, all the ^{13}C- and ^{39}K-NMR measurements were performed using the sample sealed in this L-shaped Pyrex tube.

Although the sample coil should be placed horizontally in principle in the case of our spectrometer, we gave the coil a slope about 10 degree from the horizontal direction in order to locate the sample powder in the center of the coil. This resulted in obtaining higher homogeneity, better S/N, and reproducibility in the measurements.

In the case of our resonance circuit, as shown in Fig. 4-2, the better the impedance is matched, the higher is the possibility of arching *between* the *resonance* inductor, which is coupled to the capacitor and denoted as L_{res} in the figure, *and* the *input* or *pick-up* inductor, L_{in} or L_{out} in the figure. Then, molding the inductors with insulating materials is inevitable. In order to avoid picking up the NMR signals from the materials of the coil, it is required that the sample coil (not only the inductors but also the materials for the insulation) should not include the same nuclei as contained in the sample. For ^{39}K NMR study, we used an epoxy (Ciba-Geigy Ltd., Rapid Araldite) as the insulator because the constituents are mainly proton and carbon, free from potassium. In the case of ^{13}C NMR study, however, we are not allow to use epoxies since they contain so many carbon nuclei. Thus, the sample coil was made exclusively of carbon-free materials for ourselves. The process is as follows: first, we prepared a cylinder (the length is 25 mm and the diameter is 5 mm) made of Macor (no carbon included). On the surface of the cylinder, we craved a ditch so that we can wind easily and firmly the Ag-wires for the inductors. Instead of epoxies, we insulated the wound Ag-wires with glass paste (Tanaka Kikinzoku LS- 402). Although the paste needs to be molded in a furnace firmly, we had to dry it beforehand to the extent that it does not melt down in the furnace because of its rather low

viscosity. Thus, the sample coil painted with the glass paste on the wound Ag-wires was dried by the radiation heat of a 500-W infrared lamp, by rotating the coil in roughly horizontal direction. This pre-drying process was repeated several times before molding the paste in the furnace. In addition, the molding process in the furnace was done several times in order to insulate the inductors of the sample coil sufficiently. The molded glass paste is confirmed to be proof of heat cycling. It is to be noted that the prepared carbon-free sample coil should not be used for ^{39}K NMR study, because potassium is one of the constituents of the glass paste.

^{13}C- and ^{39}K- NMR spectra are obtained by a fast Fourier transformation of their free induction decays (FIDs) under a static magnetic field H_0 of 7.06 tesla. As already mentioned, the spectrometer is more stable than 0.1 ppm/day and more homogeneous than 0.2 ppm. Quite generally, it is inevitable to check whether the RF pulse irradiates the overall line shapes sufficiently in obtaining spectra by the FFT of FIDs, as in the case of measuring T_1 and T_2. Otherwise, the incomplete RF irradiation results in experimental artifacts, hence misled conclusion. Typical net RF pulse power, which is supplied to the NMR probe by the power amplifier (Doty Scientific DSI 1000B), can be measured by a pulse power meter of the amplifier and is found to be 200 W (20 W) for ^{13}C (for ^{39}K). The smaller pulse power for ^{39}K is consistent with the longer pulse width: specifically, the width of 90° pulse for ^{13}C (for ^{39}K) is 13.7 μsec (50 μsec). The corresponding amplitude of the alternating field H_1 for ^{13}C (for ^{39}K) is calculated to be $^{13}H_1 = 17$ Oe ($^{39}H_1 = 25$ Oe). The ratio of $^{13}H_1$ ($^{39}H_1$) to H_0 results in 240 ppm (360 ppm), which is found to be sufficiently larger than the width of the overall ^{13}C- (^{39}K-) NMR spectra. Therefore, it is safely confirmed that the RF irradiation is sufficient for both the ^{13}C- and ^{39}K-NMR study.

Pulse repetition time (*Rep*) for averaging the ^{13}C- and ^{39}K-FID was set to be roughly several times of the T_1 at a given T. Typical *Rep* for ^{13}C (^{39}K) spectra was 1 sec (30 sec) at 300 K and 15 sec (4 min) at 20 K. Substantial

number of averaging, in addition to the rather long *Rep*, took us long time to obtain reliable data. Since the gyromagnetic ratio (γ), which is a measure of NMR sensitivity, of ^{13}C nucleus is almost the same as that of ^{63}Cu nucleus, the poor S/N of ^{13}C in our 50-mg K_3C_{60} sample is mainly explained by the smaller number of the ^{13}C nuclei. The number of ^{63}Cu nuclei in a 1 g-$YBa_2Cu_3O_7$ sample is 1.8×10^{21}, whereas that of ^{13}C nuclei of natural abundance (1 %) in a 50-mg K_3C_{60} is only 2.2×10^{19}. Moreover, as the K_3C_{60} powder is sealed in a Pyrex tube, the filling factor in the coil is less than 1/10. Thus, the S/N in the present case is roughly estimated to be about 1/1000 of the $YBa_2Cu_3O_7$ case. On the other hand, the S/N of the ^{39}K NMR was much poorer than that of the ^{13}C NMR, although the number of the ^{39}K nuclei is 5 times larger than that of the ^{13}C nuclei. This is because, at a constant field, the sensitivity of ^{39}K nucleus is 0.03 of that of ^{13}C nucleus by nature, which is considered to be mainly due to the smaller γ of ^{39}K ($^{39}\gamma$ = 2.0 MHz/tesla, $^{13}\gamma$ = 10.7 MHz/tesla). Typical number of averaging for the ^{13}C (for the ^{39}K) spectrum was 3,000 (30,000) at 300 K and 3,000 (1,000) at 20 K. (Quite generally, we have to average the signal at higher T more than that at lower T in principle. Thus, the actual averaging needed for the ^{13}C signal at low T is more than expected. This is because, with decreasing T, the ^{13}C recovery process deviates from the single-exponential behavior and longer component progressively appears, as will be discussed in Chapter 5.) As a result, it took 15 min (7 days) at 300 K and 4 hours (3 days) at 20 K to obtain reliable ^{13}C- (^{39}K-) NMR spectra.

One of the troubles in performing pulsed NMR is the so-called *ringdown*. This is observed as a spurious wave in the time domain just after the input RF pulses. Since an FID also appears just after the pulses, if the "lifetime" of the ringdown happens to be the same as that of the FID (which actually happens when the quality factor of the probe is sufficiently large), the apparent "signal" is the superimposition of the intrinsic FID and the spurious ringdown. If the signal is obtained as a spin-echo (SEO), there exists a "prescription" to deduce

only the SEO by eliminating the ringdown, which is known as *phase cycling technique*. However, this technique does not work in principle when the signal is acquired as an FID. Thus, we had to subtracted the ringdown in a different manner. Fortunately, the ringdown appeared mainly on the ^{39}K-FID signal. Thus, we made use of the fact that the T_1 of the ^{39}K NMR signal is very long: specifically, after we finished averaging an FID in the presence of the ringdown under an appropriate long *Rep*, we successfully obtained only the ringdown under much shorter *Rep*. We did this subtraction process soon after the signal averaging was finished, because it depends on the subtle change in the spectrometer sensitively (such as the configuration of the coil, the flow of gas helium, the impedance of the resonance circuit, and so forth).

All the T_1 values of the ^{13}C nuclei are measured by saturation recovery. Most of them are taken by recovering a spin-echo with the condition that an interval (τ) between 90°- and 180°-pulses is long enough (1 ms) in order that an FID is not superimposed on the SEO. However, some are taken by recovering an FID to confirm that our τ is sufficiently long. Unlike obtaining the ^{13}C- and ^{39}K-NMR spectra, the T_1 at low T are measured under a magnetic field of 2.93 tesla, using a superconducting magnet for broadband use which was made to our order (Cryogenic Ltd., NbTi-wire, 8-tesla). Since the value of T_1 can possibly depend on the strength of applied magnetic field below T_C, which is actually the case for the cuprate superconductors, the fixed magnetic field of 7.06 tesla by the Oxford300/89 can be too strong to clarify the superconducting mechanisms. This is why the magnet for broadband use is employed although the homogeneity of the Cryogenic is worse (10 ppm) than that of the Oxford300/89 (0.2 ppm). Moreover, the insufficient homogeneity matters little in this case. This is because it is the completeness of the RF pulse irradiation on the overall line shapes, rather than high homogeneity, that counts for measuring T_1. As already mentioned, this condition is safely satisfied.

In addition to the complete irradiation, the following conditions should

be satisfied for obtaining reliable values of T_1. First, the *Rep* should be sufficiently long. We confirmed that the *Rep* was more than 10 times larger than the obtained value of T_1, as usual. Second, the recovery data of the ^{13}C nuclear magnetization, which is defined as $P(t) = 1 - M(t)/M_0$ (where $M(t)$ (M_0) is the magnetization at time t after saturation (at thermal equilibrium)), was acquired until $P(t)$ decreases about 1 %. This is particularly important when the time evolution of $P(t)$ does not follow a single exponential function, which is actually the case for the ^{13}C in K_3C_{60} at low T. Otherwise, the value of T_1, which is derived by the fitting of the recovery curve, can possibly be misleading. Third, the recovery data were obtained by iteration, that is, signal averaging was done by sweeping the time t repeatedly. This was performed to exclude the effect of the drift in the spectrometer on the value of M_0. Moreover, the recovery data was employed only when the drift in the values of M_0 was less than 10 %. These three measurement conditions consequently required long *Rep* (10 minutes at 8.2 K) and substantial averaging (300 at 30 K), hence very long time to obtain a reliable data at a given T (no less than 2 weeks).

Chapter 5. ^{13}C NMR Study

§5-1. Static Properties --- Results of ^{13}C NMR Spectra

^{13}C NMR spectra at typical temperatures are shown in Fig. 5-1. At room T, symmetrical line shape is observed, which is considered to be due to the motion of the C_{60} molecules. With decreasing T, the shape starts to show an asymmetric structure with a sub peak at 140 ppm below 235 K (= "$T_{rotation}$", hereafter). It is tempting to attribute this sub peak to unreacted pristine C_{60} because the ^{13}C NMR shift of the pristine C_{60} is the same as that of the sub peak. If this were so, the intensity of the sub peak would be substantially larger with longer pulse repetition time at 250 K [Tycko *et al.*, 1991a; Holczer *et al.*, 1993; Yoshinari *et al.*, 1993]. However, the inset of Fig. 5-1 clearly shows that this is not true. Moreover, since the T_1 of the ^{13}C signal of the pristine C_{60} is, below 100 K, reported to be larger by the orders of more than two, the C_{60} signal is not observable under the measurement conditions of the present study [Tycko *et al.*, 1991a; Maniwa *et al.*, 1992a]. Therefore, the sub peak should not be due to the pristine C_{60}. Taking into account that the motion of the C_{60} molecules in K_3C_{60} freezes with decreasing T, and that the molecule is regarded, in the nucleus length scale, as an almost "planar segment" formed by one C=C bond and two C-C bonds, the anisotropy in the ^{13}C NMR shift $^{13}K_i$ should be observable. In this case, the ^{13}C NMR spectrum is expected to show a powder pattern because, as illustrated in Fig. 5-2, the planar segments possessing ^{13}C nuclei in all the C_{60} molecules (hence the crystallites) have random orientations with respect to the static magnetic field H_0. Therefore, as shown in Fig. 5-3, we attempted to reproduce the spectra using powder patterns, whose asymmetry is caused by anisotropic $^{13}K_i$ (denoted as $^{13}K_x$, $^{13}K_y$, and $^{13}K_z$ in descending order). In addition to the shift tensors $^{13}K_i$ ($i = x, y, z$), line broadening $^{13}\Gamma$ is taken into account as a fitting parameter. It is to be noted that the full-width at

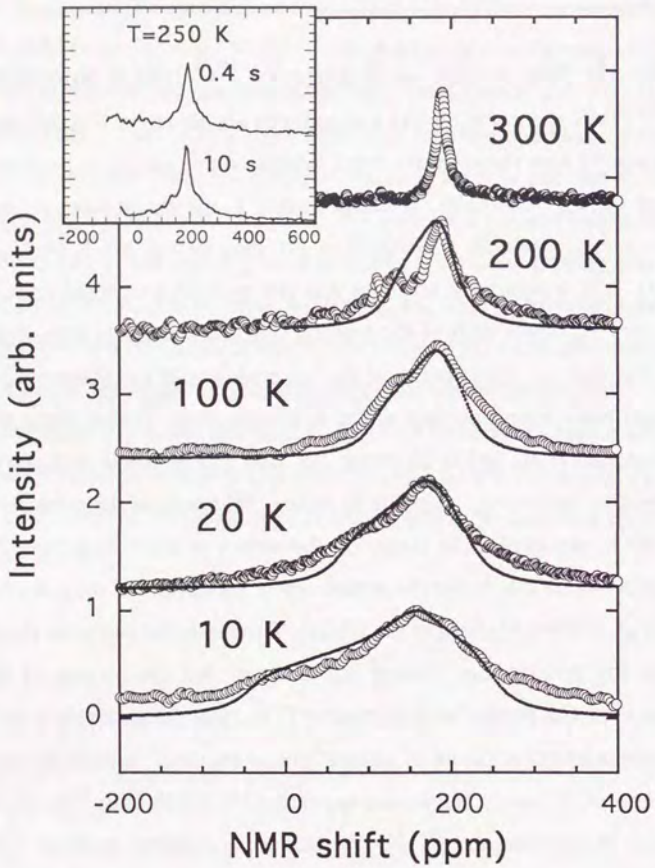

Fig. 5-1

Open circles show the ^{13}C NMR spectra of our superconducting fulleride K_3C_{60} (T_C = 19.4 K) at typical T under a static field of 7.06 tesla.

Symmetrical line shape at room T starts to show an asymmetric shape at 235 K (= $T_{rotation}$). Powder patterns with anisotropic NMR shifts $^{13}K_i$ (i = x, y, z) using the Monte-Carlo simulation (shown by the solid curves) reproduce the essential features of the spectra below $T_{rotation}$.

Inset: Pulse repetition time (*Rep*) dependence of the ^{13}C NMR spectra of K_3C_{60} at 250 K. If there existed the unreacted pristine C_{60}, the signal at ~140 ppm should get substantially larger under *Rep* = 10 sec. The inset shows that our K_3C_{60} sample contains the pristine phase too little to be detected.

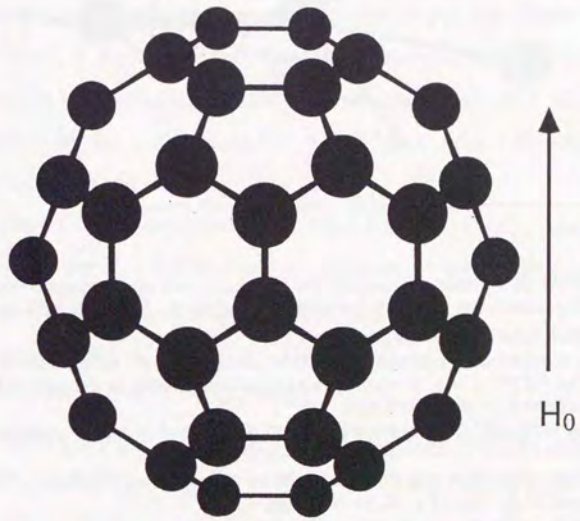

Fig. 5-2

Crystal structure of the soccer-ball shaped C_{60} molecule under a static magnetic field of H_0. Seen from the nucleus length-scale, the local structure of the molecule is regarded approximately as a "planar segment" which consists of two C-C bonds and one C=C bond. In the presence of H_0, the planar segments are randomly distributed with respect to H_0.

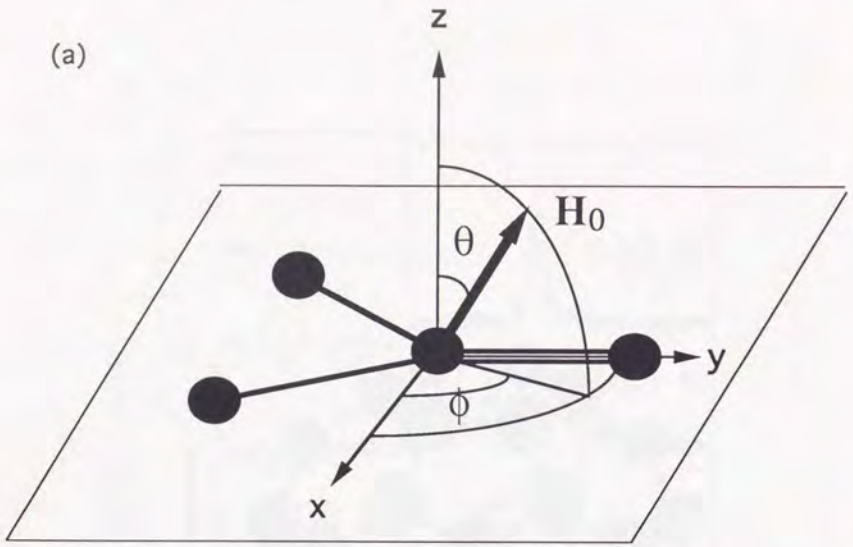

Fig. 5-3

(a) Configuration of a planar segment of the C_{60} molecules under a static magnetic field of H_0. The simulation in Fig. 5-1 was performed by the random direction of H_0 (i.e., the random values of θ and ϕ).

The principal axes of the Knight shifts $^{13}K_i^{spin}$ are found to be the same as those of the chemical shifts $^{13}K_i^{orb}$ ($i = x, y, z$). The z-axis (x- and y-axis) is the perpendicular (parallel) direction of the planar segment.

In this "planar segment" model, the x-axis (y-axis) is found to be the perpendicular (parallel) direction of the C=C bond, from the discussion in Section 5-3-A.

(b) The random values of θ and ϕ result in the so-called "powder pattern". The line shape in the case of $K_x - K_y < K_y - K_z$ is illustrated below.

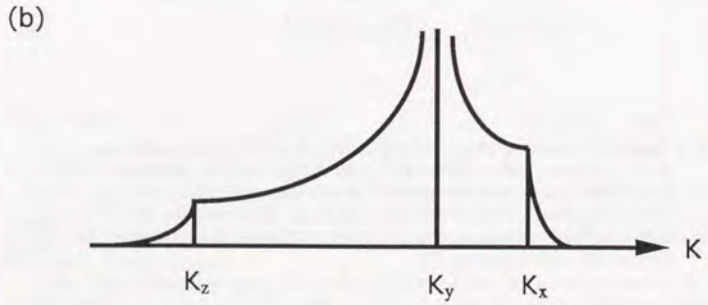

half-maximum of the overall spectrum is not given by the broadening $^{13}\Gamma$ but by the anisotropy ($\approx [(^{13}K_x+^{13}K_y)/2-^{13}K_z]$). All the calculations were done by Monte-Carlo simulation. The simulation program was written by Dr. A. Matsuda. In this simulation, we assumed that the electronic states of the 60 carbon sites of a C_{60} molecule are *equivalent* despite the presence of crystallographically inequivalent sites when the molecular motion is frozen. This assumption is proved to be a good approximation in Section 5-3-C. As shown in the Fig. 5-1, the simulation reproduces the essential feature of the line shapes. The poorer fitting at 200 K is due to an experimentally spurious effect: the "ring-down" in the FID at 200 K forced us to reduce the time range of the FFT. This resulted in the reduction of the intensity at ^{13}K = 155 ppm, which is observed as the apparent dip in the line shape.

Fig. 5-4 shows the T dependence of $^{13}K_i$. Isotropic ($^{13}K_{iso}$) and anisotropic ($^{13}K_{ax}$) parts of the $^{13}K_i$ and asymmetric parameter ($^{13}\eta$) are defined as

$$^{13}K_{iso} = (^{13}K_x + {}^{13}K_y + {}^{13}K_z)/3,$$
$$^{13}K_{ax} = [^{13}K_z - (^{13}K_x + {}^{13}K_y)/2]/3,$$
$$^{13}\eta = |^{13}K_x - {}^{13}K_y|/|2\,{}^{13}K_{ax}|. \qquad (5\text{-}1)$$

Fig. 5-5 represents the T dependences of $^{13}K_{iso}$, $^{13}K_{ax}$, and $^{13}\Gamma$. With decreasing T, both $^{13}K_{iso}$ and $^{13}K_{ax}$ decrease. In Fig. 5-6, $^{13}K_{iso}$ is plotted against $^{13}K_{ax}$ with T as an implicit parameter. This indicates that, in the normal state ($T_C < T < T_{rotation}$), $^{13}K_{iso}$ has the same T dependence as $^{13}K_{ax}$.

§5-2. Dynamical Properties --- Results of ^{13}C NMR T_1

Since one of our purposes of measuring ^{13}C spin-lattice relaxation time T_1 is to clarify the electronic properties instead of the C_{60} molecular motions in K_3C_{60}, we obtained the values of T_1 mainly at low T (< 55 K) where the molecular motion is sufficiently frozen, including those in the superconducting state. We show typical examples of the ^{13}C magnetization recovery data in Fig. 5-7. Since we found that the recovery data $P(t)$ cannot be fitted to a single

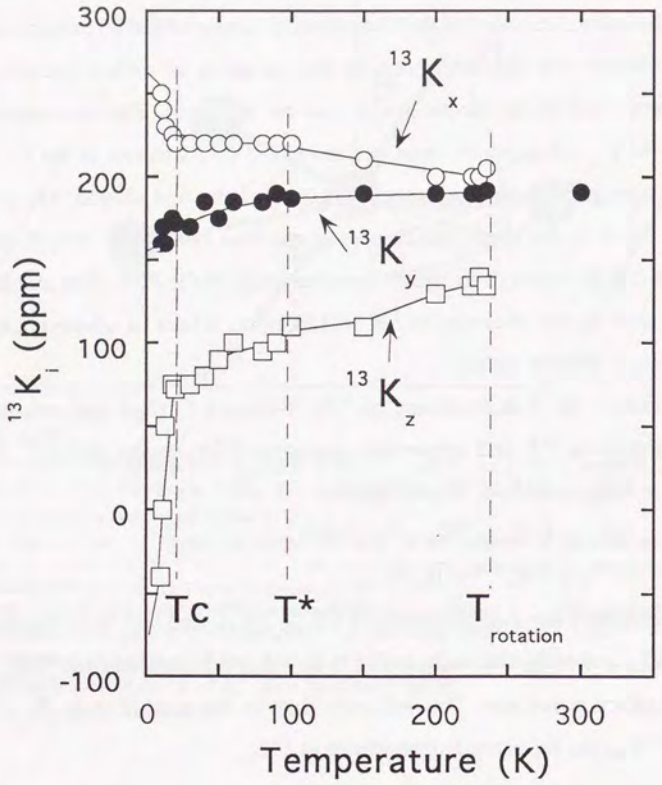

Fig. 5-4

T dependences of the anisotropic NMR shift $^{13}K_i$ ($i = x, y, z$). At each T, the value of $^{13}K_i$ is obtained by the Monte-Carlo simulation for the spectrum, as typically shown in Fig. 5-1. From the discussion of ^{39}K NMR spectra (Chapter 6), the orientational order of the C_{60} molecules is found to be incomplete below T^*.

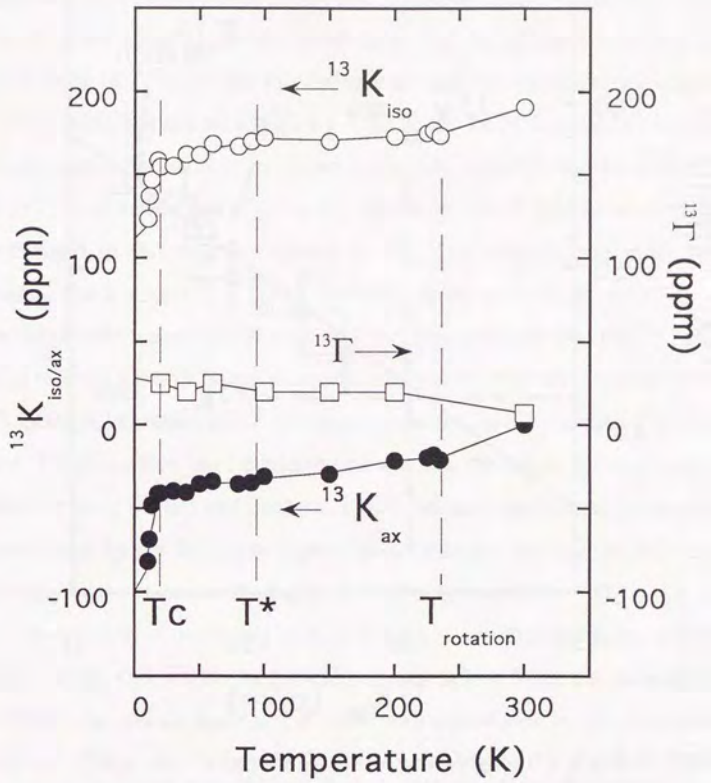

Fig. 5-5

T dependences of isotropic ($^{13}K_{iso}$) and anisotropic ($^{13}K_{ax}$) part of the ^{13}C NMR shift, which are defined by Eq. (5-1), are shown in the left-vertical axis.

In the right axis, T dependence of the broadening parameter ($^{13}\Gamma$) to reproduce the spectrum is shown. Note that $^{13}K_{iso}$ and $^{13}K_{ax}$ have the same T dependence.

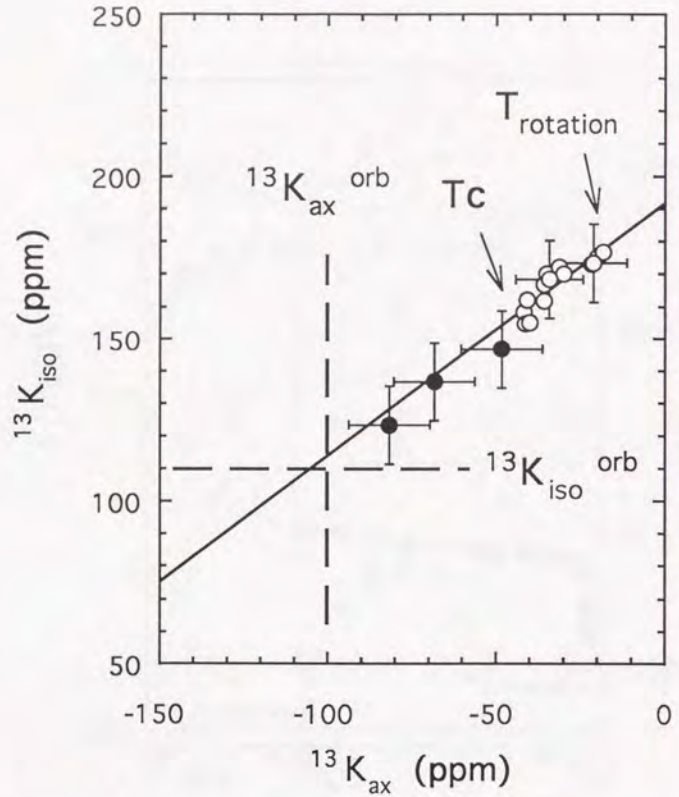

Fig. 5-6

Isotropic ^{13}C NMR shift $^{13}K_{iso}$ is plotted as a function of anisotropic one $^{13}K_{ax}$ for $T < T_{rotation}$ with T as an implicit parameter. Solid line, which is obtained by the least-squares fitting for $T > T_C$, indicates that $^{13}K_{iso}$ and $^{13}K_{ax}$ have the same T dependence as expected from Fig. 5-5.

Below T_C, the contribution of the superconducting diamagnetism $^{13}(\Delta H/H)$ to the NMR shifts, which is given in principle by the reduction of $^{13}K_{iso}$ from the solid line at a given value of $^{13}K_{ax}$, is found to be negligible (< 5 ppm). Chemical shifts ($^{13}K_{iso}^{orb}$ and $^{13}K_{ax}^{orb}$) are obtained by extrapolating the values of $^{13}K_{iso}$ and $^{13}K_{ax}$ to those at $T = 0$, assuming the Yosida function [Stenger *et al.*, 1993].

exponential function, we attempted to fit it to a 2-exponential function:

$$P(t) = 1 - M(t)/M_0 = F^S \exp(-t/T_1^S) + F^L \exp(-t/T_1^L), \quad (5\text{-}2)$$

with F^S, T_1^S, F^L, and T_1^L being the fitting parameters. Here, $M(t)$ (M_0) is the magnetization at time t after saturation (at thermal equilibrium), T_1^S (T_1^L) is defined by the initial slope (the "final slope") of the recovery data, and F^S (F^L) is the fraction of T_1^S (T_1^L). By this fitting, we found that the non-single exponential recovery (NSER) data taken at all $T < 55$ K can be normalized to an identical recovery shape. Specifically, as shown in Fig. 5-8, almost T- independent relations of $T_1^L/T_1^S = 3.4 \pm 0.4$ and $F^S/F^L = 2.0 \pm 0.6$ hold. The T dependences of T_1^S and T_1^L defined in this way are shown in Fig. 5-9, whereby we point out two features. First, above T_C, T_1T = constant holds at least up to 55 K within acceptable error range. As is verified later, this indicates that the ^{13}C nuclei in K_3C_{60} relax to a Fermi liquid where the electron interaction is treated within the RPA. Second, below T_C, $1/T_1T$ decreases gradually and has a convex T dependence curve. This behavior can be interpreted not as a clear-cut, but as a suppressed coherence peak [Hebel and Slichter, 1959], because the bulk superconductivity is confirmed by the Meissner signal detected as the increase in the resonance frequency of the resonance circuit under the magnetic field.

In addition to the values of T_1 at $T < 55$ K, we obtained those at high T of 300 K, 310 K, and 320 K. As typically shown in Fig. 5-10, the recovery data at $T > 300$ K are, unlike those at $T < 55$ K, well reproduced by single exponential functions. Thus, the values of T_1 were unambiguously defined. This is in accordance with the result mentioned in Section 5-1 that the line shapes at $T > T_{rotation}$ are symmetric.

§5-3. Analyses and Discussions on ^{13}C NMR Study

§5-3-A. Analyses of ^{13}C NMR Spectra

First, we analyze the spectra in the normal state on which those in the superconducting state are based. As mentioned in Chapter 2, in general, observed

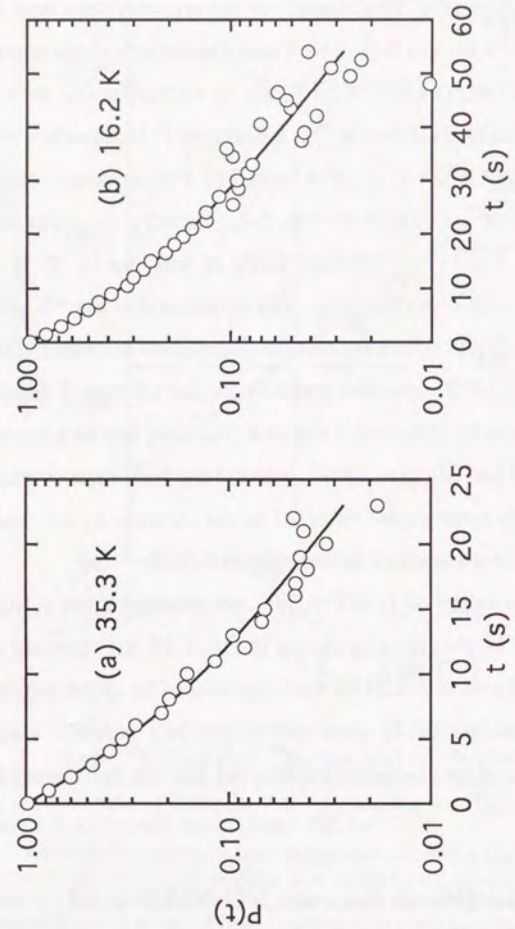

Fig. 5-7

Typical examples of ^{13}C spin-lattice relaxation recovery data (open circles) (a) at 35.3 K ($> T_C$) and (b) at 16.2 K ($< T_C$) under a static magnetic field of 2.93 tesla. Solid line is obtained by least-squares fitting. Above and below T_C, the data at all T (< 55 K) have the same recovery shape.

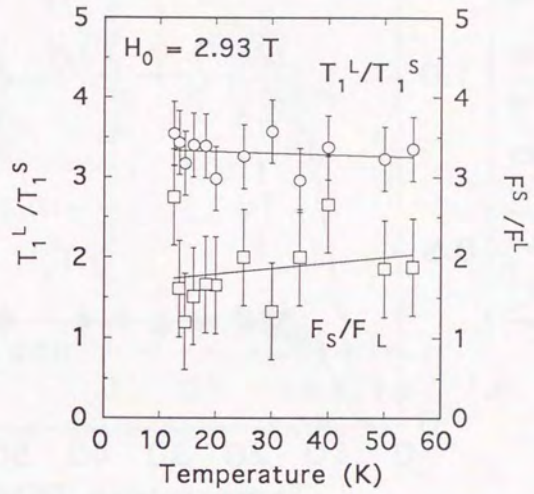

Fig. 5-8

T dependences of the ratios of T_1^L/T_1^S and F^S/F^L defined by the 2-exponential fitting: $P(t) = F^S\exp(-t/T_1^S) + F^L\exp(-t/T_1^L)$. Note that the both ratios are almost T independent above and below T_C at low T (< 55 K), which means that the recovery data are scaled to the same shape, as expected from Fig. 5-7.

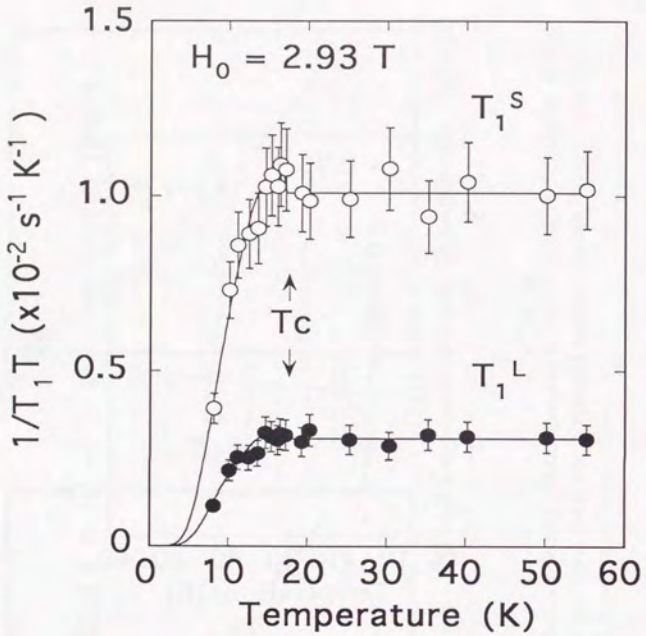

Fig. 5-9

T dependences of the values of $1/(T_1T)$ for T_1^S and T_1^L. Note that they have the same *T* dependence, as indicated by Fig. 5-8. In this *T* range, T_1T is *T* independent above T_C, and a suppressed coherence peak is observed just below T_C. The solid curves, which Nakamura *et al.* calculated with a model $\alpha^2F(\omega)$ based on the Eliashberg equation, reproduce our data well. From the *T* dependence of the fitted curves, the reduced superconducting gap $2\Delta/k_BT_C$ is found to be 4.3.

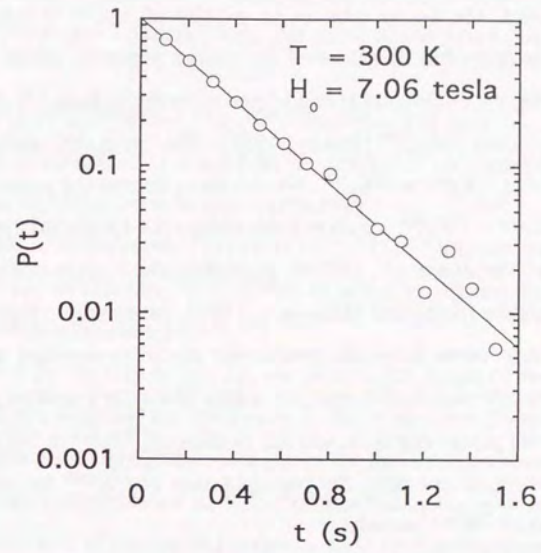

Fig. 5-10

Spin-lattice relaxation recovery curve at 300 K ($> T_{rotation}$). Unlike the data at low *T* (< 55 K) which are typically shown in Fig. 5-7, the recovery data at high *T* shows a single-exponential time evolution expected for ^{13}C nuclei with spin one-half.

NMR shift K consists of the Knight shift K^{spin} and the chemical shift K^{orb}. However, in the case of a powder pattern, we need to discuss whether the principal axes of $^{13}K^{spin}$ have the same directions as those of $^{13}K^{orb}$. Since every carbon site has one C=C bond and two C-C bonds which are regarded as a planar segment, the z-axis (the x- or y-axis) of $^{13}K^{orb}$ is assigned to the perpendicular (parallel) direction of the planar segment. Since the chemical shielding along the z-direction is considered to be the largest, $^{13}K_z^{orb}$ is expected to be smaller than $^{13}K_{x/y}^{orb}$ [Bovey, 1988]. The "in-plane" anisotropy of the bonds results in $^{13}K_x^{orb} \neq {}^{13}K_y^{orb}$. We therefore denote the principal values as $^{13}K_x^{orb} > {}^{13}K_y^{orb} > {}^{13}K_z^{orb}$, which is indeed observed for the pristine C_{60} [Tycko *et al.*, 1991a; Maniwa *et al.*, 1992b]. Regarding the Knight shifts, as the band calculation shows [Saito and Oshiyama, 1991], the isotropic (anisotropic) part is considered to come from the conduction electrons residing on the carbon s-orbitals ($p\pi$-orbitals). In this case, the z-axis (the x- or y-axis) is perpendicular (parallel) to the planar segment, and the relation of $^{13}K_z^{spin} > {}^{13}K_x^{spin} = {}^{13}K_y^{spin}$ holds. Therefore, in our case, the principal axes of $^{13}K^{spin}$ are taken to be the same as those of $^{13}K^{orb}$, namely,

$$^{13}K_i = {}^{13}K_i^{orb} + {}^{13}K_i^{spin} \ (i = x, y, z), \tag{5-3}$$

and the inequivalence of $^{13}K_x$ and $^{13}K_y$ comes from that of the chemical shifts instead of the Knight shifts (i.e., $^{13}K_x^{orb} \neq {}^{13}K_y^{orb}$ and $^{13}K_x^{spin} = {}^{13}K_y^{spin}$). We assume, as is common, that $^{13}K_i^{orb}$ is T independent and the observed decrease in $^{13}K_i$ is due to $^{13}K_i^{spin}$. Then, the reduction in $^{13}K_i$ is due to the decrease in the spin susceptibility χ^{spin}. As will be shown later in this Chapter (Section 5-3-C2), the T dependence of the T_1 value renormalized by the anisotropy in hyperfine couplings (AHC) is well explained by the T-dependent $\chi^{spin}(T)$. In this case,

for $T > T_{rotation}$,

$$[^{13}K_{iso}(T) - {}^{13}K_{iso}^{orb}]/{}^{13}A_{iso}^{spin} = \chi^{spin}(T),$$

$$^{13}K_{ax}^{orb} \approx 0, \ ^{13}K_{ax}^{spin} \approx 0 \text{ (within the line width)}, \tag{5-4a}$$

for $T_C < T < T_{rotation}$,

$$[^{13}K_{iso}(T) - {}^{13}K_{iso}^{orb}]/{}^{13}A_{iso}^{spin}$$

$$= [^{13}K_{ax}(T) - {}^{13}K_{ax}^{orb}]/\ {}^{13}A_{ax}^{spin} = \chi^{spin}(T), \tag{5-4b}$$

holds where $^{13}A_{iso}^{spin}$ ($^{13}A_{ax}^{spin}$) is the isotropic (anisotropic) hyperfine coupling due to the conduction electrons residing on the carbon s- (p-) orbitals. If the hyperfine couplings are T independent, the slope of the fitted line in Fig. 5-6 gives

$$^{13}K_{iso}^{spin}(T)/{}^{13}K_{ax}^{spin}(T) = {}^{13}A_{iso}^{spin}/{}^{13}A_{ax}^{spin} = 0.78 \pm 0.1. \tag{5-5}$$

Thus, we have experimentally solved the controversial problem of which ^{13}C hyperfine coupling is dominant in superconducting K_3C_{60}: isotropic or anisotropic. [Tycko *et al.*, 1991b; Antropov *et al.*, 1993]. Equation (5-5) means that the ^{13}C hyperfine is basically anisotropic, but, at the same time, substantially isotropic.

Regarding the spectra below T_C, we observe no traces of the "Redfield patterns" which are expected for the spectra in the vortex state [Redfield, 1967], since Fig. 5-1 shows no qualitative changes in the line shapes above and below T_C except for the T dependence of $^{13}K_i$. The Redfield pattern originates from the spatial distribution of the applied magnetic field penetrating from the vortex cores into the superconducting region. Thus, the absence of the Redfield patterns means that the penetration depth λ is much larger than the distance of the vortex lattice d. Since the spectra shown in Fig. 5-1 were obtained under the magnetic field of 7.06 tesla, the d value is estimated to be 180 Å. On the other hand, Uemura *et al.* report that the penetration depth λ of K_3C_{60} is 4800 ~ 6000 Å, which is much larger than that of usual type-II superconductors [Uemura *et al.*, 1991]. Thus we obtain

$$\lambda/d = 30 \pm 3. \tag{5-6}$$

This is consistent with the absence of the Redfield patterns, as expected. It should be noted that we can conclude from the following reasons that the *long tails* observed in the spectra are *not* the traces of the Redfield pattern. First, the long tail of the Redfield pattern is, in principle, observed at *only higher frequencies*

if the line shape is shown as a function of *frequency* instead of *magnetic field.* However, our long tails are observed at *both* higher and lower frequencies than the main structure. Second, the long tail of the Redfield pattern should have *a small edge* at a resonance frequency of the normal cores, which is actually not observed in our case. Third, our long tails are observed in the *normal state as well* as in the superconducting state, whereas the tail of the Redfield pattern is observable *only* below T_C. Since the tails are observed down to 10 K where χ^{spin} is sufficiently small [Stenger *et al.*, 1993], it is concluded that the long tails do *not* come from the *Knight* shifts, *but* from the locally distributed *chemical* shifts corresponding to the inequivalent carbon sites (ICS) of a C_{60} molecule in A_3C_{60}.

It is to be noted that the ^{13}C NMR probes the presence of the crystallographically ICS only by the chemical shifts but not by the Knight shifts, as is proved in Section 5-3-C.

In general, the decrease in K below T_C comes both from the reduction in K^{spin} (or χ^{spin}) due to the formation of spin-singlet Cooper pairing and from the superconducting diamagnetism $\Delta H/H$. In many cases, it is difficult to estimate $\Delta H/H$, although several methods have been proposed [Takigawa *et al.*, 1989; Barrett *et al.*, 1990]. Since we have found that no traces of the Redfield patterns are observed in the spectra below T_C, we can present a way of determining $^{13}(\Delta H/H)$ unambiguously, as is shown in what follows. Since $^{13}(\Delta H/H)$ cancels out in deducing $^{13}K_{ax}$ on the natural assumption that $\Delta H/H$ is isotropic, Eq. (5-4b) is modified to the following expression for $T < T_C$ as

$$[^{13}K_{iso}(T) - {}^{13}K_{iso}{}^{orb} - {}^{13}(\Delta H/H(T))]/{}^{13}A_{iso}{}^{spin}$$
$$= [^{13}K_{ax}(T) - {}^{13}K_{ax}{}^{orb}]/{}^{13}A_{ax}{}^{spin} = \chi^{spin}(T). \quad (5\text{-}7)$$

We can estimate $^{13}(\Delta H/H)$ as the *difference between* an *experimental* value of $^{13}K_{iso}$ (given by Eq. (5-7)) and a *fictitious* value which is given by assuming the absence of $^{13}(\Delta H/H)$ (the $^{13}K_{iso}$ value given in Eq. (5-4b)). As shown in Fig. 5-6, $^{13}(\Delta H/H)$ is found to be smaller than the error in $^{13}K_{iso}{}^{orb}$, hence negligible,

i.e.,

$$^{13}(\Delta H/H) \leq 5 \text{ ppm}. \quad (5\text{-}8)$$

Using the results by Stenger *et al.* that $\chi^{spin}(T)$ follows the Yosida function [Yosida, 1958; Stenger *et al.*, 1993], the chemical shift $^{13}K_{iso}{}^{orb}$ ($^{13}K_{ax}{}^{orb}$) is estimated to be 110 ±10 ppm (-100 ±5 ppm).

In order to obtain the Knight shifts $^{13}K_i{}^{spin}(T)$ ($i = x, y, z$), here we discuss the T dependences of the observed NMR shifts $^{13}K_i$ ($i = x, y, z$) which is shown in Fig. 5-4. Equation (5-8) derived from the $^{13}K_{iso}$ vs. $^{13}K_{ax}$ diagram (Fig. 5-4) assures that we can obtain the chemical shifts by extrapolating $^{13}K_i$ (T) as $T \rightarrow 0$ K, hence

$$^{13}K_x{}^{orb} = 258 \pm 5 \text{ ppm},$$
$$^{13}K_y{}^{orb} = 158 \pm 5 \text{ ppm},$$
$$^{13}K_z{}^{orb} = -74 \pm 5 \text{ ppm}. \quad (5\text{-}9)$$

These values yield $^{13}K_{iso}{}^{orb}$= 114 ±5 ppm and $^{13}K_{ax}{}^{orb}$= -94 ±5 ppm, which are consistent with the results obtained from Fig. 5-6. With the values of $^{13}K_i{}^{orb}$, we obtain $^{13}K_i{}^{spin}(T)$ as $^{13}K_i(T)$ - $^{13}K_i{}^{orb}$. The T dependences of $^{13}K_i{}^{spin}(T)$ are shown in Fig. 5-11. In the inset, we show the T dependences of $[^{13}K_{ax}{}^{spin}/{}^{13}K_{iso}{}^{spin}](T)$ (= $[^{13}A_{ax}{}^{spin}/{}^{13}A_{iso}{}^{spin}]$) using the values of $^{13}K_i{}^{spin}$. The inset shows that the ratio is almost T independent with the value of 1/(0.76 ±0.10). This agrees with the result of Eq. (5-5) which is deduced from Fig. 5-6.

One may be tempted to argue that the negative value of $^{13}K_x{}^{spin}$ (or $^{13}A_x{}^{spin}$) is not intrinsic but should be some experimental or analytical artifact of, for example, merely regarding the line widths that grow at low T as the T-dependent $^{13}K_x{}^{spin}$. However, the negative $^{13}K_x{}^{spin}$ is found to be intrinsic: as is shown in Fig. 5-12, the relation of $^{13}K_x{}^{spin}(T) \propto {}^{13}K_z{}^{spin}(T) \propto \chi^{spin}(T)$ holds because of the same T dependence of $^{13}K_x{}^{spin}$ as that of $^{13}K_z{}^{spin}$, and because both $^{13}K_x{}^{spin}$ and $^{13}K_z{}^{spin}$ approach zero as $T \rightarrow 0$. Moreover, we can prove in what follows that the negative $^{13}K_x{}^{spin}$ results from the assumed "$p\pi$-orbitals" picture: the conduction electrons producing $^{13}A_{ax}{}^{spin}$ reside dominantly on the

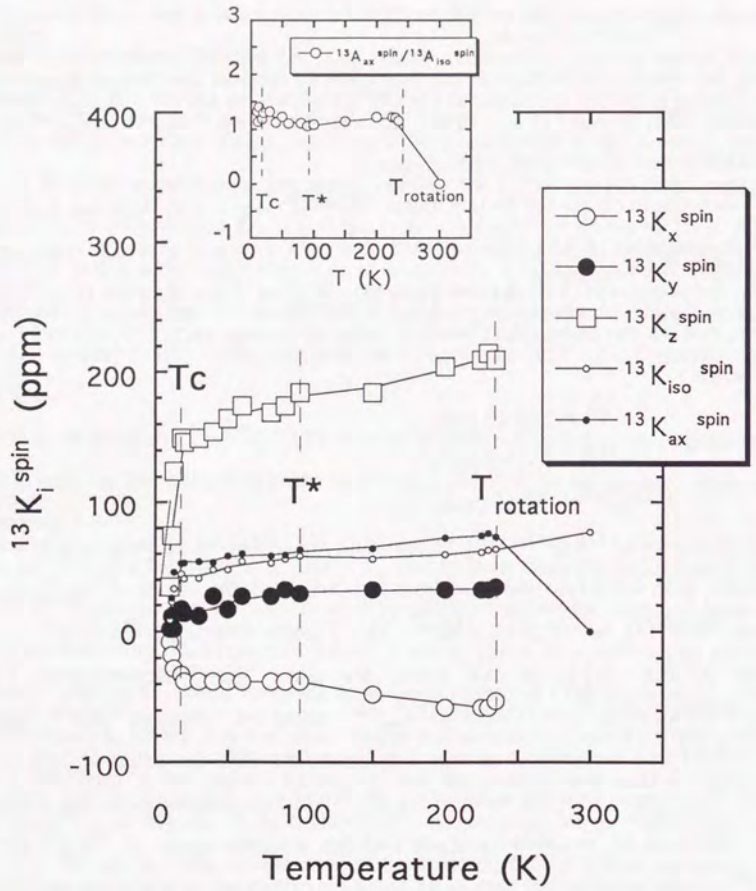

Fig. 5-11

T dependences of the Knight shifts of $^{13}K_i{}^{spin}$ (i = x, y, z, iso, or ax). Solid lines are the eye-guides.

In the inset, the ratios of the hyperfine couplings $^{13}A_{ax}{}^{spin}/^{13}A_{iso}{}^{spin}$ (= $^{13}K_{ax}{}^{spin}/^{13}K_{iso}{}^{spin}$), which are obtained from the values of $^{13}K_{iso}{}^{spin}$ and $^{13}K_{ax}{}^{spin}$ in the main figure, are shown as a function of T. Solid line is the eye-guide. Note that the almost T-independent value of $^{13}A_{ax}{}^{spin}/^{13}A_{iso}{}^{spin}$ below $T_{rotation}$ is consistent with the result obtained from Fig. 5-6.

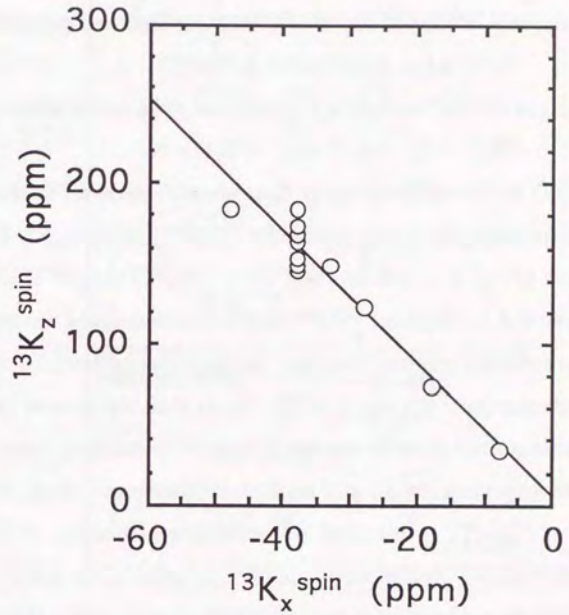

Fig. 5-12

The z-component Knight shift $^{13}K_z{}^{spin}$ is plotted as a function of the x-component one $^{13}K_x{}^{spin}$ with T as an implicit parameter. Solid line is obtained by least-squares fitting. Note that, in addition to the same T dependence of $^{13}K_x{}^{spin}$ and $^{13}K_z{}^{spin}$, both values approach zero with $T \rightarrow 0$.

carbon $p\pi$-orbitals. For this purpose, we show that anisotropic Knight shift $^{13}K_i^{ax}$, which is defined as $^{13}K_i^{spin} - {}^{13}K_{iso}^{spin}$ ($i = x, y, z$), is equal to the Knight shift $^{13}K_i^{dipole}$ which is due to the dipolar field of the conduction electrons residing mainly on the carbon $p\pi$-orbitals. First, the relation

$$^{13}K_x^{ax}(T) + {}^{13}K_y^{ax}(T) + {}^{13}K_z^{ax}(T) = 0 \qquad (5\text{-}10)$$

holds at every T, as is evident from the definition of $^{13}K_i^{ax}$. Quite generally, it is known that the same relation as Eq. (5-10) holds for dipolar Knight shifts

$$K_x^{dipole}(T) + K_y^{dipole}(T) + K_z^{dipole}(T) = 0. \qquad (5\text{-}11)$$

Second, the signs of $^{13}K_i^{ax}$ shown in Fig. 5-13 are to be noted, namely,

$$^{13}K_x^{ax} < 0, \quad {}^{13}K_y^{ax} < 0, \quad {}^{13}K_z^{ax} > 0. \qquad (5\text{-}12)$$

Equation (5-12) is consistent with the "$p\pi$-orbitals" picture [Yoshinari *et al.*, 1990]. Third, following the discussion of the $^{13}K_z^{spin}(T)$ vs. $^{13}K_x^{spin}(T)$ plot (Fig. 5-12), the inset of Fig. 5-13 means $^{13}K_x^{ax}(T) \propto {}^{13}K_z^{ax}(T) \propto \chi^{spin}(T)$. Therefore, we have proved that the negative $^{13}K_x^{spin}$ is not an experimental nor an analytical artifact, but is naturally resultant from the "$p\pi$-orbitals" picture.

Here we compare the result of Eq. (5-5) with theoretical predictions. Since $1/T_1$ is proportional to the square of hyperfine coupling [Moriya, 1963] and the orbital hyperfine coupling is negligible [Kawamoto *et al.*, 1995b], the contribution of $^{13}A_{iso}^{spin}$ to the total $1/T_1$ calculated from Eq. (5-5) is 38 %. Therefore, the $^{13}A_{iso}^{spin}$ contribution is neither as small as the prediction based on local density approximation (LDA) (5 %) [Antropov *et al.*, 1993], nor is it dominant as was predicted by Hartree-Fock approximation (HFA) [Tycko *et al.*, 1991b].

From the viewpoint of the crystal structure of the C_{60} molecule (Fig. 5-2), the result of Eq. (5-5) is reasonable, since the local structure of a carbon atom in the molecule is, as already mentioned, regarded as a microscopic "planar segment" to a good approximation: the bonding length is 1.46 Å for C-C and 1.40 Å for C=C, whereas the diameter of the molecule is 11.1 Å [Tanigaki *et al.*, 1992; Mizuki *et al.*, 1994]. This planarity results in the contribution of carbon atomic

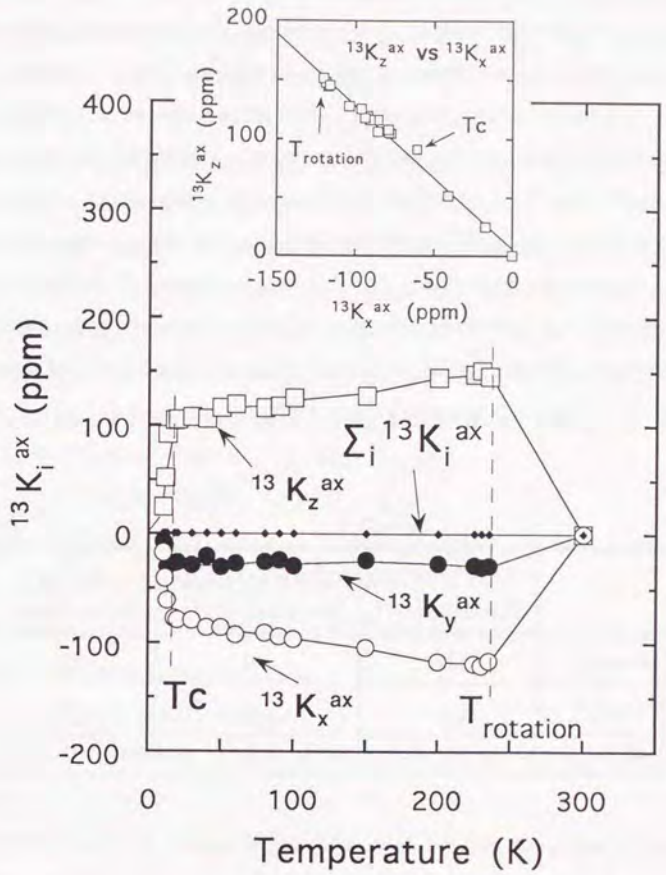

Fig. 5-13

T dependences of the Knight shift $^{13}K_i^{ax}$, which is defined as $^{13}K_i^{spin} - {}^{13}K_{iso}^{spin}$ ($i = x, y, z$). From the definition of $^{13}K_i^{ax}$, the summation of the x-, y-, and z-components is zero at every T.

In the inset, $^{13}K_z^{ax}$ is plotted as a function of $^{13}K_x^{ax}$ with T as an implicit parameter. As in the case of the $^{13}K_z^{spin}$ vs. $^{13}K_x^{spin}$ plot (Fig. 5-12), the inset shows that $^{13}K_x^{ax}$ and $^{13}K_z^{ax}$ have the same T dependence as well as that they approach zero as $T \to 0$.

p-orbitals to the molecular orbitals on the Fermi level. In addition to the planarity, the non-planarity that shapes the C_{60} molecule is expected to produce the contribution of carbon *s*-orbitals to some extent. In order to examine this interpretation for K_3C_{60}, we compared our result with the data for other carbon-based superconductors [Takigawa *et al.*, 1986; Kawamoto *et al.*, 1995a]. As Table 5-I shows, the larger the dimensionality as a conductor, the larger the value of $A_{iso}^{spin}/A_{ax}^{spin}$, as expected. In addition, it is interesting to note that K_3C_{60} shows the largest $A_{iso}^{spin}/A_{ax}^{spin}$ and the highest T_C among these materials. This may suggest the importance of *s*-orbitals or higher dimensionality in achieving higher T_C in carbon-based superconductors. However, more examples are required to confirm the empirical relation, since we have no way of logically explaining the relationship between T_C and A_i^{spin}.

Table 5-I

	$(TMTSF)_2ClO_4$ [Takigawa *et al.*]	κ-$(BEDT\text{-}TTF)_2X$ [Kawamoto *et al.*]	K_3C_{60} [present study]
dimensionality	1D	2D	3D
$A_{iso}^{spin}/A_{ax}^{spin}$	0.39	0.62	0.78
T_C (K)	1.2	11.6	19.4

Ordinarily, an experimental value of $^{13}A_i^{spin}$ is obtained from the K–χ plot [Clogston *et al.*, 1964]. In our case, however, this is almost impossible because reliable value of χ^{spin} is unavailable, due to the larger magnetization of the Pyrex glass that seals the sample. This is why we obtained only the ratio of $^{13}A_{iso}^{spin}/^{13}A_{ax}^{spin}$ from the NMR shifts alone, without using the ambiguous χ^{spin}. Nevertheless, as in the case of $^{13}K_{iso/ax}^{spin}$, we observed the qualitative behavior that χ^{spin} decreases with decreasing T by subtracting the Pyrex

magnetization. This means that both $^{13}A_{iso}^{spin}$ and $^{13}A_{ax}^{spin}$ are positive. The positive $^{13}A_{ax}^{spin}$ confirms again the assumed "$p\pi$-orbitals" picture [Yoshinari *et al.*, 1990] which was concluded from Eq. (5-12) or Fig. 5-13. The qualitative T dependence of χ^{spin} and Fig. 5-13 result in

$$^{13}A_x^{spin} < 0,\ ^{13}A_y^{spin} < 0,\ ^{13}A_z^{spin} > 0. \tag{5-13}$$

In Fig. 5-14(a), we show the T dependence of the $^{13}\eta$ value given by Eq. (5-1). It is to be noted that the relation of $^{13}\eta < 1$ (i.e., $^{13}K_x - {}^{13}K_y < {}^{13}K_y - {}^{13}K_z$) holds at every T. This relation, as well as the unchanging order of $^{13}K_x > {}^{13}K_y > {}^{13}K_z$, verifies that the obtained $^{13}K_{iso}$, $^{13}K_{ax}$, and $^{13}\eta$ are self-consistent. As is shown in the figure, on lowering T, the $^{13}\eta$ value increases without discontinuity (roughly linear in T) with $^{13}\eta\,(T \to 0\ \mathrm{K}) = 0.53 \pm 0.15$. Asymmetric parameter for the Knight shifts and that for the chemical shifts is defined as

$$^{13}\eta^{spin} = |{}^{13}K_x^{spin} - {}^{13}K_y^{spin}|/|2\,{}^{13}K_{ax}^{spin}|, \tag{5-14a}$$

$$^{13}\eta^{orb} = |{}^{13}K_x^{orb} - {}^{13}K_y^{orb}|/|2\,{}^{13}K_{ax}^{orb}|, \tag{5-14b}$$

respectively. Since $^{13}\eta\,(T \to 0\ \mathrm{K}) = {}^{13}\eta^{orb}$ owing to Eq. (5-8), we obtain

$$^{13}\eta^{orb} = 0.53 \pm 0.15. \tag{5-15a}$$

As is shown in Fig. 5-14(b), the $^{13}\eta^{spin}$ value is small ($= 0.17 \pm 0.08 \ll 1$) and almost T independent below $T_{rotation}$

$$^{13}\eta^{spin} = 0.17 \pm 0.08 \ll 1. \tag{5-15b}$$

This result is considered to be in good agreement with the assumed $^{13}K_x^{spin} = {}^{13}K_y^{spin}$.

Within the assumed "planar segment" model, we can show that the observed "in-plane" anisotropy in the Knight shifts (i.e., the small but *finite* value of $^{13}\eta^{spin}$) is ascribed to the electron dipolar field of the carbon $p\sigma$-orbitals (which is smaller than that of the $p\pi$-orbitals), if we take into account that the bond length of C=C (C-C) is 1.40 Å (1.46 Å). Along with the experimental result of $0 > {}^{13}K_y^{spin} > {}^{13}K_x^{spin}$, the *x*- (*y*-) axis is assigned to the *perpendicular* (the *parallel*) direction to the C=C bond in the planar segment.

It is tempting to argue that the substantial T dependence of $^{13}\eta$ contradicts the

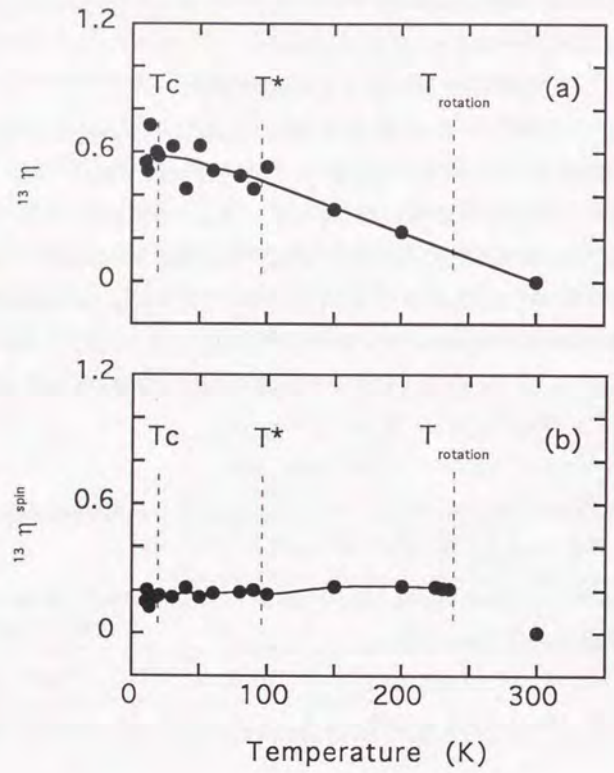

Fig. 5-14

T dependence of the asymmetric parameter of (a) $^{13}\eta$ for the NMR frequency shifts $^{13}K_i$ ($i = x, y, z$), and that of (b) $^{13}\eta^{spin}$ for the Knight shifts $^{13}K_i^{spin}$ ($i = x, y, z$). Solid lines are the eye-guides.

The relation of $^{13}\eta < 1$, as well as the unchanging order of $^{13}K_x > {}^{13}K_y > {}^{13}K_z$, proves that the obtained $^{13}K_i$ are self-consistent. The almost T-independent and small value of $^{13}\eta^{spin}$ (« 1) verifies the "$p\pi$-orbitals" picture. The value of $^{13}\eta$ depends on T although neither $^{13}\eta^{spin}$ nor $^{13}\eta^{orb}$ does. This is due to both the general relation of $\eta \neq \eta^{spin} + \eta^{orb}$ and the T-dependent $^{13}K_i^{spin}$.

T-independences of $^{13}\eta^{spin}$ and $^{13}\eta^{orb}$. However, this is not true because, both the general relation of $^{13}\eta \neq {}^{13}\eta^{spin} + {}^{13}\eta^{orb}$ (which is seen from Eqs. (5-1) and (5-14)) and the T-dependent $^{13}K_i^{spin}$ make the $^{13}\eta$ value depend on T, although neither $^{13}\eta^{spin}$ nor $^{13}\eta^{orb}$ does.

As is shown in Fig. 5-15(a), the line shapes do not clearly depend on the pulse repetition time (t) for $t \sim T_1^S$ (= 1.8 sec at T = 50 K), where the value of T_1^S is defined by the initial slope of the recovery curve. In what follows, we show that the t independence is explained by our powder-pattern model which comes from the anisotropic $^{13}A_i^{spin}$, but not by the model without the anisotropy in $^{13}A_i^{spin}$.

For simplicity, we neglect the "in-plane" anisotropy for the Knight shifts, (i.e., $^{13}\eta^{spin} = 0$). In this case, the T_1^{-1} value of a planar segment is given as

$$T_1^{-1}(\theta, \phi) = [4(\alpha^{spin})^2 - 2(\alpha^{spin})(1+3\cos 2\theta) + (7-2\cos 2\theta)]C, \quad (5\text{-}16a)$$

$$C \equiv [(\gamma_I^2 k_B T)/(4\gamma_e^2 \hbar^2 (A_{ax}^{spin})^2)] \sum_q [\chi''(q, \omega_0)/\omega_0], \quad (5\text{-}16b)$$

where $\alpha^{spin} \equiv A_{iso}^{spin}/A_{ax}^{spin}$, γ_I (γ_e) is the gyromagnetic ratio of the nucleus (electron), $\chi''(q, \omega_0)$ is the imaginary part of the dynamical spin susceptibility at the resonance frequency of ω_0 [Kawamoto *et al.*, 1995]. As illustrated in Fig. 5-3, θ (ϕ) is the polar (azimuth) angle of the H_0 field with respect to the z- (x-) axis. It is to be noted that Eq. (5-16) is valid even in the case of $\eta \neq 0$, so long as $\eta^{spin} = 0$. On the other hand, the line intensity I in the absence of broadening at a given NMR shift K (*not* at a Knight shift K^{spin}) is expressed as

$$I(c) = [c(1-f)]^{-1} \mathcal{K}[(1-c)f/c(1-c)], \quad (5\text{-}17a)$$

$$c \equiv (K - K_x)/(K_z - K_x) = f\sin^2\phi + (1 - f\sin^2\phi)\cos^2\theta, \quad (5\text{-}17b)$$

$$f \equiv (K_x - K_y)/(K_x - K_z) = 2\eta/(3 + \eta), \quad (5\text{-}17c)$$

where $\mathcal{K}[.]$ is an elliptic function given in the Slichter [Slichter, 1989]. It is to be noted that although $T_1^{-1}(\theta, \phi)$ depends on only the θ value because of $\eta^{spin} = 0$, the intensity $I(c)$ at a given c is, due to $\eta \neq 0$, integrated by the segments whose orientations are different from each other. In Fig. 5-15(b), we show this integration as contours for typical c values in the case of $f = 0.3$, corresponding

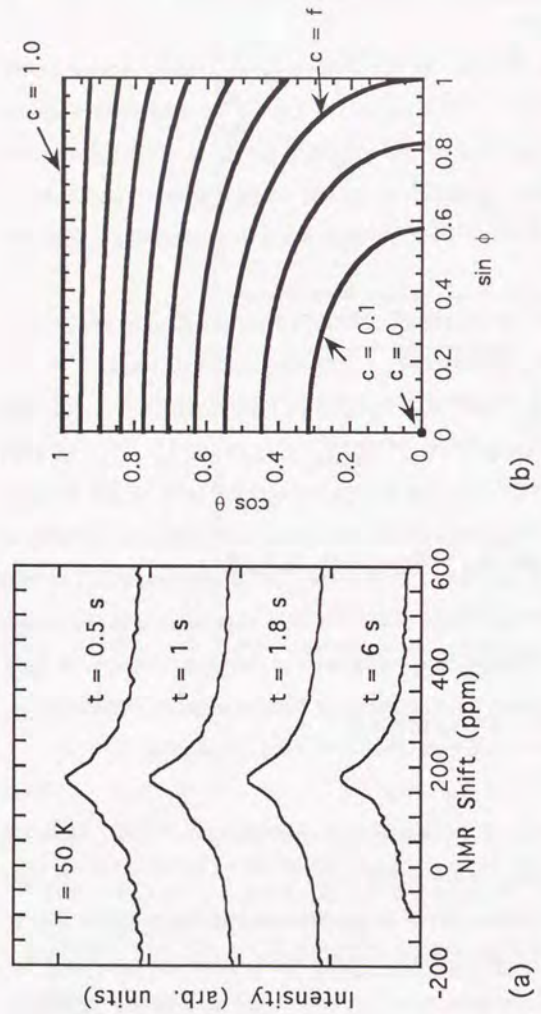

Fig. 5-15

(a) Pulse repetition time (t) dependence of the ^{13}C NMR line shapes at 50 K. The ratio of the intensity of the sub peak ($\sim {}^{13}K_z$) to that of the main peak ($\sim {}^{13}K_y$) does not clearly depend on t, for the t values around T_1^S which is defined by the initial slope of the non-single exponential recovery data and is found to be 1.8 s at 50 K.

(b) Contours for typical c values in the case of the line shapes shown in (a) (i.e., $f = 0.3$), illustrated based on Eq. (5-17). The θ and ϕ values represent the angles shown in Fig. 5-3. It is to be noted that the intensity at a given c value is *integrated* by the planar segments whose orientations, with respect to H_0, are different from each other.

to the spectra shown in Fig. 5-15(a). Along with Eq. (5-16), the contours indicate that the T_1^{-1} value at a given c is *distributed* except exactly at $c = 0$ (at K_x) and at $c = 1$ (at K_z). In order to see how the line shape depends on the t values, we estimate the t dependence of the nuclear magnetization at a c value, $M_c(t)$. We represent the t dependence of the "main peak" (the "sub peak") of the line shape by $M_{c=f}(t)$ ($M_{c=1}(t)$). For this estimation, we first need the relationship between $T_1^{-1}(\theta, \phi)$ and $(T_1^S)^{-1}$. The $(T_1^S)^{-1}$ is expressed as [Kawamoto *et al.*, 1995]

$$(T_1^S)^{-1} = 4C[(\alpha^{spin})^2 + 2]. \quad (5\text{-}18)$$

Second, we assume that $M_c(t)/M_c(\infty)$ ($\equiv m_c(t)$) is approximated by the minimum and maximum value of T_1, namely,

$$1 - m_c(t) = a\exp[-t/(T_1)^{min}] + (1 - a)\exp[-t/(T_1)^{max}]. \quad (5\text{-}19)$$

For the parameters of a, $(T_1)^{min}$, and $(T_1)^{max}$, we take into account the broadening obtained in the fitting (shown in Fig. 5-5), wherein the half-width at half-maximum is 25 ppm (corresponding to $\Delta c = \pm 0.2$). This is because the clear-cut edges at $^{13}K_x$ and $^{13}K_z$, which are expected for a powder pattern in the absence of broadening, are not observed. Specifically, the parameters are taken as $\alpha^{spin} = 1/3$, $(T_1)^{min} = T_1[\cos\theta=0.85]$ and $(T_1)^{max} = T_1[\cos\theta=1]$ for $c = 1 \pm \Delta c$, and $\alpha^{spin} = 1/4$, $(T_1)^{max} = T_1[\cos\theta=0.70]$, $(T_1)^{min} = T_1[\cos\theta=0]$ for $c = f \pm \Delta c$. From Eqs. (5-5), (5-16), (5-18), (5-19), and Fig. 5-15(b), the t dependence of the estimated intensity ratio $r^{powder}(t) \equiv m_{c=1}(t)/m_{c=f}(t)$ is shown in the upper of Table 5-II. It is found that, in our case, the $r^{powder}(t)$ value is almost t independent for $t \sim T_1^S$, as expected.

Table 5-II

t (s)	0.5	1.0	1.8 (= T_1^S)	6.0	∞
$r^{powder}(t)$	0.23 ±0.1	0.23 ±0.04	0.25 ±0.03	0.34 ±0.02	1
$r^{sub/main}(t)$	22	19	16	7.8	1

(The arbitrary choice of the a values in Eq. (5-19) results in the errors shown in Table 5-II. The intensity at $\sim{}^{13}K_z$ shown in Fig. 5-15(a) may appear to be larger than the estimated $r^{\text{powder}}(t)$ values for t = 1 and 1.8 sec. This is considered to result from the experimental inaccuracy (i.e., the non-linearity) in the intensity of a spectrum: the signal intensity at lower K is larger than the real intensity, because the carrier frequency for obtaining an FID is smaller than the signal frequencies, in addition to the inequivalent sensitivity of our resonance circuit. Moreover, the non-linearity in the power spectrum makes the smaller intensities appear to be larger than the real ones.)

It should be noted that we find, in the course of this estimation, that the comparable value of ${}^{13}A_{\text{iso}}{}^{\text{spin}}$ to ${}^{13}A_{\text{ax}}{}^{\text{spin}}$ (i.e., Eq. (5-5)) causes the fact that the condition of $t \sim T_1{}^{\text{S}}$ is *insufficient* to grow the intensities at around $\sim{}^{13}K_z$. Indeed, as already mentioned in Section 4-3, the simulated spectra (typically shown in Fig. 5-1) were obtained under the condition of $t = (5 \sim 10) \times T_1{}^{\text{S}}$. In other words, this means that the *shoulder-like structure* at around $\sim{}^{13}K_z$ in the line shape is *not clearly observed* under the condition of $t \sim T_1{}^{\text{S}}$, and that the very fact shown in Fig. 5-15(a) evidences the validity of the obtained value of α^{spin} (= ${}^{13}A_{\text{iso}}{}^{\text{spin}}/{}^{13}A_{\text{ax}}{}^{\text{spin}}$).

Without the anisotropy in ${}^{13}A_i{}^{\text{spin}}$, on the other hand, it would be correct to assign the NMR shift of the main peak ($\approx {}^{13}K_y$) and the sub peak ($\approx {}^{13}K_z$) to two independent symmetrical lines coming from inequivalent sites, and the peak separation to ${}^{13}K_y{}^{\text{spin}} - {}^{13}K_z{}^{\text{spin}}$ and/or to ${}^{13}K_y{}^{\text{orb}} - {}^{13}K_z{}^{\text{orb}}$. It is found that the separation results from ${}^{13}K_y{}^{\text{spin}} - {}^{13}K_z{}^{\text{spin}}$ rather than ${}^{13}K_y{}^{\text{orb}} - {}^{13}K_z{}^{\text{orb}}$, since the reduction in ${}^{13}K_y - {}^{13}K_z$ below T_C is quite different from that above T_C, as is seen from Fig. 5-4. In this case, following the derivation of ${}^{13}A_{\text{iso}}{}^{\text{spin}}/{}^{13}A_{\text{ax}}{}^{\text{spin}}$ based on the ${}^{13}K_{\text{iso}}$ vs. ${}^{13}K_{\text{ax}}$ plot, we obtained ${}^{13}K_z{}^{\text{spin}}/{}^{13}K_y{}^{\text{spin}} = 5 \pm 2$, hence $T_1{}^{\text{main}}/\ T_1{}^{\text{sub}} = 25 \pm 15$. The model of two independent symmetrical lines unambiguously gives the t dependence of the intensity ratio $r^{\text{sub/main}}(t)$ of the

sub peak to the main peak, because of their single-exponential recoveries. As shown at the bottom of Table 5-II, the estimated $r^{\text{sub/main}}(t)$ value depends on t more prominently than the $r^{\text{powder}}(t)$ value does. Moreover, this model clearly contradicts the recovery data (shown in Fig. 5-8) that the fraction of $T_1{}^{\text{S}}$ is 0.67, because the integrated intensity of the sub peak, which would correspond to the fraction of $T_1{}^{\text{S}}$ in this model, is no more than 0.3.

Therefore, we can conclude that *only* models assuming the *anisotropic* ${}^{13}A_i$ can reproduce the spectra.

§5-3-B. Analyses of ^{13}C NMR T_1

First let us discuss the relaxation results above T_C, on which the analyses below T_C are based. As shown in Fig. 5-9, T_1T is constant within the acceptable error range. This is consistent with other NMR results [Holczer *et al.*, 1993; Maniwa *et al.*, 1992b] and it is likely that a Korringa relation holds for the ^{13}C nuclei. However, as mentioned in Chapter 2, the constancy of T_1T does not always mean a Korringa relation. The *modified* Korringa relation, which treats the electron interaction within the random phase approximation (RPA), is described as

$$T_1T({}^{13}K_{\text{iso}}{}^{\text{spin}})^2 = S/K(\alpha), \tag{5-20}$$

where S is the Korringa constant (for ^{13}C nucleus, ${}^{13}S = 4.34\times10^{-6}$ Ks), $K(\alpha)$ is a factor representing the electron interaction [Korringa, 1950; Moriya, 1963]. Since the ^{13}C nuclear spin (${}^{13}I$) is 1/2, it is expected that the nuclear magnetization recovery $P(t) \equiv 1 - M(t)/M_0$ (where $M_0 \equiv M(\infty)$) shows a single exponential time evolution in principle, and thus the unique value of T_1 is defined unambiguously. The modified Korringa relation is verified by the T-independent values of $T_1T({}^{13}K_{\text{iso}}{}^{\text{spin}})^2$ (but not T_1T). In our case, however, since the $P(t)$ showed non-single exponential recoveries (NSER), Eq (5-20) cannot be applied. It is tempting to ascribe the NSER to some experimental artifacts such as the existence of an extrinsic phase in the sample, or insufficient irradiation of RF pulses. However,

these are unlikely, since the former possibility is denied by the T-independent recovery shapes below 55 K (including those below T_C), and the latter is denied by the fact that, as mentioned in Section 4-3, the value of H_1 is confirmed to be larger than the width of overall line shapes. We could decompose the NSER data into an exponential function with more than two components. However, the T independences of F^S/F^L and T_1^L/T_1^S indicate that the 2-exponential decomposition is sufficient to describe the essential feature of the NSER curve. Since we found that the random distribution of the planar segments (hence the distribution of the anisotropic hyperfine coupling (AHC) of $^{13}A_i$) with respect to the external field H_0 causes the asymmetric ^{13}C NMR powder patterns, it is expected that the NSER is also caused by the random distribution of $^{13}A_i^{spin}$. In this case, it is naturally concluded that, even in the case of $I = 1/2$, the recovery $P(t)$ does not follow a single-exponential time evolution in principle. As mentioned in Section 2-3, the modified Korringa relation Eq. (5-20) is extended to the formula as [Kawamoto *et al.*, 1995a]

$$T_1^S T(K_{iso}^{spin})^2 = S/[K(\alpha)\{1 + 2(A_{ax}^{spin}/A_{iso}^{spin})^2\}]. \quad (5\text{-}21)$$

In the absence of anisotropy in the hyperfine couplings (i.e., $A_{ax}^{spin} = 0$ and $T_1^S = T_1$), the extended relation (5-21) is reduced to the conventional formula Eq. (5-20). Using the values of $^{13}K_{iso}^{spin}$, T_1^S, and Eq. (5-5), it is found that $T_1^S T(K_{iso}^{spin})^2$ is almost T independent with

$$K(\alpha) = 5.7 \pm 1.0 > 1, \quad (5\text{-}22)$$

for $T_C < T < 55$ K. Equation (5-22) means that the relaxation is enhanced to that of independent electrons, and that the susceptibility $\chi(q)$ of K_3C_{60} is enhanced *antiferromagnetically* at the *finite* wave vector $q = Q$. This is consistent with other results: the Coulomb interaction on the C_{60} molecule is found to be 1.6 ±0.2 eV, according to the Auger spectrum [Lof *et al.*, 1992], whereas the calculated bandwidth is 0.4 ~ 0.6 eV [Erwin and Picket, 1991] for K_3C_{60}. Nevertheless, the electron interaction is treated within the RPA because of the validity of the Korringa relation at $T_C < T < 55$ K.

Since the Korringa relation is found to hold above T_C, we can safely analyze the results below T_C. Although no clear-cut coherence peak is observed, the gradual decrease in $1/T_1T$ with decreasing T is consistent with BCS s-wave pairing. In order to obtain more detailed parameters, we fit the data using the following conventional formula:

$$\frac{(1/T_1)_S}{(1/T_1)_N} = 2\int_{\Delta(T)}^{\infty} \{N_S^2(E) + M_S^2(E)\}(-\frac{\partial f(E)}{\partial E})dE, \quad (5\text{-}23)$$

where $N_S(E)$ is the BCS superconducting density of states, $M_S(E)$ is the so-called anomalous density of states arising from the BCS coherence factor, and $f(E)$ is the Fermi distribution function. We first employ the Dynes' density of states [Dynes *et al.*, 1978] with the phenomenological parameters of the broadening due to the lifetime of the thermally-activated quasi particles and the superconducting gap $2\Delta(0)/k_BT_C$. We assumed BCS-type T dependence on $\Delta(T)$. However, we could obtain no satisfactory fittings with these densities of states. Instead, we found that a more accurate treatment of the density of states, based on the Eliashberg equation, could reproduce our experimental data. Nakamura *et al.* calculated the NMR relaxation rate [Nakamura *et al.*, 1993] using model $\alpha^2F(\omega)$ spectra, which predicts the correct T_C value. The spectra and the corresponding calculated results are shown in Fig. 5-16 from the reference. The theoretical curve based on their "model C" is found to be quite satisfactory (solid lines in Fig. 5-9). Its $\alpha^2F(\omega)$ ranges from 0 to 60 meV and has two peaks at 43 meV and 48 meV. The obtained $\Delta(0)$ is 3.52 meV, hence $2\Delta(0)/k_BT_C$ = 4.3. Therefore, our results show that the superconductivity of K_3C_{60} is well explained as a conventional s-wave superconductor in the strong coupling regime. Strong coupling suggests the importance of the low-frequency (that is, inter-molecular or intra-molecular radial) phonons rather than the high-frequency (that is, intra-molecular tangential) phonons. However, we do not exclude the possibility that a theory in the weak coupling regime, if any, can reproduce our data. In the case of weak coupling, the characteristic phonon frequency [Prassides *et al.*, 1991] should be comparable to the bandwidth [Erwin and Picket, 1991]

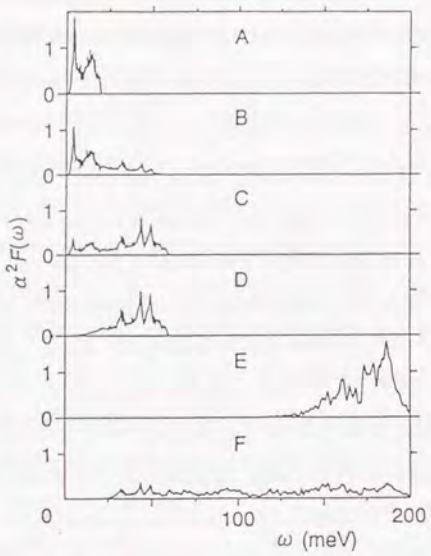

model	A	B	C	D	E	F
λ	2.99	2.21	1.36	0.793	0.442	0.559
Δ_0 (meV)	4.46	4.07	3.52	3.11	2.84	2.82
$2\Delta_0/k_BT_c$	5.48	4.98	4.31	3.80	3.54	3.62
ω_{ln} (meV)	5.94	7.36	11.8	31.4	171	75.6

Fig. 5-16

Upper: Various models of phonon spectra $\alpha^2F(\omega)$.

Lower: Values of the superconducting gap Δ_0, the reduced gap $2\Delta_0/k_BT_C$, the coupling parameter λ, and the averaged phonon frequency ω_{ln} calculated for the spectra of model A to F based on the Eliashberg equations [Nakamura *et al.*, 1993].

of K_3C_{60}, which invalidates the condition on which Migdal's approximation is based. Therefore, a theory in the weak coupling regime, which fully renormalizes the vertices, is expected to be developed.

§5-3-C. Discussions on ^{13}C NMR Study

§5-3-C1. Origin of the non-single exponential recovery (NSER) --- anisotropic hyperfine coupling (AHC) vs. local density of states (LDOS)

In Section 5-3-A, we have shown that the asymmetric ^{13}C NMR line shapes are reproduced by the powder patterns which result from random distribution of the "planar segments" whose hyperfine couplings $^{13}A_i$ (*not only* $^{13}A_i^{spin}$ *but also* $^{13}A_i^{orb}$) are anisotropic. On the other hand, contrary to the expectation for ^{13}C nucleus ($I = 1/2$), we observed that the T_1-recovery processes show non-single exponential recoveries (NSER). In Section 5-3-B, we found that the NSER are scaled to an identical shape above and below T_C, the feature of which is well reproduced *empirically* by Eq. (5-2), 2-exponential fitting. However, to be consistent with the analysis on the asymmetric line shapes, we need to discuss whether or not the observed NSER can be reproduced by the value of $^{13}A_{iso}^{spin}/^{13}A_{ax}^{spin}$ ($= 0.78 \pm 0.1$) obtained from the spectra.

The origin of the NSER for the ^{13}C nuclei of K_3C_{60} in the presence of anisotropic hyperfine coupling (AHC) $^{13}A_i^{spin}$ is qualitatively understood as follows. Owing to Eq. (5-15b) and for simplicity, we regard the Knight shifts as axially symmetric (i.e., $^{13}K_x^{spin} = {}^{13}K_y^{spin} \equiv {}^{13}K_{x/y}^{spin}$) for the "planar segment" (Fig. 5-3). In this case, as mentioned in Chapter 2, the anisotropy in $^{13}A_i^{spin}$ results in the difference between $(T_1)_z$ and $(T_1)_{x/y}$, as well as that between $^{13}K_z^{spin}$ and $^{13}K_{x/y}^{spin}$. Since a planar segment in the C_{60} molecules has random direction with respect to H_0 by nature (Fig. 5-2), the observed relaxation process, which is the spacial average on $(T_1)_z$ and $(T_1)_{x/y}$, shows the NSER.

Specifically, the NSER are simulated as follows. Since the T_1-recovery of a planar segment shown in Fig. 5-3 follows a single-exponential time evolution

exp[$-t/T_1(\theta, \phi)$], where the $T_1(\theta, \phi)$ value is given by Eq. (5-16), it is the spatial average on the orientation of H_0 (hence on the values of θ and ϕ) that causes the NSER. Equation (5-18) is needed to normalize the t values to the T_1^S. It is to be noted that, in this simulation, a recovery shape depends *only* on the value of α^{spin} ($\equiv A_{iso}^{spin}/A_{ax}^{spin}$). In Fig. 5-17, we show the simulated recovery curve for $\alpha^{spin} = 0.78$, along with typical recovery data above and below T_C. The figure shows that the simulated curve well reproduces the recovery data and that the 2-exponential fitting in Section 5-2, which was found to *empirically* reproduce the identical recovery shape, can be regarded as a good approximation for the present simulation. Therefore, we have proved that the random distribution of the "planar segments" with AHC causes *both* the asymmetric NMR line shapes (Section 5-3-A) *and* the NSER. In other words, we found that the parameter of α^{spin}, which was derived from the analysis on the line shapes, reproduces the shape of the T_1-recovery processes successfully as well.

As mentioned in Section 3-1, Holczer *et al.* first proposed that the NSER should be ascribed to the existence of inequivalent carbon sites (ICS) [Holczer *et al.*, 1993]. It is known that *three* crystallographic ICS *would* exist in A_3C_{60} if the orientations of the C_{60} molecules *were* completely ordered at low T; *all* of the four C_{60} molecules, which form a tetrahedron with its center of gravity occupied by an alkali ion (denoted as "T-site"), face their hexagons to the T-site. Assuming this orientational order, Antropov *et al.* have shown by calculation using the local density approximation (LDA) that *three* ICS do have *different* local density of states (LDOS) [Antropov *et al.*, 1993], which results in the presence of the NSER [Holczer *et al.*, 1993]. From an experimental viewpoint, Maniwa *et al.* argued later that the contribution of the LDOS due to the ICS was found to be indispensable to reproduce the observed NESR [Maniwa *et al.*, 1994]. Their argument was based on the logic that the observed recovery data was so deviated from the single-exponential function that even purely dipolar hyperfine field (i.e., $\alpha^{spin} = A_{iso}^{spin}/A_{ax}^{spin} = 0$) is insufficient to account for the

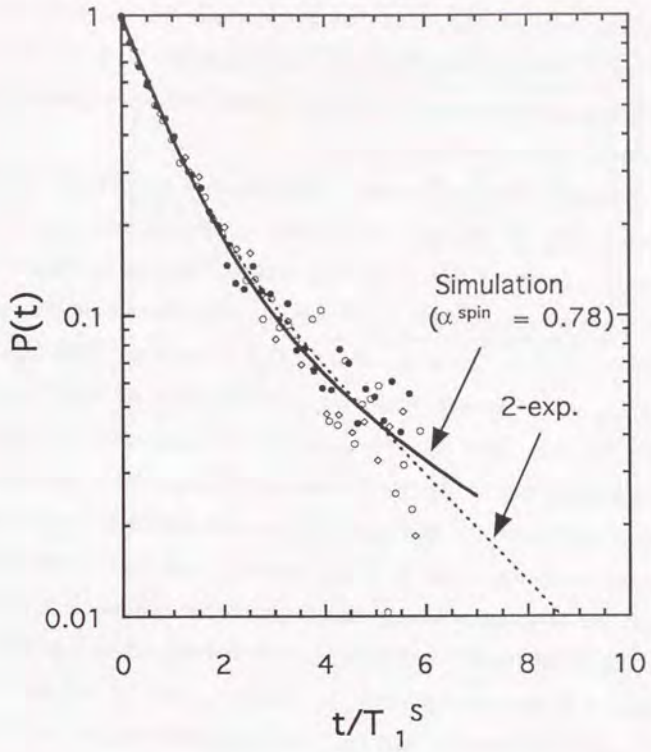

Fig. 5-17

Non-single exponential recovery processes of the ^{13}C NMR at typical low T (< 55 K). The time after saturation (t) is normalized by the value of T_1^S, where T_1^S is given by the initial slope of the data.

Open diamonds represent the data at 35.3 K (> T_C), open circles at 16.2 K (< T_C), and closed circles at 12.5 K (< T_C). The data at low T are scaled to the same recovery shape above and below T_C, as already shown by Fig. 5-7 and Fig. 5-8.

The broken curve stands for the 2-exponential fitting (Eq. (5-2)), which reproduced the recovery shape empirically, as already illustrated in Fig. 5-7 and Fig. 5-8. The solid curve stands for the simulation based on the anisotropy in $^{13}A_i^{spin}$. It should be noted that *no adjustable parameters* are used in this simulation, since the value of α^{spin} (= $^{13}A_{iso}^{spin}/^{13}A_{ax}^{spin}$) is obtained from only the analysis of the spectra. The empirical 2-exponential fitting is found to be a good approximation of this simulation.

NSER.

However, from the following reasons, we can conclude that the contribution of the LDOS to the NSER is negligible and that the electronic states of the 60 carbon sites of a C_{60} molecule are effectively *equivalent* despite the presence of ICS when the molecular motion is frozen.

First, one of the theoretical predictions by Antropov *et al.* that $^{13}A_{ax}{}^{spin}$ dominates to the value of $1/T_1$ (82 %) clearly contradicts our experimental result (38 %), as mentioned in Section 5-3-A. Second, as will be discussed in Chapter 6, the ^{39}K NMR study reveals that the orientations of the molecules are *incompletely* ordered below ~100 K. This means that the ICS at low T are more than three. Consequently, it is *physically misleading* to decompose the NSER into a 3-exponential function. Third, it is to be noted that the argument by Maniwa *et al.* assumes implicitly that the deviation from a single-exponential function is the largest when the hyperfine coupling is purely anisotropic (in the case of $\alpha^{spin} = 0$). However, as shown in Fig. 5-18, this assumption is found to be *incorrect*, but instead, *the deviation is larger when the hyperfine coupling is substantially isotropic* (i.e., $A_{iso}{}^{spin}/A_{ax}{}^{spin} \approx 0.5$) for $0.01 < P(t) < 1$. Thus, it is found that their argument is physically misleading. Fourth, it is also to be noted that our model (i.e., the random distribution of a planar segment) assumes only the AHC of carbon sites with *uniform* density of states but not the LDOS due to the ICS. The very fact that, *both* the asymmetric line shapes *and* the NSER are successfully reproduced by our model, means that the AHC is the main origin of the NSER, and that the electronic states of the 60 carbon sites are found to be equivalent to a good approximation.

Finally in this section, we discuss the so-called "stretched exponential" fitting which was done by Tycko *et al.* and Stenger *et al.* for the ^{13}C NSER [Tycko *et al.*, 1992; Stenger *et al.*, 1995]. It is expressed as

$$P(t) \equiv 1 - M(t)/M_0 = \exp[-(t/T_1)^{\beta}], \tag{5-24}$$

where $M(t)$ (M_0) is the nuclear magnetization at time t after saturation (at

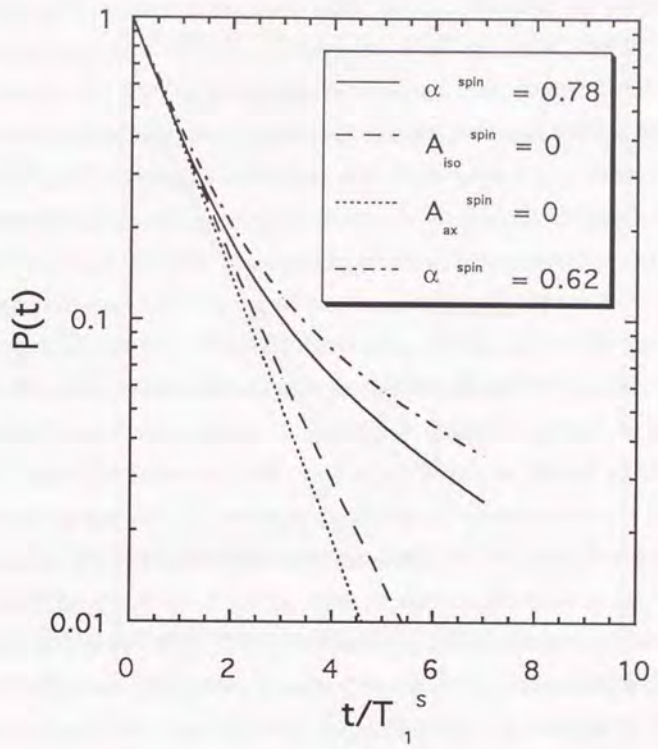

Fig. 5-18

Nuclear spin-lattice relaxation processes ($I = 1/2$) simulated for a powder sample in the presence of anisotropy in the hyperfine coupling $A_i{}^{spin}$. The anisotropy is represented by the ratio of α^{spin} ($= A_{iso}{}^{spin}/A_{ax}{}^{spin}$).

If the hyperfine coupling is *purely isotropic* (i.e., $A_{ax}{}^{spin} = 0$ or $\alpha^{spin} = \infty$), the relaxation is single-exponential, as shown by the dotted line. Note that $P(t/T_1{}^S = 1) = e^{-1} = 0.368$. On the contrary, in the case of *purely anisotropic* hyperfine coupling (i.e., $A_{iso}{}^{spin} = 0$ or $\alpha^{spin} = 0$), the relaxation deviates from the singe-exponential time evolution, as shown by the broken curve.

It is tempting to argue that the deviation from the single-exponential would be largest in the case of $A_{iso}{}^{spin} = 0$. However, as shown by the solid curve ($\alpha^{spin} = 0.78$) and the broken-dotted curve ($\alpha^{spin} = 0.62$), *the deviation is found to be largest when the hyperfine coupling is substantially isotropic* (i.e., $\alpha^{spin} = 0.5$).

thermal equilibrium), and β is a parameter (less than unity) which empirically characterizes the deviation from the single-exponential function: the smaller the value of β than unity, the more the recovery data deviates from the single-exponential time evolution. Stenger *et al.* argue that *all* their ^{13}C recovery data (10 K < T < 500 K) are well fitted by the stretched exponential functions with β = 0.85 (which is T independent), and regard the anisotropic $^{13}A_{ax}^{spin}$ as the origin of the NSER [Stenger *et al.*, 1995]. We attempted to fit our recovery data by the stretched exponential functions. As typically shown in Fig. 5-19, the data at *all* T < 55 K are *insufficiently* reproduced by the stretched exponential fittings: specifically, where the nuclear spins recover more than 90 % (i.e., $P(t) < 0.1$), the real nuclear spins relax *slower* than the stretched exponential curves. Moreover, the value of β is found to be 0.79 ± 0.02 in our case, which is smaller than that (β = 0.85) by Stenger *et al.* and Tycko *et al.*. We have no way to make clear the origin of this discrepancy because their recovery data are not published. In addition, it is to be noted that their recovery data at high T (~300 K > $T_{rotation}$) are reported to be NSER as well as those at low T. As Fig. 5-10 shows, our finding clearly contradicts their report and agrees to the report by Holczer *et al.* where the T dependence of the recovery shape is extensively studied for 8 K ≤ T ≤ 300 K [Holczer *et al.*; 1993]. Here we point out again that *both* our single-exponential recovery data (Fig. 5-10) *and* our symmetrical line shapes (Fig. 5-1) at $T > T_{rotation}$ are explained by the absence of the AHC as a result of the isotropic molecular motion.

§5-3-C2. Validity of the Korringa relation --- Up to room T

In Section 5-3-B, we concluded that the extended Korringa relation holds in the normal state from the T independence of $T_1^S T(K_{iso}^{spin})^2$, or equivalently, from the fact that both $\chi^{spin}(T)$ and T_1T are almost T independent below T < 55 K. Strictly speaking, however, their T independences are not true in the entire T range, since, with decreasing T below room T, not only $^{13}K_i^{spin}(T)$ (as

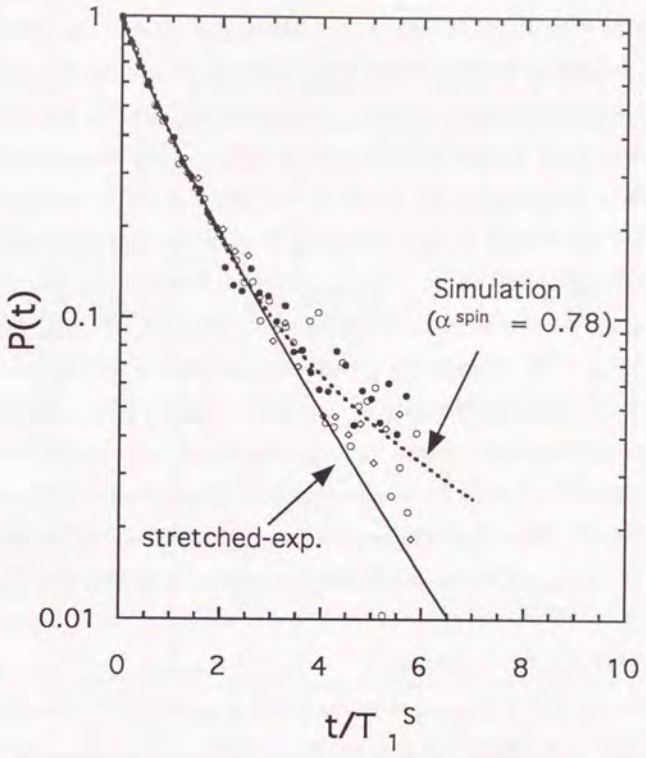

Fig. 5-19

As already shown in Fig. 5-17, the ^{13}C NMR spin-lattice relaxation data at low T (< 55 K) are found to be well reproduced by the simulation (the broken curve) for a powder sample in the case of α^{spin} = 0.78.

For the non-single exponential relaxation data, Tycko *et al.* and Stenger *et al.* argued that they were fitted by the so-called "stretched exponential" function given by Eq. (5-24). However, the stretched exponential function (the solid curve) does not reproduce the relaxation data satisfactorily: the stretched exponential fitting clearly fails for $0.1 > P(t) > 0.01$ although the fitting reproduces the data only for $1 > P(t) > 0.1$.

mentioned in Section 5-3-A) but also $1/(T_1T)$ decreases [Tycko *et al.*, 1992; Kiefl *et al.*, 1993; Stenger *et al.*, 1995]. In Fig. 5-20, in addition to the values of $1/(T_1^S T)$ at $T < 55$ K (where the magnetization $P(t)$ follows the NSER), we show three values of $1/(T_1T)$ at 300 K $\leq T \leq$ 320 K (where the $P(t)$ follows a single-exponential function). Apparently, the values of $1/(T_1T)$ at high T ($\geq$ 300 K) are almost equal to those of $1/(T_1^S T)$ at low T (< 55 K). However, it is not appropriate to interpret that the values of $1/(T_1^S T)$ at low T is extrapolated to those of $1/(T_1T)$ at high T with increasing T, since the electronic properties probed by the ^{13}C NMR above $T_{rotation}$ is different from those below $T_{rotation}$. Above $T_{rotation}$, the anisotropy in $^{13}K_i$ is not observable: $^{13}K_{ax}^{spin} \approx 0$, $^{13}K_{ax}^{orb} \approx 0$ (hence $^{13}K_{ax} \approx 0$), because the correlation rate $1/\tau_M$ of the C_{60} molecular motion is faster than the difference in the NMR frequency ($^{13}K_x$ - $^{13}K_z$) which would become finite if the motion were sufficiently slow. Indeed, the relation $^{13}K_{ax} \approx 0$ naturally explains the symmetrical line shapes (Section 5-1), and the relation $^{13}K_{ax}^{spin} \approx 0$ leads to the single-exponential recovery of $P(t)$. In other words, at $T > T_{rotation}$, the *modified* Korringa relation (Eq. (5-20)) is expected to hold as

$$T_1T(K_{iso}^{spin})^2 = S/K(\alpha) \qquad (\text{for } T > T_{rotation}). \tag{5-20}$$

On the contrary, at $T < T_{rotation}$, since the correlation rate $1/\tau_M$ is slower than the difference in the NMR frequency ($^{13}K_x$ - $^{13}K_z$), the anisotropy in $^{13}K_i$ is observable. In this case, as already discussed in Section 5-3-B, the modified Korringa relation is extended as

$$T_1^S T(K_{iso}^{spin})^2 = S/[K(\alpha)D_{ax}] \qquad (\text{for } T < T_{rotation}), \tag{5-21}$$

where

$$D_{ax} \equiv 1 + 2(A_{ax}^{spin}/A_{iso}^{spin})^2. \tag{5-25}$$

The D_{ax} value parameterizes the AHC: if the hyperfine coupling is purely isotropic ($A_{ax}^{spin} = 0$), the D_{ax} value is equal to unity. The larger the anisotropy, the larger the value of D_{ax} than unity. Here we define the value of $(T_1)_{iso}$ which is "renormalized" by the parameter D_{ax} as

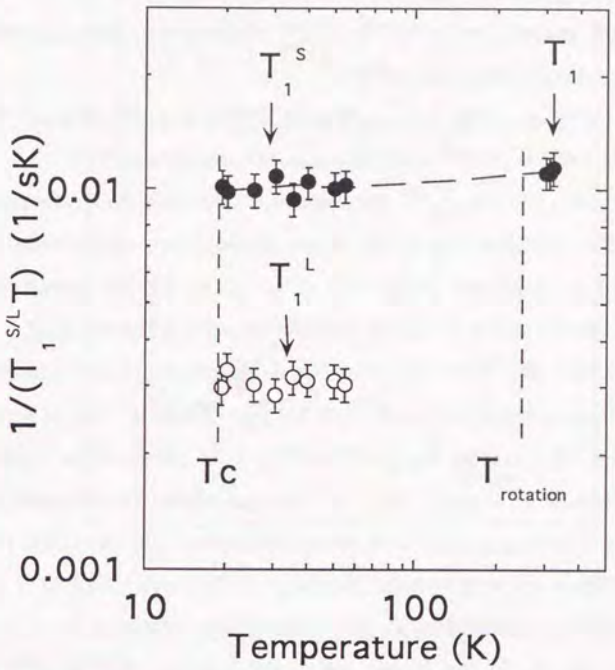

Fig. 5-20

T dependence of the ^{13}C-NMR $1/(T_1T)$ in the normal state at both low T (< 55 K) and high T (= 300, 310, and 320 K). At low T where the relaxation data show non-single exponential recoveries, the values of $1/(T_1T)$ are represented by T_1^S and T_1^L, which is defined by the initial and the "final" slope in the recovery data, respectively (Eq. (5-2)). At high T, the T_1 values are unambiguously defined owing to the single-exponential recoveries.

It is tempting to argue that the values of T_1^S at low T are extrapolated to the T_1 values at high T. However, in Section 5-3-C2, this interpretation is found to be physically *incorrect*.

$$(T_1)_{iso} \equiv T_1{}^S D_{ax}. \qquad (5\text{-}26)$$

Then, the extended Korringa relation (5-21) is expressed as

$$(T_1)_{iso} T (K_{iso}{}^{spin})^2 = S/K(\alpha) \qquad (\text{for } T < T_{rotation}). \qquad (5\text{-}27)$$

The value of D_{ax} in Eq. (5-25) is obtained by assuming axial $A_i{}^{spin}$: $A_x{}^{spin} = A_y{}^{spin}$. In the general case of $A_x{}^{spin} \neq A_y{}^{spin}$, the parameter for anisotropy D_{ax} is modified to [Kawamoto *et al.*, 1995b]

$$D_{ax} = 1 + (2/3)[(A_{ax,x}{}^{spin})^2 + (A_{ax,x}{}^{spin})(A_{ax,y}{}^{spin}) + (A_{ax,y}{}^{spin})^2]/[A_{iso}{}^{spin}]^2,$$

$$\text{where } A_{ax,x}{}^{spin} = (A_z{}^{spin} - A_x{}^{spin})/3, \; A_{ax,y}{}^{spin} = (A_z{}^{spin} - A_y{}^{spin})/3. \qquad (5\text{-}28)$$

In the case of $A_{ax,x}{}^{spin} = A_{ax,y}{}^{spin}$, this formula is reduced to the axial representation of Eq. (5-25). Hereafter, in order to discuss quantitatively the extended Korringa relation of Eqs. (5-26) and (5-27) for $T < T_{rotation}$, we use the general formula of Eq. (5-28) instead of Eq. (5-25) for the renormalization factor D_{ax}.

With the values of $^{13}K_i{}^{spin}$ shown in Fig. 5-11, which are found to be reliable owing to the negligible value of $^{13}(\Delta H/H)$ (Eq. (5-8)), we can now obtain the general value of D_{ax} from Eq. (5-28). In Fig. 5-21, we show the T dependence of the values of $1/[(T_1)_{iso}T]$ for $T < T_{rotation}$, which are obtained from Eq. (5-26). For $T > T_{rotation}$, we show the unambiguous value of $1/(T_1T)$ at 300 K owing to the single-exponential function of $P(t)$ and $^{13}K_{ax}{}^{spin}(T) \approx 0$. For comparison, the values of $1/[(T_1)_{iso}T]$ at low T are normalized to the value of $1/(T_1T)$ at 300 K. In the figure, the T dependences of $[^{13}K_{iso}{}^{spin}(T)]^1$ and $[^{13}K_{iso}{}^{spin}(T)]^2$ are also plotted. The values of $[^{13}K_{iso}{}^{spin}(T)]^1$ and $[^{13}K_{iso}{}^{spin}(T)]^2$ are both normalized to those at 300 K. The figure shows that $1/[(T_1)_{iso}T]$ has the same T dependence as $[^{13}K_{iso}{}^{spin}(T)]^2$, not as $[^{13}K_{iso}{}^{spin}(T)]^1$. In addition, the upper of Fig. 5-22 shows that the value of $(T_1)_{iso}T[^{13}K_{iso}{}^{spin}(T)]^2$ is T independent whereas the value of $(T_1)_{iso}T[^{13}K_{iso}{}^{spin}(T)]^1$ is substantially T dependent. The lower of the figure shows that $1/[(T_1)_{iso}T]$ is proportional to $[^{13}K_{iso}{}^{spin}(T)]^2$ not to $[^{13}K_{iso}{}^{spin}(T)]^1$. Therefore, we have confirmed that the extended Korringa relation holds for the electronic normal states of K_3C_{60} *above and below* $T_{rotation}$.

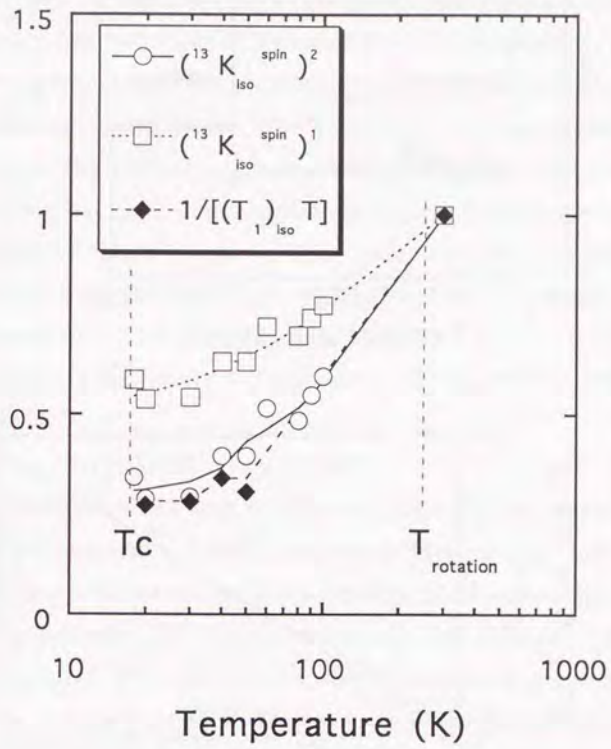

Fig. 5-21

Values of $(^{13}K_{iso}{}^{spin})^2$ (open circles) and $(^{13}K_{iso}{}^{spin})^1$ (open squares), both of which are normalized to those at high T (= 300 K), are plotted as a function of T, where $^{13}K_{iso}{}^{spin}$ is the isotropic part of the Knight shift. Also plotted are the values of $1/[(T_1)_{iso}T]$ (shown by closed diamonds) at low T (< 55 K) and the value of $1/(T_1T)$ at high T (= 300 K), where $(T_1)_{iso}$ represents the T_1 value renormalized by the anisotropy in the hyperfine couplings. The $1/[(T_1)_{iso}T]$ values at low T are normalized by the $1/(T_1T)$ value at 300 K.

This figure indicates that the extended Korringa relation holds up to room T, where both the anisotropy in the hyperfine couplings and the T dependence of the density of states are taken into account, since the $1/[(T_1)_{iso}T]$ has the same T dependence as $(^{13}K_{iso}{}^{spin})^2$, not as $(^{13}K_{iso}{}^{spin})^1$.

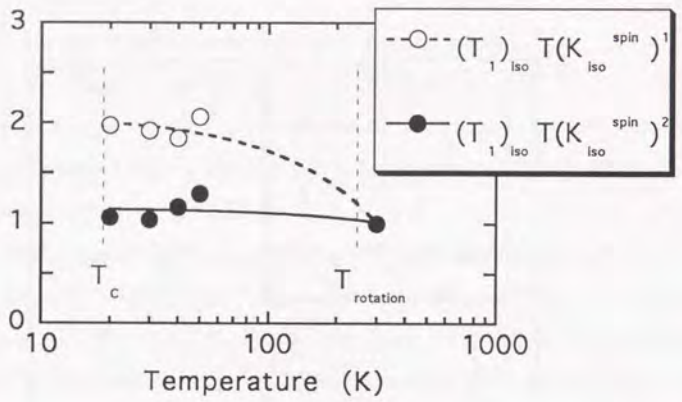

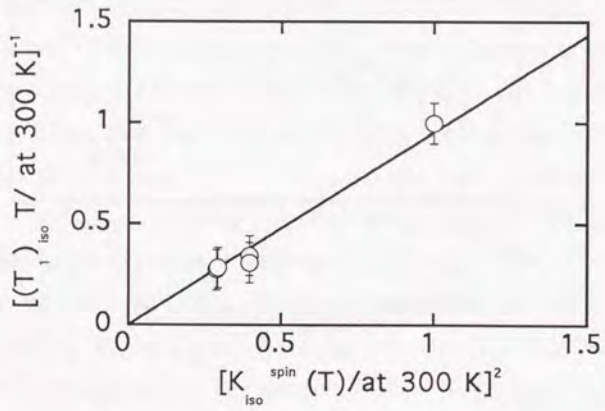

Fig. 5-22

Upper: values of $[(T_1)_{iso}T(^{13}K_{iso}{}^{spin})^1]$ (open circles) and $[(T_1)_{iso}T(^{13}K_{iso}{}^{spin})^2]$ (closed circles), both of which are normalized to those at high T (= 300 K), are plotted as a function of T, where $(T_1)_{iso}$ represents the T_1 value renormalized by the anisotropy in the hyperfine couplings and $^{13}K_{iso}{}^{spin}$ is the isotropic part of the Knight shift. Solid and broken line is an eye-guide.

Lower: values of $1/[(T_1)_{iso}T]$ at low T, which are normalized to the $1/(T_1T)$ value at 300 K, are plotted as a function of $[^{13}K_{iso}{}^{spin}/$ at 300 K$]^2$ with T as an implicit parameter. Solid line is the eye-guide obtained by least-squares fitting. It is found that the reduction of the value of $1/[(T_1)_{iso}T]$ is proportional to the decrease in the value of $[N_0(T)]^2$, owing to the validity of the extended Korringa relation (upper figure and Fig. 5-21).

Moreover, this proves the validity of the assumption that the decreases in the observed NMR shift $^{13}K_i$ are caused by the T-dependent Knight shift $^{13}K_i{}^{spin}(T)$ (equivalently, the T-dependent $\chi^{spin}(T)$). In this picture, the decrease in $1/[(T_1)_{iso}T]$ with decreasing T is well explained by the reduction in the density of states at the chemical potential $N_0(T)$. It should be noted that these results are sharply different from the results of the ^{17}O- and ^{89}Y-NMR in the cuprate oxide superconductors of $YBa_2Cu_3O_{6+x}$ [Pennington and Slichter, 1990; Yoshinari *et al.*, 1990]. In the case of the cuprate oxides, the apparent T independence of T_1T for the ^{17}O NMR of planar oxygen in $YBa_2Cu_3O_{6.9}$ does *not* mean a Korringa relation, since it is not $T_1T(K_{iso}{}^{spin})^2$ but $T_1T(K_{iso}{}^{spin})^1$ that is T independent for $YBa_2Cu_3O_{6+x}$ (x = 0.6 ~ 0.9) [Yoshinari *et al.*, 1990].

From Eqs. (5-20), (5-27), and the relation of $^{13}K_{iso}{}^{spin}(T) \propto \chi^{spin}(T) \propto N_0(T)$, we obtain

$$N_0(T_C)/N_0(300\ \mathrm{K}) = 0.55 \pm 0.08. \qquad (5\text{-}29)$$

It should be noted that such a large dependence of N_0 on T is *not* reproduced by *only* the thermal contraction of the lattice distance [Fleming *et al.*, 1991; Sparn *et al.*, 1991], but should be resultant from the effect of the *narrow band*. As is seen from Fig. 1-2, substantial T dependence is expected for the value of $N_0(T)$, since $N_0(T)$ represents the density of states at the *T-dependent* chemical potential (*not* at the Fermi energy) in general. Therefore, we believe that this result of Eq. (5-29) will be an experimental constraint on theoretical predictions, such as band calculation.

Since we found that the extended Korringa relation holds above and below $T_{rotation}$, we can obtain the $K(\alpha)_{nonax}$ value using the general formula of Eq. (5-28) for the renormalization factor D_{ax} , instead of the axial formula of Eq. (5-25). The T dependences of both $K(\alpha)_{nonax}$ (using Eq. (5-28)) and $K(\alpha)_{uniax}$ (using Eq. (5-25)) are shown in Fig. 5-23. The T-independent and large value of $K(\alpha)_{nonax}$ (= 7.4 ±1.2 > 1) verifies that the electronic system of the normal state is well described by the Fermi-liquid picture *above and below* $T_{rotation}$, where

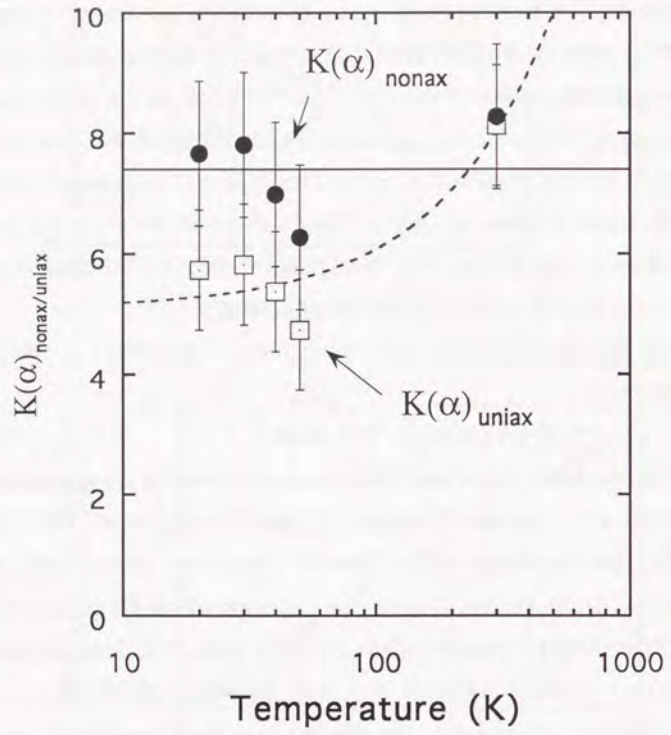

Fig. 5-23

T dependences of the values of $K(\alpha)_{nonax}$ and $K(\alpha)_{uniax}$, both of which are given by the *modified* Korringa relation of Eq. (5-20) at high T (= 300 K > $T_{rotation}$) and by the *extended* Korringa relation of Eq. (5-21) at low T (< 55 K < $T_{rotation}$).

At low T, the value of $K(\alpha)_{nonax}$ ($K(\alpha)_{uniax}$) is obtained using the renormalization factor D_{ax}, which is expressed by Eq. (5-28) (by Eq. (5-25)), in the presence (the absence) of the in-plane anisotropy of $^{13}K_x^{spin} \neq {}^{13}K_y^{spin}$. Both the solid line and the broken curve are obtained by least-squares fitting.

The T independence of $K(\alpha)_{nonax}$ above and below $T_{rotation}$, which is larger than unity, indicates that the electronic system of K_3C_{60} behaves as a Fermi liquid where the *antiferromagnetic* electron interaction can be treated *within the RPA up to 300 K*.

the *antiferromagnetic* electron interaction is treated within the RPA. Although this picture was already derived in Section 5-3-B *only* for T < 55 K < $T_{rotation}$ with the use of axial D_{ax}, it should be noted that, quite generally, the Korringa relation does *not* hold any more *at elevated T* for the electronic system where the antiferromagnetic interaction *could* be treated within the RPA *at low T* (< 300 K). This is because, as Moriya and Kawabata showed [Moriya and Kawabata, 1973], the interaction of spin-density fluctuation between *different* wave-vector q ("mode-mode coupling"), which was ignored by the RPA, should be taken into account self-consistently at high T. Therefore, this is the first time, to the knowledge of the author, that the Korringa relation holds up to room T with the $K(\alpha)$ value being enhanced. Indeed, in the case of BEDT-TTF superconductors, the ^{13}C NMR study revealed that the Korringa relation does *not* hold but their $1/T_1T$ ($\propto \sum_q[\chi''(q,\omega_0)/\omega_0]$) shows a Curie-Weiss-like T dependence with $K(\alpha)$ > 10 [Kawamoto *et al.*, 1995a]. The comparison on the electronic sates of K_3C_{60} and the BEDT-TTF superconductors [Kawamoto *et al.*, 1995; Mayaffre *et al.*, 1995] are shown in Table 5-III.

Table 5-III

	K_3C_{60} [present study]	κ-(BEDT-TTF)$_2$X [Kawamoto *et al.*; Mayaffre *et al.*]
coherence peak	present	absent
$[T_1T]^{-1}$ ($T < T_C$)	BCS s-wave	T^3-law (d-wave?)
$[T_1T]^{-1}$ ($T > T_C$)	extended Korringa $[(T_1)_{iso}T(K_{iso}^{spin})^2 = \text{const.}]$ up to 300 K	Curie-Weiss-like $[C/[T + \theta]]$ spin gap (?) above T_C
$K(\alpha)$	$7.4 \pm 1.2 < 10$	> 10

Chapter 6. ^{39}K NMR Study

§6-1. Static Properties --- Results of ^{39}K NMR Spectra

^{39}K NMR spectra at typical T (for $T_C < T < 300$ K) are shown in Fig. 6-1. The NMR shift is defined as the difference in the frequency between the ^{39}K NMR signal of the K_3C_{60} sample and that of the liquid KF at room T.

Below room T, two symmetrical lines are observed down to about 100 K (denoted as T^*). The higher (lower) NMR frequency, denoted as $^{39}K_T$ ($^{39}K_O$), is assigned to two tetrahedral (T) (one octahedral (O)) potassium sites which are intercalated per unit C_{60}, since the intensity of the T-line is about twice as that of the O-line. For $T > T^*$, the two lines are well reproduced by least squares fitting with two Gaussian or Lorentzian lines. Although no substantial differences in the reproducibility were observed between the two fittings, the Gaussian (Lorentzian) ones were slightly better at higher (lower) T. It is to be noted that, despite the finite electric quadrupole moment (^{39}Q) of the ^{39}K nucleus ($^{39}Q = 0.11 \times 10^{-24}$ cm^2, which is comparable to the quadrupole moment of the copper nucleus $^{63/65}$Q of $0.15/0.16 \times 10^{-24}$ cm^2), no quadrupole splittings were observed for both the T- and O-lines within the resolution of the present study. This means that the electric field gradient at both the T- and O-sites is too small to be observed (close to zero), due to the high symmetries of the both sites. Below T^*, an additional line (which we denote as T'-line) starts to appear whose NMR frequency and width are larger than those of the T-lines. With decreasing T (~ 60 K $< T < T^*$), the intensity of the T'-line increases whereas that of the T-line decreases. However, the sum of the intensity of the T- and T'-lines is roughly twice as the intensity of the O-line for $T_C < T < T^*$. The similar behaviors for the additional T'-line are also observed in the ^{87}Rb NMR spectra in Rb_3C_{60} [Walstedt *et al.*, 1993]. In their study, they revealed that the T'-sites are connected to the T-sites using the spin echo double resonance (SEDOR) technique, in

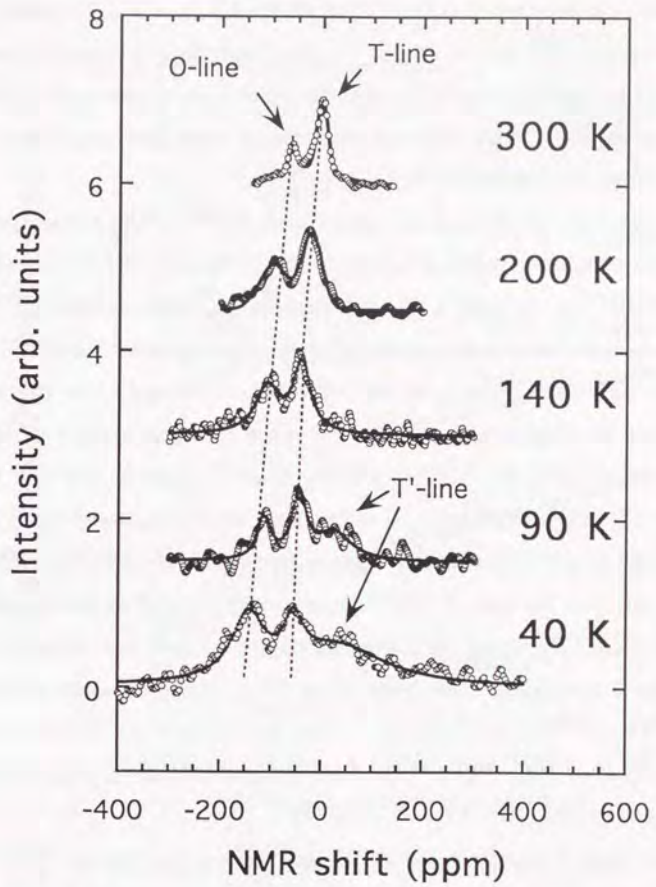

Fig. 6-1

Open circles show the ^{39}K NMR spectra of our superconducting fulleride K_3C_{60} (T_C = 19.4 K) at typical T ($T_C < T < 300$ K) under a static magnetic field of 7.06 tesla.

Two symmetrical lines are observed down to ~100 K (= T^*). From the intensity ratio of 2 to 1, the higher and lower peak frequency, denoted as $^{39}K_T$ and $^{9}K_O$, is assigned to the T- and O-site potassiums. Below T^*, an additional line at ~ 50 ppm (denoted as T'-line) starts to grow whereas the T-line intensity decreases. As shown by the solid curves, the spectra are fitted by two (three) Gaussians or Lorentzians above T^* (below T^*). Note that no quadrupole-split lines are observed.

addition to the relationship for the intensity of the T-, T'-, and O-lines. Thus, it is very likely to conclude that the T'-line for the K_3C_{60} at $T < T^*$ comes from the T-line above T^*. Below T^*, the observed overall line shapes were well reproduced by least squares fitting with three Gaussian or Lorentzian lines. As in the case of $T > T^*$, no substantial differences were observed between the Gaussians and the Lorentzians for $T_C < T < T^*$.

In Fig. 6-2, we show the T dependences of $^{39}K_T$, $^{39}K_O$, $^{39}K_T$', and the half-widths at half-maximum (HWHM) of the T-, O-lines. With decreasing T, both $^{39}K_T$ and $^{39}K_O$ decrease with small step-like reductions at about 235 K (= $T_{rotation}$). As mentioned in the previous chapter, the decreases in the NMR shifts are also observed in the case of the ^{13}C NMR and found to be due to the decreases in the Knight shifts ($^{13}K_i^{spin}$) instead of the chemical shifts ($^{13}K_i^{orb}$). Since the relationship of $^{13}K_i^{spin} \propto \chi^{spin} \propto {}^{39}K_{T/O}{}^{spin}$ (= the Knight shift at the potassium T- and O-sites) holds, it is expected that $^{39}K_{T/O}$ and $^{13}K_i$ have the same T dependence if the chemical shifts at the potassium sites ($^{39}K_{T/O}{}^{orb}$) is T independent, as in the case of $^{13}K_i^{orb}$. As shown in Fig. 6-3(a), this is actually observed in the $^{39}K_T$ versus $^{13}K_{iso}$ plot, although the values are rather scattered mainly due to the slight T dependence of the $^{13}K_{iso}$. Moreover, as shown in Fig. 6-3(b), $^{39}K_T$ and $^{39}K_O$ have the same T dependence. These two facts mean that, as in the case of $^{13}K_i$, $^{39}K_{T/O}{}^{orb}$ is T independent and the T dependence of $^{39}K_{T/O}$ is due to $^{39}K_{T/O}{}^{spin}$.

With decreasing T, the widths of the T- and O-lines (denoted as $^{39}\Gamma_T$, $^{39}\Gamma_O$, respectively) increase at about 235 K (= $T_{rotation}$). However, below $T_{rotation}$, no substantial line broadenings were observed within the error ranges of the experimental data and of the decomposing process. As is seen from Fig. 6-1, it is true that the width of the overall line shape gets broader below T^*. However, by decomposing the rather complex spectrum into three Gaussians or Lorentzians, it is found that neither $^{39}\Gamma_T$ nor $^{39}\Gamma_O$ gets larger. Instead, it is the width of the T'-line that causes the increase in the width of the overall line shape. The rather

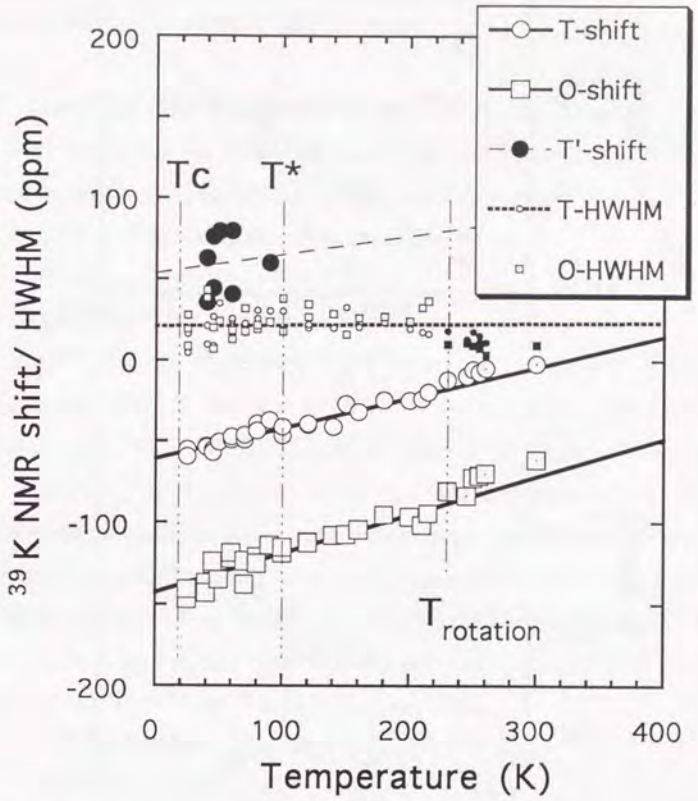

Fig. 6-2

T dependences of the ^{39}K NMR shifts for the T-, O- and T'-lines (denoted as $^{39}K_T$, $^{9}K_O$, and $^{39}K_T$') are shown by open circles, open squares, and closed circles, respectively. Both $^{39}K_T$ and $^{39}K_O$ decrease linear in T with no anomalies down to T_C, except the small step-like reductions at $T_{rotation}$. Two solid lines for the $^{39}K_T$ and $^{39}K_O$ are obtained by the least-squares fitting for the data below $T_{rotation}$.

T dependences of the half-widths at half-maximum (HWHM) for the T- and O-lines (denoted as $^{39}\Gamma_T$ and $^{39}\Gamma_O$) are shown by open circles and open squares (the sizes of which are smaller than those of $^{39}K_T$ and $^{39}K_O$), respectively. Broken line for the $^{39}\Gamma_T$ is obtained by least-squares fitting for the data below $T_{rotation}$. Except for the increases at $T_{rotation}$, both $^{39}\Gamma_T$ and $^{39}\Gamma_O$ are almost T independent below $T_{rotation}$.

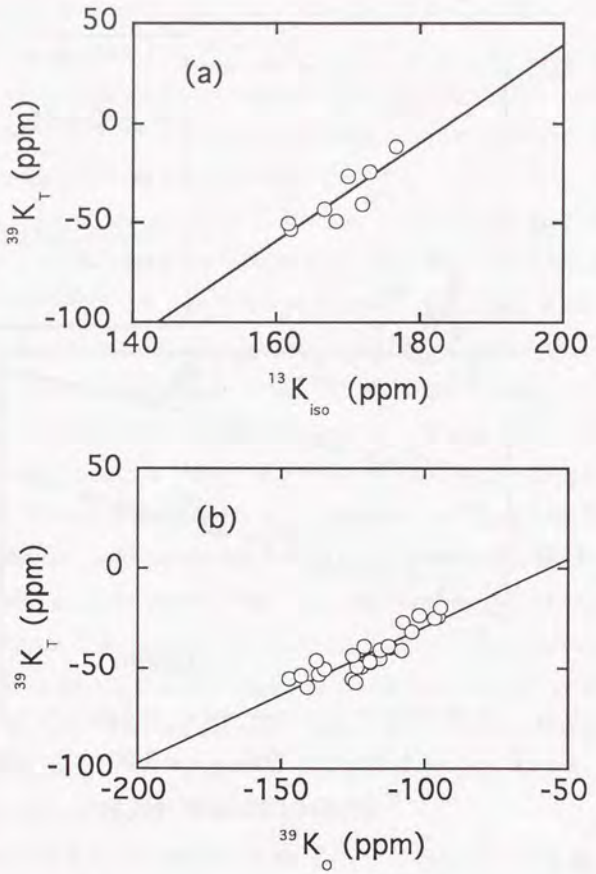

Fig. 6-3

(a) ^{39}K NMR shift for the T-line ($^{39}K_T$) is plotted as a function of isotropic part of the ^{13}C NMR shifts ($^{13}K_{iso}$) with T as an implicit parameter. Both $^{39}K_T$ and $^{13}K_{iso}$ have the same T dependence although the values of $^{13}K_{iso}$ are rather scattered due to their smaller dependence on T.

(b) $^{39}K_T$ is plotted as a function of $^{39}K_O$ (the NMR shifts for the O-line) with T as an implicit parameter. Both $^{39}K_T$ and $^{39}K_O$ have the same T dependence.

In both figures, only the data are for $T < T_{rotation}$ are shown and the solid lines are obtained by least-squares fitting.

larger scatterings in the data of $^{39}K_T$, $^{39}K_O$, $^{39}\Gamma_T$ and $^{39}\Gamma_O$ below T^* come from the ambiguities in the process of decomposing since the intensity of the T-line decreases and the width of the T'-line increases.

§6-2. Analyses and Discussions on ^{39}K NMR Study

First, we discuss the T dependences of $^{39}K_T$ and $^{39}K_O$. Unlike the case of ^{13}C nucleus, we take into account of only *isotropic* hyperfine couplings ($^{39}A_{T/O}$) for the ^{39}K NMR shifts. In general, they are expressed as

$$^{39}K_k(T) = {}^{39}K_k^{spin}(T) + {}^{39}K_k^{orb}(T),$$

$$^{39}K_k^{spin}(T) = {}^{39}A_k^{spin}\chi^{spin}(T),$$

$$^{39}K_k^{orb}(T) = {}^{39}A_k^{VV}\chi^{VV}(T) + {}^{39}A_k^{core}\chi^{core}. \qquad (k = T\text{- or O-sites})$$

As is common, $^{39}K_k^{orb}$ is considered to be T independent since the T dependence of chemical shift is ordinarily of the order of 1 ppm in the T range of the present study. However, we need to *examine* the T *independences* of $^{39}K_k^{orb}$ *experimentally*, because the lattice contraction can possibly change the valence states of the potassium ions and cause the T-dependent $^{39}K_k^{orb}$. First, it should be noted that, as proved in the previous chapter, the T dependence of $^{13}K_i$ is ascribed to the Knight shifts $^{13}K_i^{spin}$ (hence the T-dependent $\chi^{spin}(T)$), and that the chemical shifts $^{13}K_i^{orb}$ are T independent, namely,

$$^{13}K_i(T) = {}^{13}K_i^{spin}(T) + {}^{13}K_i^{orb}, \qquad (6\text{-}1a)$$

$$^{13}K_i^{spin}(T) = {}^{13}A_i^{spin}\chi^{spin}(T) \qquad (i = x, y, z, \text{iso, ax}). \qquad (6\text{-}1b)$$

Second, Fig. 6-3(a) shows that $^{39}K_T$ has the same T dependence as $^{13}K_{iso}$. Therefore, it is concluded that, also at the potassium sites, the chemical shifts $^{39}K_k^{orb}$ are T independent and the T dependence of $^{39}K_k$ comes from $\chi^{spin}(T)$, that is,

$$^{39}K_k(T) = {}^{39}K_k^{spin}(T) + {}^{39}K_k^{orb}, \qquad (6\text{-}2a)$$

$$^{39}K_k^{spin}(T) = {}^{39}A_k^{spin}\chi^{spin}(T), \qquad (6\text{-}2b)$$

$$^{39}K_k^{orb} = {}^{39}A_k^{VV}\chi^{VV} + {}^{39}A_k^{core}\chi^{core}. \qquad (k = T\text{- or O-sites}) \quad (6\text{-}2c)$$

As shown in Fig. 6-2, for $T_C < T < T_{rotation}$, both $^{39}K_T$ and $^{39}K_O$ are well

reproduced by T-linear relations (the solid lines in the figure) as

$$^{39}K_T(T) = -60.8 + 0.189T, \quad (6\text{-}3a)$$

$$^{39}K_O(T) = -142.5 + 0.235T, \quad (T_C < T < T_{rotation}) \quad (6\text{-}3b)$$

where the units are in ppm. This means that the increase in $\chi^{spin}(T)$ is approximately proportional to T. This was not deduced from the analyses of $^{13}K_i$ because of their smaller T dependences than $^{39}K_k$.

The slope in Fig. 6-3(a) gives the ratio of the isotropic hyperfine coupling at the potassium T-sites to that at the carbon sites as

$$^{39}A_T^{spin} / {}^{13}A_{iso}^{spin} = 2.46 \pm 0.45. \quad (6\text{-}4a)$$

On the other hand, from the slope in Fig. 6-3(b), we obtain the ratio of the isotropic hyperfine coupling at the potassium T-sites to that at the O-sites as

$$^{39}A_T^{spin} / {}^{39}A_O^{spin} = 0.80 \pm 0.15. \quad (6\text{-}4b)$$

Eqs. (6-2) and (6-3) give

$$[^{39}K_k(T_C) - {}^{39}K_k^{orb}] / [^{39}K_k(300\ K) - {}^{39}K_k^{orb}] = \chi^{spin}(T_C) / \chi^{spin}(300\ K). \quad (6\text{-}5)$$

Since the right-side of Eq. (6-5) is given from the ^{13}C NMR study as

$$\chi^{spin}(T_C) / \chi^{spin}(300\ K) = {}^{13}K_i^{spin}(T_C) / {}^{13}K_i^{spin}(300\ K) = 0.55 \pm 0.08, \quad (5\text{-}29)$$

we obtain the chemical shifts at the potassium sites as

$$^{39}K_T^{orb} = -121 \pm 10\ ppm, \quad (6\text{-}6a)$$

$$^{39}K_O^{orb} = -218 \pm 15\ ppm. \quad (6\text{-}6b)$$

It is desirable to obtain the chemical shifts directly from ^{39}K NMR spectra well below T_C. However, since the S/N of the ^{39}K NMR signal was poorer and their spin-lattice relaxation time was longer by about ten times than the case of ^{13}C NMR, it would have taken too much time to obtain the ^{39}K NMR spectra, thus it would not be practical. Therefore, we did not go so far as to perform the measurements but obtained Eq. (6-6) from the analysis.

Second, we discuss the origin of the additional T'-line.

The first picture to be considered is that the T'-sites is displaced from the exact center of the gravity of the tetrahedron formed by the C_{60} molecules (T-sites). The deviation from the T-sites produces a finite value of the electric field

gradient (EFG) at the T'-sites, hence the difference in the NMR shift. In this case, since the T'-line appears as a satellite line of the center T-line due to the EFG, two additional lines should be observed *above and below* the T-line symmetrically in the NMR frequency, as mentioned in Chapter 2. However, the T'-line is observed *only above* the T-line. Therefore, this picture is found not to be true.

Since the T'-line is proved not to be caused by the EFG effect, it should come from the *local* difference in the Knight shift and/or the chemical shift between the T'- and T-sites. If the T'-line is caused by the *local* difference in the *Knight shifts alone*, it is expressed as

$$^{39}K_T{}'^{orb} = {}^{39}K_T^{orb}, \quad (6\text{-}7a)$$

$$^{39}K_T{}'^{spin} - {}^{39}K_T^{spin} = \Delta(^{39}K_T^{spin}). \quad (6\text{-}7b)$$

By dividing the both sides of Eq. (6-7b) by $^{39}K_T^{spin}$, we obtain

$$^{39}K_T{}'^{spin}/{}^{39}K_T^{spin} - 1 = \Delta(^{39}K_T^{spin})/{}^{39}K_T^{spin}. \quad (6\text{-}8)$$

From Fig. 6-2, we obtain

$$^{39}K_T' = 60 \pm 25\ ppm,\ {}^{39}K_T = -50 \pm 10\ ppm\ (for\ T_C < T < T^*). \quad (6\text{-}9)$$

Since Eqs. (6-6a) and (6-7a) give $^{39}K_T{}'^{orb} = {}^{39}K_T^{orb} = -121 \pm 10$ ppm, and by using the relation of $^{39}K_k^{spin} = {}^{39}K_k - {}^{39}K_k{}'^{orb}$ (k = T, T') and Eq. (6-9), we obtain

$$^{39}K_T{}'^{spin}/{}^{39}K_T^{spin} - 1 = 2.65 \pm 0.75. \quad (6\text{-}10)$$

On the other hand, since we assumed that $\Delta(^{39}K_T^{spin})$ is caused by the *local* distribution in the Knight shifts at the T-sites, the relation

$$\Delta(^{39}K_T^{spin})/{}^{39}K_T^{spin} = \Delta(\chi^{spin})/\chi^{spin} \quad (6\text{-}11)$$

holds, where $\Delta(\chi^{spin})$ is the deviation from the mean value of the uniform susceptibility χ^{spin}, which results from the "local density of states (LDOS)" discussed in Section 5-3-C1. Thus, from Eqs. (6-8), (6-10), and (6-11), we obtain

$$\Delta(\chi^{spin})/\chi^{spin} = 2.65 \pm 0.75. \quad (6\text{-}12)$$

Clearly, this result is not appropriate from the following reasons: first, this

value (2.65 ± 0.75) is quite different from the finding by the ^{13}C NMR (Section 5-3-C1) that the LDOS, if any, contributes little to both the asymmetric spectra and the non-single exponential recoveries (NSER). Second, in this scenario, the *absence* of O'-line would lead to the picture that the value of $\Delta(\chi^{spin})/\chi^{spin}$ is ~ 0 at *all* O-sites, whereas the value is ~ 0 at T-sites, 2.65 at T'-sites, and ~ 0 at *all* carbon sites. Although it could be possible to imagine that χ^{spin} is qualitatively modulated spatially in this way, this is very unlikely since, among others, the value of the modulation at the T'-sites (which is *much larger* than unity) invalidates the assumption that the local distribution of χ^{spin} is described as the *deviation* from its mean value of the *uniform* susceptibility. Thus, we can conclude that the appearance of the T'-line cannot be explained by the *local* difference in the *Knight shifts alone*.

On the contrary, the unrealistic distribution of $\Delta(\chi^{spin})/\chi^{spin}$ expressed by Eq. (6-12) is *not* required *if* we assume that the distribution in the *chemical shifts*, instead of the Knight shifts, plays the main part of causing the presence of the T'-line, that is,

$$^{39}K_T' - {}^{39}K_T \approx {}^{39}K_T'^{orb} - {}^{39}K_T^{orb}. \quad (6\text{-}13)$$

In this case, since the chemical shift depends on the local electronic states (the valences of the potassium ions), both the *absence* of the O'-line *and* the presence of the T'-line are explained by a scenario that one and only valence state exists at the O-sites whereas there are two valence states resulting in the T- and T'-sites. Specifically, Eqs. (6-6), (6-9), and (6-13) give

$$^{39}K_T'^{orb} \approx 10 \pm 25 \text{ ppm}. \quad (6\text{-}14)$$

This indicates that the valence of the T'-sites is nearly equal to +1, since our ^{39}K NMR shift is defined relative to that of liquid KF. On the other hand, Eq. (6-6) means that the *ionization* at both the T- and O-sites is *incomplete* and the valence of the T- (O-) sites is $+1 - \delta_T$ ($+1 - \delta_O$) where $0 < \delta_T < \delta_O < 1$. In other words, the intra-ionic valences are *differentiated* at the T-, T'-, and O-sites [Pfeiffer *et al.*, 1982]. In addition, since the electrons are doped from the

potassiums to the C_{60} molecules, the result of Eq. (6-6) is understandable if we take into account that the distance from the molecule is larger at the O-sites than the distance at the T-sites.

For a specific physical picture of the T'-sites, two possibilities are thought of, as was also done by Walstedt *et al.* [Walstedt *et al.*, 1993]. As is illustrated in Fig. 6-4, one is that all the four neighboring O-sites are displaced to the T-sites *without* causing finite EFG at *any* of the O-sites. Although this could produce the differentiation in the valences at the T-sites (causing the T'-sites), it is very likely that, at the same time, this could result in the appearance of O'-sites. The other possibility is the *incomplete* orientational order of the C_{60} molecules below T^*. Since the early stage of the studies on superconducting fullerides, it has been proposed that, at low T where the molecular motion is frozen, there exists *two* orientations of the C_{60} molecules (the low-T structure of A_3C_{60} is called "*merohedral disorder*") [Stephens *et al.*, 1991]. One of the orientations is that a C_{60} molecule nearest to a T-site faces its hexagon to the T-site (denoted as "C6-T"), and the other is that the molecule faces its pentagon to the T-site (denoted as "C5-T"). In addition, it is known that the "C6-T" configuration is dominated and that the "C5-T" case occurs no more than 25 %. In Fig. 6-5, we show the peak intensity ratios of the T- and T'-lines to the O-lines (denote as I^{peak}(T/O) and I^{peak}(T'/O), respectively) as a function of T. Since, as is seen from the figure, the peak intensity of the T'-line (although rather scattered mainly due to the larger width) is found to be no more than half of the T-line, the T'-line is considered to correspond to the "C5-T" configuration. This picture is consistent with the fact that O'-line is not observed, since it is less likely that the orientational difference of the C_{60} molecules nearest to the T-site changes the local valence states at the O-site which has higher symmetry and longer distance from the C_{60} molecules than the T-site. It should be noted that the T^* for K_3C_{60} is smaller (100 K) than that for Rb_3C_{60} (370 K) [Walstedt *et al.*, 1993]. Taking into account that the ion radius of Rb^+ (1.49 Å) is larger than that

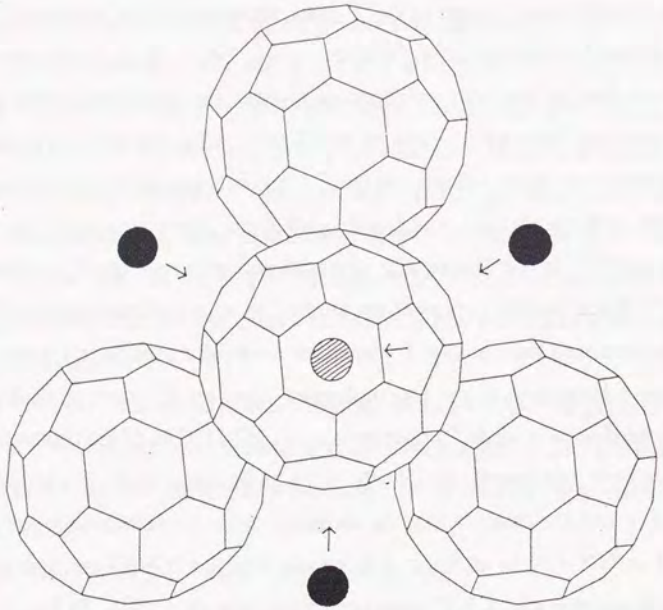

Fig. 6-4

View of the local surrounding around the T-site potassium (shown by the hatched circle) which is located through hexagonal faces of the C_{60} molecule in the foreground.
The possible clustering of neighboring O-site potassiums (shown by closed circles) is indicated by arrows.
If the orientations of the molecules were ordered completely, all the four neighboring molecules would face their hexagons to the T-site (denoted as "C6-T" case in the text). In the case of *incomplete* ordering of the C_{60} molecules, some of them face their pentagon to the T-site (denoted as "C5-T" case in the text). In this figure, the arrow on the molecule in the foreground shows a rotation from "C6-T" to "C5-T" orientation.

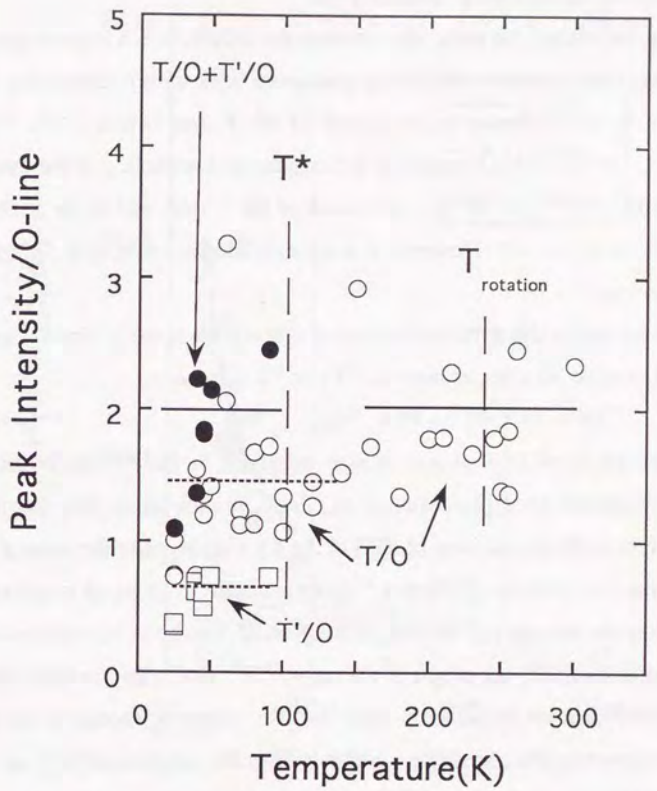

Fig. 6-5

T dependences of the peak intensity ratio of the T-line to the O-line (shown by open circles and denoted as $I^{peak}(T/O)$) and that of the T'-line to the O-line (shown by open squares and denoted as $I^{peak}(T'/O)$) for $T < T^*$. Above T^*, $I^{peak}(T/O) \approx 2$. Below T^*, as two broken lines guide the eye, $I^{peak}(T/O) \approx 1.4$ (< 2) and $I^{peak}(T'/O) \approx 0.6$. Above and below T^*, the sum rule of $I^{peak}(T/O) + I^{peak}(T'/O) \approx 2$ holds for the peak intensity.

of K^+ (1.38 Å) [Shannon and Prewitt, 1970], this means that the appearance of the T'-line is considered to come from the freezing of the C_{60} molecular motion, which also supports qualitatively the picture that the orientational disorder of the C_{60} molecules causes the potassium T'-sites .

Third, we discuss the possibility whether the LDOS, which is not observed at the carbon sites, is observable at the potassium sites, or not. Since Fig. 6-2 shows no clear-cut increases in the widths of the T- and O-line ($^{39}\Gamma_T$, $^{39}\Gamma_O$, respectively) at T^*, it could be possible to attribute the broadening of the overall line shapes below T^* *only* to the appearance of the T'-line and to its growing width, as shown in Fig. 6-6. However, this interpretation is found to be *incorrect* in the followings.

In Fig. 6-6, the half-width at the half-maximum (HWHM) of the T'-line (denoted as $^{39}\Gamma_T$') is close to 10 times as large as $^{39}\Gamma_T$ or $^{39}\Gamma_O$, namely,

$$^{39}\Gamma_T' \approx 10 \times {}^{39}\Gamma_T \approx 10 \times {}^{39}\Gamma_O. \qquad (6\text{-}15)$$

Broad width of an additional line is also observed in the $^{85/87}$Rb NMR of Rb_3C_{60} by Yoshinari *et al.* [Yoshinari *et al.*, 1994]. In their study, they ascribed the large width to the distribution of EFG at the Rb-sites because the ratio of the widths for the two isotopes (^{85}Rb and ^{87}Rb) was found to be equal to the ratio of the quadrupole moments of the two. In the present case, however, this method is not available to clarify the origin of the large $^{39}\Gamma_T$', since there exist no other isotopes which possess sufficiently large nuclear magnetic moments for the NMR measurements. In principle, whether or not the distributed EFG at the T'-sites contributes to the large $^{39}\Gamma_T$' can be verified by investigating the dependence of the value of $^{39}\Gamma_T$' on the magnetic field (H_0). However, since all the NMR spectra are obtained under the maximum field (H_0 = 7.06 tesla) of our magnet, reducing the value of H_0 results in making the poor S/N of the present ^{39}K NMR signals much poorer. Moreover, we are concerned in the presence of LDOS on the potassium sites instead of the origin of the large $^{39}\Gamma_T$'. Thus, we discuss the widths of the spectra from a different manner.

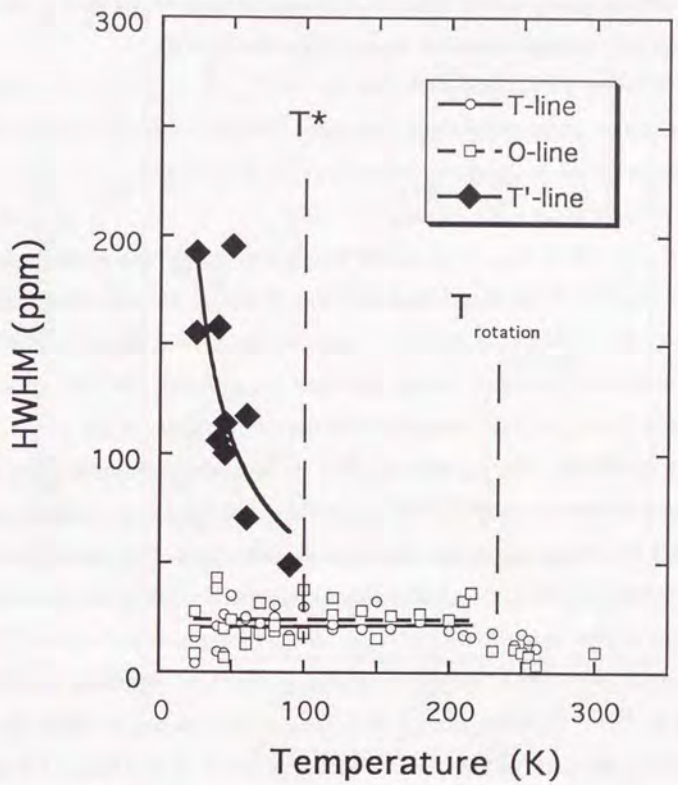

Fig. 6-6

T dependences of the half-widths at half-maximum (HWHM) of the T-, O-, and T'-line (denoted as $^{39}\Gamma_T$, $^{39}\Gamma_O$, and $^{39}\Gamma_T$') which are shown by open circles, open squares, and closed diamonds, respectively. The widths, as well as the peak frequencies and intensities, are obtained by least-squares fitting as free parameters.

With decreasing T (< T^*), the width $^{39}\Gamma_T$' anomalously increases, whereas, as shown also in Fig. 6-2, neither $^{39}\Gamma_T$ nor $^{39}\Gamma_O$ does.

As is shown in Fig. 6-5, the expected sum rule on the *peak* intensity roughly holds below T^* although the data are rather scattered, namely,

$$I^{peak}(T/O) + I^{peak}(T'/O) \approx 2. \quad (6\text{-}16)$$

On the contrary, as is shown in Fig. 6-7, the sum rule does *not* hold if we take the *integrated* intensity instead of the *peak* intensity, that is,

$$I^{integ}(T/O) + I^{integ}(T'/O) \approx 5 \pm 3\ (> 2). \quad (6\text{-}17)$$

The invalidation of the sum rule is, as is seen also from Fig. 6-7, mainly due to the anomalously larger integrated intensity of the T'-sites of

$$I^{integ}(T'/O) \approx 4.7 \pm 2.7\ (> 2). \quad (6\text{-}18)$$

Since the sum rule is found to hold for the peak intensity, the anomaly in Eq. (6-18) is ascribed to the large value of $^{39}\Gamma_T$'. It should be noted that it is not appropriate to ascribe the large $^{39}\Gamma_T$' to only the presence of distributed EFG on the T'-line (*electric* origin), if any, because the sum rule for the integrated intensity holds in general, irrespective of the origin of the width of the line; magnetic or electric. The anomaly in $^{39}\Gamma_T$' is *only* understandable *if* we take into account that the values of $^{39}\Gamma_T$, $^{39}\Gamma_O$, and $^{39}\Gamma_T$' were obtained by decomposing the overall line shape into three Gaussians or Lorentzians. The decompositions were performed by the least-squares fittings with their NMR shifts, intensities, and widths as free parameters. Thus, Eq. (6-18) means that the value of $^{39}\Gamma_T$' was obtained to be *larger misleadingly* than the *intrinsic* width of the T'-line (denoted as $^{39}\Gamma_T{}'^{real}$) in the process of the decomposition, due to the analytical artifact that some parts of the intrinsic widths of the T- and/or O-line (denoted as $^{39}\Gamma_T{}^{real}$, $^{39}\Gamma_O{}^{real}$, respectively) were added to $^{39}\Gamma_T{}'^{real}$, that is,

$$^{39}\Gamma_T{}'^{real} < {}^{39}\Gamma_T', \quad (6\text{-}19a)$$

$$^{39}\Gamma_T{}^{real} > {}^{39}\Gamma_T \quad (6\text{-}19b)$$

$$^{39}\Gamma_O{}^{real} > {}^{39}\Gamma_O. \quad (6\text{-}19c)$$

In other words, Eq. (6-19) means that *both* $^{39}\Gamma_T{}^{real}$ and $^{39}\Gamma_O{}^{real}$ should *increase* below T^*. Thus, it is *incorrect* to attribute the broadening of the overall line shapes to *only* the increase in $^{39}\Gamma_T$', and to interpret the *apparent* T independences

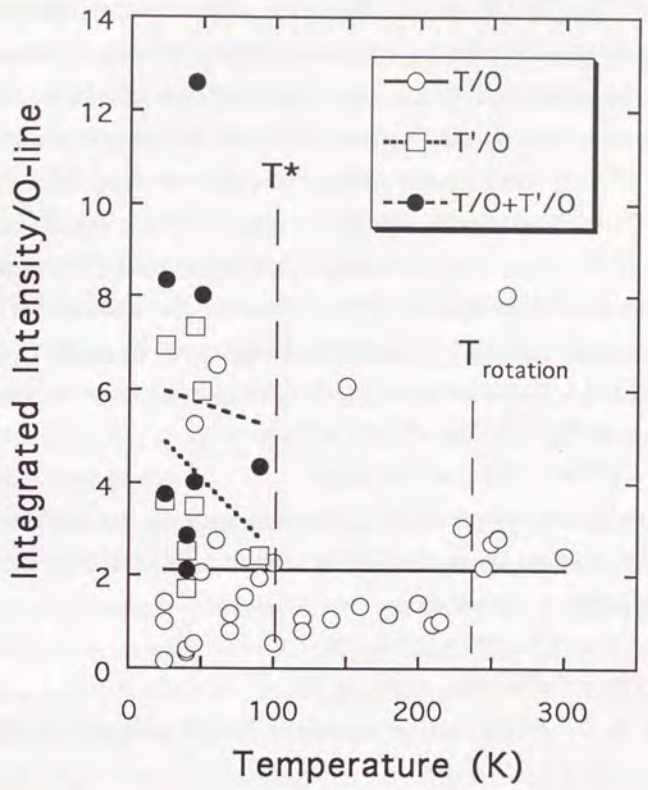

Fig. 6-7

T dependences of the integrated intensities of the T- and T'-line, both of which are normalized to the intensity of the O-line. The normalized intensities are denoted as $^{39}I^{integ}(T/O)$ and $^{39}I^{integ}(T'/O)$, and shown by open circles and open squares for the T- and T'-line, respectively.
Unlike the case of the peak intensity (Fig. 6-5), the expected sum rule of $^{39}I^{integ}(T/O) + {}^{39}I^{integ}(T'/O) \approx 2$ does *not* hold for $T < T^*$, where the integrated intensities are defined as $^{39}I^{integ}(k/O) = {}^{39}I^{peak}(k/O) \times (^{39}\Gamma_k/{}^{39}\Gamma_O)$ for k = T, T'. The invalidation of the sum rule is ascribed to the anomalously larger value of $^{39}\Gamma_T$' at lower T (Fig. 6-6).

of the values of $^{39}\Gamma_T$ and $^{39}\Gamma_O$ above and below T^* as no traces of the broadening of the T- and O-lines.

As already mentioned, we have no way of clarifying the origin of the growing widths of $^{39}\Gamma_{T/O/T}{}'^{real}$ without the spectra under different values of H_0. Thus, it remains to be solved whether the increases in $^{39}\Gamma_{T/O/T}{}'^{real}$ below T^* are caused by either the LDOS (magnetic origin) or the distribution in EFGs (electric origin), or both. Here we only check the validity of the magnetic origin. Since we found that the least-squares fitting gives the values of $^{39}\Gamma_{T/O/T}{}'$ (*not* $^{39}\Gamma_{T/O/T}{}'^{real}$), we have no other way but to "read" the real widths $^{39}\Gamma_{T/O/T}{}'^{real}$ directly from the spectra with ambiguities. In order to reduce the ambiguities, we estimate the real width at the O-line rather than the width at the T- and T'-line, because the T-line is substantially superimposed by the T'-line, as is seen from Fig. 6-1. The typical increase at 40 K, which is denoted as $\Delta[^{39}\Gamma_O{}^{real}(40\ K)]$, is given by $^{39}\Gamma_O{}^{real}(40\ K) - {}^{39}\Gamma_O\ (T>T^*)$, hence

$$\Delta[^{39}\Gamma_O{}^{real}(40\ K)] = 30 \pm 20\ ppm. \qquad (6\text{-}20)$$

The substantial error in Eq. (6-20) is due to the ambiguity in "reading" the value of $^{39}\Gamma_O{}^{real}(40\ K)$ from the spectrum. If the value of $\Delta[^{39}\Gamma_O{}^{real}(40\ K)]$ is caused by *only* the LDOS, it is expressed as

$$\Delta(^{39}\Gamma_O{}^{real}) = \Delta(^{39}K_O{}^{spin}), \qquad (6\text{-}21)$$

$$\Delta(^{39}K_O{}^{spin})/{}^{39}K_O{}^{spin} = \Delta(\chi^{spin})/\chi^{spin}. \qquad (6\text{-}22)$$

From Eqs. (6-3b), (6-6b), and the relation of $^{39}K_O{}^{spin} = {}^{39}K_O - {}^{39}K_O{}^{orb}$, we obtain

$$^{39}K_O{}^{spin}(40\ K) = 85 \pm 15\ ppm. \qquad (6\text{-}23)$$

Then, from Eqs. (6-20), (6-21), (6-22), and (6-23), we obtain

$$\Delta(\chi^{spin})/\chi^{spin} = 0.4 \pm 0.3. \qquad (6\text{-}24)$$

Equation (6-24) means that the LDOS at the potassium sites is substantial, which clearly contradicts the finding in Section 5-3-C1 that the LDOS at the carbon sites in the C_{60} molecule is found to be negligible. This discrepancy can be explained by two possibilities: one is that the ^{39}K NMR line broadening is

partly or totally caused by the *electric* origin. Specifically, unlike ^{13}C nucleus, since ^{39}K nucleus possess quadrupole moment, it is possible to attribute the substantial value of "$\Delta(\chi^{spin})/\chi^{spin}$" at the potassium sites to the distribution of EFGs, *not* to the LDOS. The other is that the value in Eq. (6-24) is *solely* due to the magnetic origin. This means substantial value of the LDOS at the potassium sites, contrary to the negligible value at the carbon sites. However, the second scenario is not appropriate from a quantitative viewpoint, since the value in Eq. (6-24) is *too large* to be caused *only* by the deviation from the uniform susceptibility, as discussed in the case of the origin of the T'-line. Thus, it is concluded that there exists the *electric* contribution to the line broadening below T^*. At present, however, we have no way of determining whether or not the *magnetic* contribution is zero at the potassium sites. Nevertheless, the LDOS on the potassium sites is expected to be negligible, if we take into account that the distribution of EFG is confirmed, and that the LDOS on the carbon sites is found to be negligible.

Finally, we roughly estimate the spin-lattice relaxation time ($^{39}T_1$) at the potassium sites. Since it is clarified in the previous chapter that the extended Korringa relation holds at the carbon sites and the hyperfine couplings $^{13}A_i{}^{spin}$ do not depend on the wave vector q in the dynamical susceptibility, the following relation is expected to hold also at the potassium sites

$$[(^{39}T_1)_k{}^{mag}]T(^{39}K_k{}^{spin})^2 = {}^{39}S/K(\alpha) \qquad (k = T, O, T'). \qquad (6\text{-}25)$$

The superscript "mag" is labelled to make it clear that the Korringa relation describes the relaxation caused by only the local *magnetic* fluctuation, since, in general, the observed $^{39}T_1$ includes the *electric* relaxation (denoted as $(^{39}T_1)_k{}^{el}$) coming from the fluctuation of the EFG. The value of ^{39}S is 1.24×10^{-4} Ks, and the value of $K(\alpha)$ which represents the electron interaction is assumed to be the same as that at the carbon sites (7.4 ±1.2). From Eqs. (6-3), (6-6), (6-25), we calculate the T dependence of the *magnetic* relaxation rates at both the T- and the O-sites as

$$[1/(^{39}T_1)_T^{mag}](T) = (215T + 1.68T^2) \times 10^{-6}\ s^{-1}, \quad (6\text{-}26a)$$

$$[1/(^{39}T_1)_O^{mag}](T) = (340T + 1.70T^2) \times 10^{-6}\ s^{-1}. \quad (6\text{-}26b)$$

Although the coefficient of the T^2-term is smaller than that of the T-linear term by the orders of two, the T^2-term is not negligible as shown in Fig. 6-8. Ordinarily, it is argued that if the observed relaxation rate for the nucleus with quadrupole moment is found to be proportional to T^2, the rate is dominated by the *electric* origin. However, as Eq. (6-26) and Fig. 6-8 show, not the electric but the *magnetic* relaxation $1/(^{39}T_1)_k^{mag}$ is expected to *do have* T^2 dependence if χ^{spin} has T-linear dependence. Therefore, it should be noted that even if the experimentally obtained relaxation rate is found to depend on T^2, it does not always mean that the rate is electric but rather *magnetic*.

From the dependence of I^{peak}(T/O) on pulse repetition time at typical T, we found that the ratio of $(^{39}T_1)_T/(^{39}T_1)_O$ is larger at lower T, although we have not directly measured the relaxation rate because of the experimental difficulties. This means that the contribution of the electric relaxation is larger at the T-sites than at the O-sites.

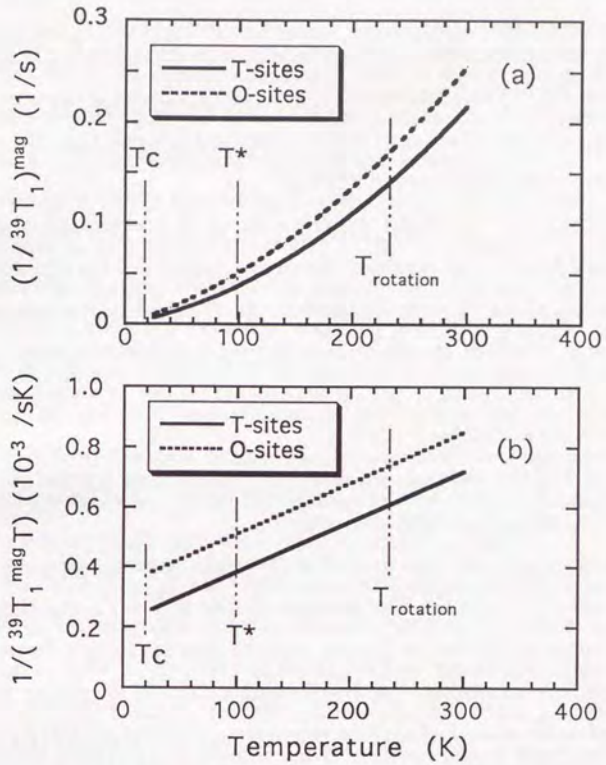

Fig. 6-8

(a) T dependences of *magnetic* spin-lattice relaxation rates $(1/^{39}T_1)^{mag}$ for both the T- and O-sites.
Note that these relaxation rates are not experimentally obtained but estimated from the T-linear Knight shifts $^{39}K_k^{spin}(T)$ (Fig. 6-2) and from the modified Korringa relation (Eq. (6-25)). Thus, the values of $(1/^{39}T_1)^{mag}$ do not consist of the *electric* origin (i.e., the relaxation mechanism due to the fluctuation of the EFGs).

(b) T dependences of the estimated magnetic relaxation rates divided by T, $(1/^{39}T_1{}^{mag}T)$ for the both sites.
The T-linear Knight shifts result in the *magnetic* relaxation rate proportional to T^2, which is ordinarily observed for *electric* relaxation rate.

Chapter 7. Summary and Conclusion

Using the spectrometer which has been built by the author in our laboratory, the ^{13}C- and ^{39}K-NMR measurements are carried out for a superconducting fulleride K_3C_{60} which does not contain unreacted pristine C_{60}. The obtained results are consistently analyzed in this study.

Regarding the ^{13}C NMR experiments, both spectra and spin-lattice relaxation rate ($1/T_1$) were obtained above and below T_C. On the other hand, only the spectra above T_C were obtained for the ^{39}K NMR. The measurements of the ^{13}C- and ^{39}K-NMR spectra were performed at typical temperatures (T) up to room T. On the contrary, the measurements of the ^{13}C-NMR $1/T_1$ were limited for $T < 55$ K, and for $T \sim 300$ K.

In what follows, the analyzed results are summarized and the answers are given to the questions presented in Chapter 3.

[1] With decreasing T, the state of the C_{60} molecular motion changes at $T_{rotation}$ ($\simeq$ 235 K) and T^* ($\simeq$ 100 K). The isotropic motion at $T > T_{rotation}$ crosses into uniaxial jumping motion below $T_{rotation}$, and the jumping motion freezes below T^*. It is concluded from the ^{39}K NMR spectra that, *in the frozen state, the orientational order of the molecules is incomplete*: the orientational order would be complete, if all the four nearest molecules of a T-site potassium face their hexagon to the potassium. In reality, however, this is found not to be true.

[2] Above T_C, the spin susceptibility $\chi^{spin}(T)$ decreases with decreasing T, which causes the decreases in the Knight shifts at both the carbon sites and the potassium sites. The T dependence of $\chi^{spin}(T)$ results from that of the density of states $N_0(T)$ at the chemical potential. Since the reduction of $\chi^{spin}(T)$ is found to be so large as $\chi^{spin}(20\ K) / \chi^{spin}(300\ K) = 0.55$, the T dependence of $N_0(T)$ is *not solely ascribed to the thermal contraction of the lattice distance, but mainly to the effect of the narrow band.*

Below T_C, the decrease in $\chi^{spin}(T)$ comes from the formation of the spin-singlet Cooper pairs.

[3] The hyperfine coupling at the carbon nucleus of the C_{60} molecules consists of its isotropic part ($^{13}A_{iso}{}^{spin}$) and its anisotropic part ($^{13}A_{ax}{}^{spin}$). The former ($^{13}A_{iso}{}^{spin}$) is due to the Fermi contact interaction by the conduction electrons on the carbon s-orbitals, and the latter ($^{13}A_{ax}{}^{spin}$) comes from the dipolar field of the conduction electrons residing on mainly the carbon $p\pi$-orbitals.

From the analysis on the anisotropic Knight shifts of the ^{13}C nucleus ($^{13}K_i{}^{spin}$), we found that the ratio on isotropy α^{spin} ($\equiv {}^{13}A_{iso}{}^{spin} / {}^{13}A_{ax}{}^{spin}$) is 0.78.

This means that we *experimentally* solved, *for the first time*, the controversial problem of which the ^{13}C hyperfine coupling is dominant in K_3C_{60}: isotropic ($^{13}A_{iso}{}^{spin}$) or anisotropic ($^{13}A_{ax}{}^{spin}$). We consider that the substantial contribution of s-orbitals reflects the crystal structure of the C_{60} molecule: the almost planar structure seen from the nucleus length scale makes the dominant contribution of anisotropic $p\pi$-orbitals, but the non-planarity that shapes the C_{60} molecule produces the comparable contribution of the carbon s-orbitals.

[4] At high T ($> T_{rotation}$), since the isotropic molecular motion quenches the anisotropy in the hyperfine coupling, the ^{13}C NMR spectra show symmetrical line shapes and the T_1 recovery processes follow the single-exponential time evolution which is expected for ^{13}C nucleus. On the contrary, below $T_{rotation}$, the ^{13}C NMR spectra show asymmetric line shapes due to the presence of the anisotropy which results from the jumping motion of the molecules. At lower T ($< T^*$) where the molecular motion is frozen, the T_1 processes show non-single exponential recoveries (NSER) which are scaled to an identical recovery shape. The value of $\alpha^{spin} = 0.78$, which was derived from the analysis on the ^{13}C NMR spectra, well reproduces the identical shape of the NSER. This means that *both* the asymmetric line shapes *and* the NSER at low T are explained by *only* the anisotropy in the ^{13}C hyperfine coupling. In addition, the contribution of the *local density of states* at the inequivalent carbon sites, which had been proposed

to account for the NSER and for the asymmetric line shapes, *is found to be less than* the contribution of the *anisotropy*.

[5] Regarding the Knight shifts and the spin-lattice relaxation time for the ^{13}C nucleus, the usual Korringa product is defined as $T_1T[^{13}K_{iso}{}^{spin}]^2$ at high T ($> T_{rotation}$), due to the quenching of the anisotropy. At low T ($< T^*$) where the molecular motion is frozen, the effective value of $(T_1)_{iso}$ is defined by renormalizing the anisotropy in the hyperfine coupling to the observed $T_1{}^S$ value (which is obtained from the initial slope of the NSER shape). In this case, the Korringa product is modified as $(T_1)_{iso}T[^{13}K_{iso}{}^{spin}]^2$. It is found that the values of $(T_1)_{iso}T[^{13}K_{iso}{}^{spin}]^2$ at low T are equal to the value of $T_1T[^{13}K_{iso}{}^{spin}]^2$ at room T. This means that the "*extended* Korringa relation", where *both* the anisotropy *and* the T-dependent density of states are taken into account, holds irrespective of the state of the molecular motion. In addition, the $K(\alpha)$ value (which is defined by the Korringa constant over the Korringa product) in our case is 7.4 times as large as the value of independent electrons. Thus, it is concluded that the normal state of K_3C_{60} is a Fermi liquid where substantial *antiferromagnetic* electron interaction is treated within the RPA. This finding is *far from self-evident* in that the Korringa relation holds *up to room T* with the $K(\alpha)$ value being enhanced.

[6] We made it clear *for the first time* that the ^{13}C nuclear spin-lattice relaxation rate $1/T_1T$ shows *a broadened coherence peak* below T_C. From this finding, it is concluded that *the superconducting gap has no nodes* in the wave-vector space and that the Cooper pairs have *s-wave* symmetry. The T dependence of $1/T_1T$ is not explained by the phenomenological fitting which parameterizes both the life time of the thermally-excited quasi particles and the superconducting gap, but is well reproduced by the theoretical prediction which treats the electron-phonon interaction based on the Eliashberg theory. Since this theory assumes the dominant contribution of the low frequency ($0 \sim 60$ meV) phonons to the relaxation rate and predicts the superconducting gap of $2\Delta(0)/k_BT_C = 4.3$, it is found that the

s-wave pairing by *low frequency phonons* in the *strong coupling* regime can explain the superconductivity of K_3C_{60}.

In conclusion, the present study has revealed *how* the consistent physical picture is like on the electronic properties of a superconducting fulleride K_3C_{60}. Consequently, *all the questions*, which were presented when this study was started, *have been cleared except but one*. The question which remains to be seen is, "*Why* is the T_C of this material *so high*?" It is true that researchers are strongly motivated by this *naive* question to study the mechanisms of superconductivity of new materials. However, it is also true that scientific researches *can* give answers to "*how*" very precisely and minutely, but, as is often, *not* satisfactorily to "*why*". In the case of a superconducting fulleride, the origin of its high T_C cannot be ascribed to the value of the density of states, since there are no experimental findings which evidence that the value is sufficiently large to account for the high T_C.

It is expected that various modes of phonons are induced both *on* a C_{60} molecule (due to its "moderately" large size) and *between* the molecules (due to the van der Waals bonding). Thus, those phonons should contribute to enhance the superconductivity *if* the Cooper pairs are found to be phonon-mediated. Since the present study has revealed that the T dependence of $1/T_1T$ is well explained by the electron-phonon mechanisms, we have proved experimentally the assumption on which the above mentioned expectation is based. This is the *safest* answer which the author can present at best, to the *naive* but *important* "*why*".

References

Antropov, V. P., Mazin, I. I., Andersen, O. K., Liechtenstein, A. I., and Jepsen, O.: Phys. Rev. B**47**, 12373 (1993).

Barrett, S. E., Durand, D. J., Pennington, C. H., Slichter, C. P., Friedmann, T. A., Rice, J. P., and Ginsberg, D. M.: Phys. Rev. B**41**, 6283 (1990).

Bloembergen, N, and Rowland, T. J.: Acta Metall. **1**, 731 (1953).

Boebinger, G. S., Palstra, T. T. M., Passner, A., Rosseinsky, M. J., Murphy, D. W., and Mazin, I. I.: Phys. Rev. B**46**, 5876 (1992).

Bovey, F. A.: *Nuclear Magnetic Resonance Spectroscopy*, 2nd ed. (Academic Press, London, UK, 1988)

Chakravarty, S. and Kivelson, S.: Europhys. Lett. **16**, 751 (1991).

Clogston, A. M., Jaccarino, V., and Yafet, Y.: Phys. Rev. **134**, A650 (1964).

Degiorgi, L., Wachter, P., Gruner, G., Huang, S. -M., Wiley, J., and Kaner, R. B.: Phys. Rev. Lett. **69**, 2987 (1992).

Ebbesen, T. W., Tsai, J. S., Tanigaki, K., Tabuchi, J., Shimakawa, Y., Kubo, Y., Hirosawa, I., and Mizuki, J.: Nature **355**, 620 (1992).

Erwin, S. C., and Picket, W. E.: Science **254**, 842 (1991).

Fleming, R. M, Ramirez, A. P., Rosseinsky, M. J., Murphy, D. W., Haddon, R. C., Zaharak, S., M., and Makhiga, A. V.: Nature **352**, 787 (1991).

Gelfand, M. P., and Lu, J. P.: Phys. Rev. Lett. **68**, 1050 (1992).

Gossard, A. G., and Portis, A. M.: Phys. Rev. Lett. **3**, 164 (1959).

Hebard, A. F., Rosseinsky, M. J., Haddon, R. C., Murphy, D. W., Glarum, S. H., Palstra, T. T. M., Ramirez, A. P., and Kortan, A. R.: Nature **350**, 600 (1991).

Hebel, L. C. and Slichter, C. P.: Phys. Rev. **113**, 1504 (1959).

Holczer, K., Klein, O., Huang, S. -M., Kaner, R. B., Fu, K. -J., Whetten, R. L., and Diederich, F.: Science **252**, 1154 (1991).

Holczer, K., Klein, O., Alloul, H., Yoshinari, Y., Hippert, F., Huang, S. -M., Kaner, R. B., and Whetten, R. L.: Europhys. Lett. **23**, 63 (1993).

Jaccarino, V.: *Proceedings of the International School of Physics, Enrico Ferimi Course* XXXVII (Academic Press, New York, 1967).

Johnson, C. E., Jiang, H. W., Holczer, K., Kaner, R. B., Whetten, R. L., and Diederich, F.: Phys. Rev. B**46**, 5880 (1992).

Kawamoto, A., Miyanaga, K., Nakazawa, Y., and Kanoda, K. (a): Phys. Rev. Lett. **74**, 3455 (1995).

Kawamoto, A., Miyanaga, K., Nakazawa, Y., and Kanoda, K. (b): Phys. Rev. BI**52**, 15522 (1995).

Kiefl, R. F., MacFarlane, W. A., Chow, K. H., Dunsiger, S., Duty, T. L., Johnston, T. M. S., Schneider, J. W., Sonier, J., Brard, L., Strongin, R. M., Fischer, J. E., and Smith III, A. B.: Phys. Rev. Lett. **70**, 3987 (1993).

Korringa, J.: Physica **16**, 601 (1950).

Kratschmer, W., Lamb, L. D., Fostiropoulos, K, and Huffman, D. R.: Nature **347**, 354 (1990).

Kroto, H. W., Heath, J. R., O'Brien, S. C., Curl, R. F., and Smalley, R. E.: Natrue **318**, 162 (1985).

Lof, R. W., van Beenendaal, M. A., Koopmans, B., Jonkman, H. T., and Sawatzky, G. A.: Phys. Rev. Lett. **68**, 3924 (1992).

MacLaughlin, D. E.: Solid State Phys. **31**, 1 (1976).

Maniwa, Y., Ohi, A., Mizoguchi, K., Kume, K., Kikuchi, K., Saito, K., Ikemoto, I., Suzuki, S., and Achiba, Y. (a): Synth. Met. Proc. ICSM 92, Goteborg, Sweden. (1992).

Maniwa, Y., Shibata, T., Mizoguchi, K., Kume, K., Kikuchi, K., Ikemoto, I., Suzuki, S., and Achiba, Y.(b): J. Phys. Soc. Jpn. **61**, 2212 (1992).

Maniwa, Y., Saito, T., Ohi, A., Mizoguchi, K., Kume, K., Kikuchi, K., Ikemoto, I., Suzuki, S., Achiba, Y., Kosaka, M., Tanigaki, K., and Ebbesen, W.: J. Phys. Soc. Jpn. **63**, 1139 (1994).

Marks, R. E.: *The Dymaxion World of Buckminster Fuller* (Reinhold, New York, 1960).

Mayaffre, H., Wzietek, P., Jerome, D., Lenoir, C., and Batail, P.: Phys. Rev. Lett. **75**, 4122 (1995).

Mitch, M. G., Chase, S. J., and Lannin, J. S.: Phys. Rev. Lett. **68**, 883 (1992).

Morikawa, T. and Takahashi, T.: Physica C**87**, 1017 (1993).

Moriya, T.: J. Phys. Soc. Jpn. **18**, 516 (1963).

Moriya, T. and Kawabata, A.: J. Phys. Soc. Jpn. **34**, 639 (1973); *ibid.*, **35**, 669 (1973).

Nakamura, Y. O., Yokoya, Y., Matsuda, N., and Shiina, Y.: Solid State Commum. **86**, 627 (1993).

Palstra, T. T. M., Haddon, R. C., Hebard, A. F., and Zaanen, J.: Phys. Rev. Lett. **68**, 1054 (1992).

Pennington, C. H. and Slichter, C. P.: in *Physical Properties of High Temperature Superconductivity II*, Ginsberg, D. M., ed. (World Scientific, Teaneck, NJ, USA, 1990).

Pfeiffer, L., Walstedt, R. E., Bell, R. F., and Kovacs, T.: Phys. Rev. Lett. **49**, 1162 (1982).

Prassides, K., Tomkinson, J., Christides, C., Rosseinsky, M. J., Murphy, D. W., and Haddon, R. C.: Nature **354**, 462 (1991).

Ramirez, A. P., Kortan, A. R., Rosseinsky, M. J., Duclos, S. J., Mujsce, A. M., Haddon, R. C., Murphy, D. W., Makhija, A. V., Zahurak, S. M., and Lyons, K. B. (a): Phys. Rev. Lett. **68**, 1058 (1992).

Ramirez, A. P., Rosseinsky, M. J., Murphy, D. W., and Haddon, R. C. (b): Phys. Rev. Lett. **69**, 1687 (1992).

Redfield, A. G.: Phys. Rev. **162**, 367 (1967).

Saito, S. and Oshiyama, A.: Phys. Rev. BII**44**, 11536 (1991).

Sasaki, S., Matsuda, A., and Chu, C. W.: J. Phys. Soc. Jpn. **63**, 1670 (1994).

Sasaki, S., Matsuda, A., and Chu, C. W.: J. Phys. Soc. Jpn. **65**, 2389 (1996).

Schluter, M., Lannoo, M., Needels, M., Baraff, G. A., and Tomanek, D.: Phys. Rev. Lett. **68**, 526 (1992).

Shannon, R. D. and Prewitt, C. T.: Acta Cryst. B**26**, 1046 (1970).

Slichter, C. P., *Principles of Magnetic Resonance*, 3rd. ed. (Springer-Verlag, New York, USA, 1989).

Sparn, G., Thompson, J. D., Huang, S. -M., Kaner, R. B., Diederich, F., Whetten, R. L., Gruner, G., and Holczer, K.: Science **252**, 1829 (1991).

Sparn, G., Thompson, J. D., Whetten, R. L., Huang, S. -M., Kaner, R. B., Diederich, F., Gruner, G., and Holczer, K.: Phys. Rev. Lett. **68**, 1228 (1992).

Stenger, V. A., Recchia, C., Vance, J., Pennington, C. H., Buffinger, D. R., and Ziebarth, R. P.: Phys. Rev. B**48**, 9942 (1993).

Stenger, V. A., Pennington, C. H., Buffinger, D. R., and Ziebarth, R. P.: Phys. Rev. Lett. **74**, 1649 (1995).

Stephens, P. W., Mihaly, L., Lee, P. L., Whetten, R. L., Huang, S. -M., Kaner, R., Deiderich, F, and Holczer, K.: Nature **351**, 632 (1991).

Takigawa, M. and Saito, G.: J. Phys. Soc. Jpn. **55**, 1233 (1986).

Takigawa, M., Hammel, P. C., Heffner, R. H., Fisk, Z.: Phys. Rev. B**39**, 7371 (1989).

Tanigaki, K., Hisosawa, I., Ebbesen, T. W., Mizuki, J., Shimakawa, Y., Kubo, Y., Tsai, J. S., and Kuroshima, S.: Nature **356**, 419 (1992).

Tinkham, M.: *Introduction to Superconductivity* (McGraw-Hill Inc., New York, 1975).

Tycko, R., Dabbagh, G., Fleming, R. M., Haddon, R. C., Makhija, A. V., and Zajurak, S. M. (a): Phys. Rev. Lett. **67**, 1886 (1991).

Tycko, R., Dabbagh, G., Rosseinsky, M. J., Murphy, D. W., Fleming, R. M., Ramirez, A. P., and Tully, J. C. (b): Science **253**, 884 (1991).

Tycko, R., Dabbagh, G., Rosseinsky, M. J., Murphy, D. W., Ramirez, A. P., and Fleming, R. M.: Phys. Rev. Lett. **68**, 1912 (1992).

Uemura, Y. J. *et al.*: Nature **352**, 605 (1991).

Walstedt, R. E., Murphy, D. W., and Rosseinsky, M.: Nature **362**, 611 (1993).

Wong, W. H., Hanson, M. E., Clark, W. G., Gruner, G., Thompson, J. D., Whetten, R. L., Huang, S. -M., Kaner, R. B., Diederich, F., Petit, P., Andre, J.

-J., and Holczer, K.: Europhys. Lett. **18**, 79 (1992).

Xiang, X. -D., Hou, J. G., Briceno, G., Vareka, W. A., Mostovoy, R., Zettl, A., Crespi, V. H., and Cohen, M. L.: Science **256**, 1190 (1992).

Xiang, X. -D., Hou, J. G., Crespi, V. H., Zettl, A., and Cohen, M. L.: Nature **361**, 54 (1993).

Yoshinari, Y., Yasuoka, H., Ueda, Y., Koga, K., and Kosuge, K.: J. Phys. Soc. Jpn. **59**, 3698 (1990).

Yoshinari, Y., Alloul, H., Kriza, G., and Holczer, K.: Phys. Rev. Lett. **71**, 2413 (1993).

Yoshinari, Y., Alloul, H., Holczer, K., and Forro, L.: Physica C **235-240**, 2479 (1994).

Yosida, K.: Phys. Rev. **110**, 769, (1958).

Zhang, Z., Chen, C. C., Kelty, S. P., Dai, H., and Lieber, C. M.: Nature **353**, 333 (1991).

Zhang, F. C., Ogata, M., and Rice, T. M.: Phys. Rev. Lett. **67**, 3452 (1991).

43